AD-A118 583 DAVID W TAYLOR NAVAL SHIP RESEARCH AND DEVELOPMENT CE--ETC F/G 12/1
CALCULATION OF CONTACT PRESSURES AND FRICTIONAL EFFECTS ON MECH--ETC(U)
AUG 82 D E LESAR
UNCLASSIFIED DTNSRDC-82/033 NL

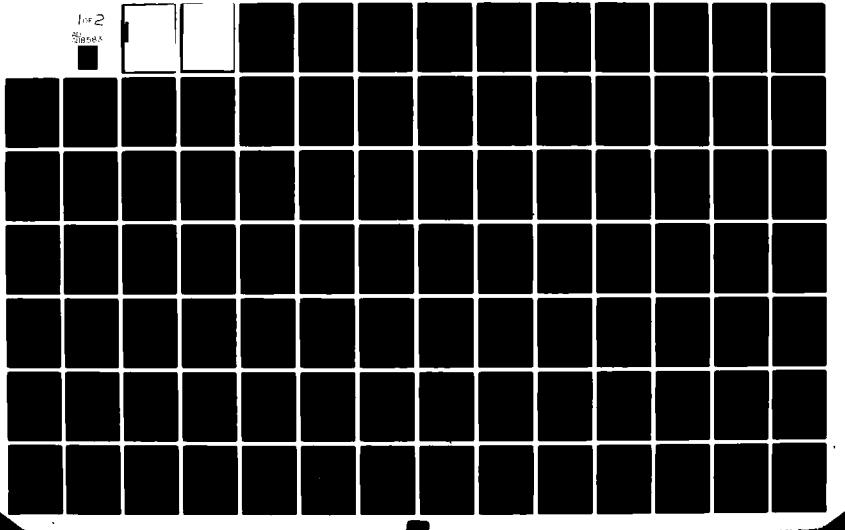

UNCLASSIFIED

SECURITY CLASSIFICATION OF THIS PAGE *(When Data Entered)*

REPORT DOCUMENTATION PAGE	READ INSTRUCTIONS BEFORE COMPLETING FORM
1. REPORT NUMBER: DTNSRDC-82/033	2. GOVT ACCESSION NO.: AD A118583
3. RECIPIENT'S CATALOG NUMBER	
4. TITLE *(and Subtitle)*: CALCULATION OF CONTACT PRESSURES AND FRICTIONAL EFFECTS ON MECHANICAL CONTACT SURFACES BY FINITE ELEMENT METHODS WITH APPLICATION TO FRETTING DAMAGE PREDICTION	5. TYPE OF REPORT & PERIOD COVERED
	6. PERFORMING ORG. REPORT NUMBER
7. AUTHOR(s): Douglas E. Lesar	8. CONTRACT OR GRANT NUMBER(s)
9. PERFORMING ORGANIZATION NAME AND ADDRESS: David W. Taylor Naval Ship R&D Center, Bethesda, Maryland 20084	10. PROGRAM ELEMENT, PROJECT, TASK AREA & WORK UNIT NUMBERS: Program Element 61152N, Task Area ZR0230301, Work Unit 1720-110
11. CONTROLLING OFFICE NAME AND ADDRESS: Dr. Alan Powell, Technical Director, DTNSRDC, Code 01	12. REPORT DATE: August 1982
	13. NUMBER OF PAGES: 136
14. MONITORING AGENCY NAME & ADDRESS *(if different from Controlling Office)*: Director of Laboratory Programs, Naval Material Command, Code 08L	15. SECURITY CLASS. *(of this report)*: UNCLASSIFIED
	15a. DECLASSIFICATION/DOWNGRADING SCHEDULE

16. DISTRIBUTION STATEMENT *(of this Report)*

APPROVED FOR PUBLIC RELEASE: DISTRIBUTION UNLIMITED

17. DISTRIBUTION STATEMENT *(of the abstract entered in Block 20, if different from Report)*

18. SUPPLEMENTARY NOTES

19. KEY WORDS *(Continue on reverse side if necessary and identify by block number)*

Contact Stress
Coulomb Friction
Finite Element Methods
Frictional Slip
Fretting Damage
Shrinkfit Assemblies

20. ABSTRACT *(Continue on reverse side if necessary and identify by block number)*

Contact stresses, contact forces, relative contact surface displacements, and the dissipative effects of friction are computed, by the finite element method, for various two- and three-dimensional contact problems. The finite element technique is verified by analysis of several two-dimensional frictionless contact problems; the Hertz contact of two cylinders, a rigid sleeve/elastic shaft shrinkfit, and an elastic sleeve/elastic

(Continued on reverse side)

DD FORM 1 JAN 73 1473 EDITION OF 1 NOV 65 IS OBSOLETE

S/N 0102-LF-014-6601

UNCLASSIFIED

SECURITY CLASSIFICATION OF THIS PAGE *(When Data Entered)*

(Block 20 continued)

shaft shrinkfit. In these cases the finite element calculations compare favorably to existing solutions. The contact analysis capability is extended to frictional contacts by considering plane stress and axisymmetric contact problems with friction and slip, for which reasonable results are produced. The capability is further extended to complex three-dimensional contacts by an effort to determine the contact forces and frictional dissipation taking place in the cyclic bending of a shrinkfit assembly. This work demonstrates that advanced nonlinear finite element methods can be used to solve a variety of mechanical engineering problems involving unlubricated contact surfaces and the effects of friction.

TABLE OF CONTENTS

LIST OF FIGURES

LIST OF TABLES

NOTATION

a_i, b_i etc.	Lengths of element sides
a/h	Punch half width to slab depth ratio
b	Sleeve half length or contact zone half length
b/h	Sleeve length to thickness parameter
F_A, F_B, etc.	Contact forces at nodes A, B, etc.
F_N	Normal contact force
F_T	Tangential friction force intensity
H	Sleeve thickness
h	Shrinkfit interference
K_f	Frictional stiffness
M	Bending moment
P	Pressure
P_A, P_B, etc.	Contact Pressures at nodes A, B, etc.
P_N	Normal contact pressure
P_T	Frictional shear stress
r	Radius
r_i	Shaft inner radius
r_o, r_1, A	Shaft outer radius
r_2	Sleeve outer radius
u_r	Radial deflection
u_z	Axial deflection
u_r^i, u_z^i	Contact surface nodal displacement of body i in r,z polar coordinates
u_x^i, u_y^i, u_z^i	Contact surface nodal displacements of body i in x,y,z cartesian coordinates

Z	Shaft length from cent[illegible]plane of symmetry
μ	Coefficient of friction
υ	Poisson's ratio
θ	Circumferential angle
σ_A, σ_B, etc.	Stresses at integration points A, B. etc.
σ_{AB}, σ_{CD}, etc.	Extrapolated contact surface stresses from integration points A, B, etc.
σ_{RR}	Radial stress
$\sigma_{\theta\theta}$	Hoop stress
σ_{zz}	Axial stress
σ_{Rz}	Shear stress

LIST OF ABBREVIATIONS

cm	Centimeter
deg	Degrees
DTNSRDC	David W. Taylor Naval Ship Research and Development Center
in.	Inch
in-lb	Inch pound
J	Joule
kg	Kilogram
lb	Pound
lb/in	Pound per inch
N/cm	Newtons per centimeter
N/cm^2	Newtons per square centimeter
psi	Pounds per square inch
vs.	Versus
2-D	Two-dimensional
3-D	Three-dimensional

ABSTRACT

Contact stresses, contact forces, relative contact surface displacements, and the dissipative effects of friction are computed, by the finite element method, for various two- and three-dimensional contact problems. The finite element technique is verified by analysis of several two-dimensional frictionless contact problems; the Hertz contact of two cylinders, a rigid sleeve/elastic shaft shrinkfit, and an elastic sleeve/elastic shaft shrinkfit. In these cases the finite element calculations compare favorably to existing solutions. The contact analysis capability is extended to frictional contacts by considering plane stress and axisymmetric contact problems with friction and slip, for which reasonable results are produced. The capability is further extended to complex three-dimensional contacts by an effort to determine the contact forces and frictional dissipation taking place in the cyclic bending of a shrinkfit assembly. This work demonstrates that advanced nonlinear finite element methods can be used to solve a variety of mechanical engineering problems involving unlubricated contact surfaces and the effects of friction.

ADMINISTRATIVE INFORMATION

The work described in this report was performed at the David W. Taylor Naval Ship Research and Development Center (DTNSRDC) under the In-house Research/In-house Engineering Development (IR/IED) program, Program Element 61152N, Task Area ZR0230301, and Work Unit 1720-110.

METRIC CONVERSION

All numerical quantities in this report are expressed in U.S. customary units. Use the following factors to convert to metric units:

1 in.	=	2.54 cm
1 lb	=	0.454 kg
1 psi	=	0.690 N/cm^2
1 lb/in	=	1.751 N/cm
1 in-lb	=	0.113 J

INTRODUCTION

In many cases, the reliability of machine elements in power transmission and power generation systems depends on the integrity of contact surfaces between system components. Although the wear resistance of component surfaces is a vital consideration, the performance of contact surfaces in a structural mechanical sense is also very important. All machinery components deform under load, and such deformations influence both the contact pressures and the frictional forces transmitted between contact surfaces. These forces are also influenced by the materials and lubricants involved.

Many examples can be cited in which contact stresses and the frictional behavior of contact surfaces affect the various possible failure modes of naval ship and submarine machine components. Often, the contact surface is lubricated (e.g. the concentrated contacts arising in gear and bearing assemblies). Surface fatigue failure mechanisms such as pitting and fretting, which occur in reduction gear and propulsion shaft bearings, respectively, are influenced by contact pressure and frictional stress. Contact pressure and friction resulting from component deformation influence the performance of mechanical fastenings (bolts, joints, rivets, threaded fasteners) and seal systems (O-rings and gaskets). The influence of contact stresses on failures is an important consideration in high-speed machinery components, such as turbine blade/rotor fastenings. Finally, contact surface gapping is sometimes a potential problem (e.g. the behavior of preloaded bolts and blade palm/hub surfaces in controllable pitch propeller systems).

When dealing with contact surface integrity problems, the navy engineering community has traditionally devoted much attention to the materials aspects. Solutions to wear, galling and surface fatigue problems have typically been sought through extensive and expensive experimentation and materials evaluations. The ongoing concern with submarine shaft seals provides a prime example. These machinery component problems have been addressed almost exclusively from a materials standpoint, with relatively little attention to the structural mechanical performance. Clearly, a seal cannot perform as intended unless the component deformations and the geometry of seal and surrounding components assure an optimum contact surface load transmission pattern. The experimental line of attack was the only available recourse when analytical methods for contact and friction analysis were limited, impractical, or impossible. The rapid development of finite element methods to

analyze structural mechanical systems of complex geometry and treat previously intractable nonlinear phenomena has changed this situation completely.

As naval machinery systems have become more complex, the need for a contact/friction structural analysis capability has become more acute. Although they retain their importance, experiments and materials evaluations that account for the influence of all variables are difficult and expensive to conduct. An analytical tool is needed which is capable of mathematically evaluating the performance of contact surfaces in mechanical component designs. Such an analytical tool may also be of assistance in failure assessment.

OBJECTIVE AND SCOPE

The purpose of this study is twofold:

(1) To verify evaluate, and refine newly developed nonlinear finite element techniques for contact stress and friction analysis.

(2) To apply these new techniques to a complex practical engineering problem, fretting corrosion fatigue, in an attempt to correlate calculated contact and friction behavior to experimental evidence of fretting.

The scope of this study is limited in several ways:

(1) The theory is limited to dry, unlubricated contacts. The important problem area of elastohydrodynamic lubrication is not considered.

(2) Of principal concern are interference contacts over a large surface area; concentrated contacts are not considered.

(3) Mixed contact/gapping is not considered, although the theory is capable of straightforward treatment of such problems.

(4) This study is limited to static and quasi-static cyclic loadings, although theories exist which can handle dynamic impact problems.

(5) The theory describes the effects of contact behavior only in a macroscopic structural mechanical sense. No attempt is made to address the tribological issues of contact and friction behavior (asperity interaction, contact surface irregularity, local cold welding and cracking, etc.)

These limitations can be placed in proper perspective by realizing that this study is only a first attempt to apply state-of-the-art structural mechanics analysis methods to a wide class of complex, practical contact problems.

BACKGROUND

CLASSICAL MATHEMATICAL APPROACHES TO CONTACT PROBLEMS OF SOLID MECHANICS

The mathematical techniques of elasticity theory have long been used to solve the static contact problems of solid mechanics. The standard work of Timoshenko (reference 1,* pp. 409-420) contains a treatment of the so-called Hertzian contact of spheres and cylinders, the simplest type of contact problem and the first one reduced by rational analysis. The Hertz problems are also discussed by Lubkin (reference 2, Chapter 42) and by Love (reference 3, pp. 192-200). Many Russian mathematicians have specialized in contact research, and three treatises on such problems have been produced.[4-6] The English-language literature also contains a vast number of papers on a wide variety of contact problems; a few recent samples are referenced.[7-12]

The elasticity approach is important for fundamental understanding and has provided many useful solutions to engineering problems. From the engineer's standpoint, however, the purely mathematical approach presents three difficulties:

(1) Complexity

The commonly used *specialized techniques* (integral transforms, potential functions) require a in-depth understanding of the theory of partial differential equations and integral equations. As a result, solutions tend to be involved mathematical expressions that are not always presentable in closed form.

(2) Geometrical limitations

In order for elasticity solutions to be tractable, the problem must be posed in simple coordinate systems (Cartesian, radial). Many practical contact problems are characterized by complex geometry that does not fit a standard coordinate system. Also, because specialized elasticity solutions contain assumptions on boundary conditions and symmetry planes, their validity is restricted.

(3) Limited threatment of nonlinear effects in mathematical solutions

When friction is considered,for example, (which is rare) the ideal assumption of full adherence is usually invoked, while the real situation may involve mixed slip and adherence. In contact and gapping situations, the extent of gapping must be assumed "a priori," an assumption which may be difficult to

*A complete listing of references is given on page 117.

justify. The nonlinearity of dynamic contact-impact kinetics is also very difficult to treat analytically.

This brief critique of classical methods demonstrates the desirability of an approximate numerical approach to analysis of contact effects in complex naval engineering problems.

FINITE ELEMENT APPROACHES IN CONTACT, FRICTION, AND GAPPING PROBLEMS IN SOLID MECHANICS

The finite element method has recently been extended to handle nonlinear contact problems in solid mechanics. For many years, the thrust of research has been to devise specialized techniques for specific classes of contact problems. Earliest efforts addressed frictionless contact arising from a prescribed indentation without gapping.[13] Techniques were then developed to handle frictionless contact/gap problems (reference 14, and work by Gifford*); frictionless interference fits without gapping;[15-17] and combinations of contact, gapping, and interference.** The first finite element treatment for contact and gapping with friction[18-20] considered two-dimensional contacts modelled by low-order finite elements. This capability has been extended to three-dimensional problems.[21] The general approach of this work is to formulate the contact problem in terms of conventional incremental equilibrium equations subject to nonlinear constraint conditions on contact surface displacements and/or forces. This approach can be conveniently generalized in terms of the classicial Lagrange multiplier method, in which nonlinear contact constraint equations and conventional incremental equilibrium equations are solved simultaneously in an iterative manner. The Lagrange multiplier approach[22] is considered in this study.

Another line of attack is to model contact interfaces as a fictitious layer of material possessing empirical constitutive properties that approximately describe observed contact and friction behavior. Contact and gap phenomena can be modelled with "bilinear springs" that possess very high stiffness when contact is detected and are assigned vanishingly small stiffness when gapping occurs.[23] Analogous "friction springs" can similiarly be activated and deactivated according to whether

---

*Unpublished work by L.N. Gifford of the Structures Department of DTNSRDC.

**Unpublished work by R. A. Lindeman of the U.S. Naval Weapons Laboratory, Dahlgren, Virginia.

adherence or slip is occurring.[24,25] Contact surfaces have also been modelled as a continuous layer of material with bilinear stiffness.[26] The bilinear spring approach has been used in general-purpose nonlinear finite element programs.[27,28] These works share a common feature; a contact surface stiffness parameter is assigned which supplements the conventional stiffnesss coefficients of the incremental equilibrium equations. The "stiffness" (also called "penalty") approach has advantages in some situations and is also considered in this study.

More advanced lines of finite element contact research have also been pursued. An advanced stiffness-like method which models complex frictional behavior by "bond elements" has been proposed.[29] Complex adherence and slip rules closely resembling classical plasticity theories have been formulated for two- and three-dimensional problems.[30,31] These works model frictional behavior by rational constitutive relations. The constitutive equation approach holds promise for modeling finer details of friction behavior for a wide variety of materials; however, it is not conveniently applicable to the problems considered here. Finally, a method has been devised for finite element solution of dynamic contact-impact problems,[32,33] which are vitally important but of little relevance to this study.

These recent works have made possible the approximate numerical analysis of a wide variety of contact problems. The limitations of classical mathematical methods, geometry-dependence, and need for special boundary conditions are eliminated quite naturally by finite element techniques. Highly nonlinear contact phenomena, such as mixed contact and gapping, mixed adherence and slip, and contact/impact, are accomodated quite generally by finite element codes. Finally, most of those engineers who do not have the extensive mathematical background needed to understand elasticity methods can work with even nonlinear finite element methods.

The finite element techniques which have been applied to problems considered in this study are more fully described in the following section.

APPROACH

LAGRANGE MULTIPLIER METHOD FOR FINITE ELEMENT MODELLING OF CONTACT, GAP, AND FRICTION PROBLEMS

The elastic stiffness matrix and the incremental load vector in the structural incremental equilibrium equations are formulated in this approach by the generalized principle of minimum potential energy (or alternatively, the principle of virtual work). The incremental equilibrium equations are supplemented, however, by constraint terms of the Lagrange multiplier type which impose the contact or gap conditions existing at the current load step. Finite element meshes representing the solid bodies in the problem are modelled in the usual way by arrays of elements interconnected at nodal points. The nodal arrangement on surfaces that initially interfere (as in a shrinkfit), initially contact, and initially contact but gap apart as loading proceeds, must be such that opposing nodes are paired; that is, their initial coordinates are either coincident (interference and contact), or spatially close together and in line with one another (initial gapping, see Figure 1). It is assumed that displacements in the problem are small, so that opposing nodes which are initially close together remain so in the course of loading. The analyst specifies "contact elements" or "contact kinematic constraints" between chosen pairs of candidate contact nodes. The relative normal displacements are monitored at these node pairs as the structure is loaded. The Lagrange multipliers, which are calculated unknowns as are the nodal displacements, turn out to be the normal contact forces transmitted between the node pairs. The initial interference case, which exists if all node pairs are overlapping, is a linear problem which can be solved in one step since all Lagrange multipliers are active. In the general case, however, the contact conditions change in the course of loading (i.e. gaps close or open) and the Lagrange multipliers are made active (gap closed, contact force transmitted) or set to zero (gap open, no contact force), depending on the current normal relative displacements. This constitutes the nonlinearity of the problem. A complete mathematical description of the Lagrange multiplier theory and the associated finite element equations are given, in vectorial form, by Hibbitt and Rubin.[22] Specialized examples of finite element equation systems have been developed from the general forms in reference 22. These

unpublished developments* illustrate the adherence/slip constraints and the solution process for various contact conditions of practical interest.

The Lagrange multiplier approach is also used to model the frictional behavior of contact surfaces.[22] Classical Coulomb friction theory is applied; this assumes that an adherence condition exists at a contact node pair when the local frictional force (force tangential to the contact surface) is below the local static frictional force limit. Slip (relative tangential displacement) occurs when the frictional force reaches this limit. The friction limit is defined by an empirical relation of the normal contact force F_N, in which μ is the experimentally measured static friction coefficient:

$$F_T < \mu \cdot F_N \qquad \text{(adherence)} \qquad (1)$$

$$F_T = \mu \cdot F_N \qquad \text{(slip)} \qquad (2)$$

In the complete adherence condition, all relative tangential displacements on the contact surface are constrained to zero, and the frictional forces are unknown. In the mixed adherence and slip condition, the frictional force is constrained to $F_T = \mu \cdot F_N$ at slipping node pairs, and the slip is the unknown quantity associated with those node pairs. The displacement response to external loading is nonlinear in a load step; this causes the Coulomb slip limit to be reached at some node pairs while the others remain adhered. The nonlinear problem is solved by monitoring the relation of normal force to frictional force, the appropriate constraints being imposed according to whether equations (1) or (2) hold. After a trial solution that assumes full adherence everywhere, final equilibrium at the current load is found through an iterative process that unlocks adhered nodes not satisfying the Coulomb limit.

The Lagrange multiplier approach for both normal contact/gapping and friction behavior has been incorporated as the "contact elements" of the MARC general purpose nonlinear finite element code.[34] Several finite element contact approaches[19-22] are very similar to the MARC method but do not contain a frictional slip degree of freedom. They can be considered to be special cases of the MARC approach. As it turns out, the Lagrange multiplier method works quite well for the normal contact

*Authored by D. E. Lesar of the Structures Department of DTNSRDC.

force/gap part of the contact problem but does not always work well for friction. Hibbitt, the developer of this method, has indicated that the Lagrange multiplier approach for friction and slip suffers mathematical instabilities and leads to convergence difficulties in cases where adherence to slip transitions occur.[35] The method appears to predict adherence/slip behavior reasonably well in the 2-D analysis,[19] as long as the extent of slip is small. Attempts to apply MARC to the 3-D friction problems considered here resulted in severe convergence problems. This poor performance led to the consideration of a new friction theory which borrows from the so-called "penalty method" used in finite element solutions of contact problems. This improved friction theory is discussed in the next section.

STIFFNESS METHOD FOR FINITE ELEMENT MODELLING OF FRICTIONAL BEHAVIOR IN CONTACT/GAP AND FRICTION PROBLEMS

The penalty (or stiffness) method has been used in the past to model the contact/gap aspects of contact problems. Candidate contact node pairs are linked by what amount to simple truss elements that possess a "bilinear stiffness." These elements are assigned a very high stiffness when the current nodal displacements indicate a closed gap and a very low stiffness when gapping occurs. This method, used in ANSYS[27] and a previous version of MARC,[36] tends to predict physically invalid contact surface overlap when the "stiffnesses" are not optimally tuned to the particular problem at hand. This poor performance led to development of the Lagrange multiplier approach discussed earlier.

Some penalty method concepts have been resurrected in development of a new friction-constraint element that circumvents possible convergence problems often encountered in the Lagrange multiplier friction approach. This feature, contained in the ABAQUS general-purpose nonlinear finite element program[37], retains Lagrange multiplier contact/gap modelling but makes use of a completely new friction approach described briefly in the following paragraphs.

The ABAQUS theory assumes that the frictional shear force magnitude F_T is linearly proportional to the tangential contact surface displacement by a "frictional stiffness" or "stiffness in stick" parameter K_f as long as the frictional shear force is less that the static frictional limit. Because of K_f, the contacting solids behave as if connected by elastic springs that are capable or transmitting frictional force. These "springs" represent, in a gross way, the resistance of the

contact surface to shear force and can be interpreted as the integrated effect of the microscopic asperity interaction occurring in reality. This approach, which allows relative tangential dispacements on the contact surface, is more realistic than the Lagrange multiplier method, which assumes that all such displacements are zero in the adherence regime. A danger exists, however; K_f must be carefully chosen so as to produce neither unrealistic results nor numerical instability problems. This matter is discussed in the analysis section.

The slip condition is defined in ABAQUS by a frictional shear force limit similar to equation 2. Instead of calculating Lagrange multipliers associated with slip, ABAQUS directly imposes the frictional slip constraint on the frictional forces by a so-called "radial return" algorithm.[38]

ABAQUS regards an incremental solution as "converged" when all nonequilibrated (residual) nodal forces resulting from the approximate nature of the piecewise linear solution to the nonlinear problem are within some selected tolerance. This convergence criterion is quite stringent and is particularly amenable to reliable solution of contact and friction problems where the nonlinearities are related to forces.

Although finite element equations for the ABAQUS contact and friction approach are completely developed in vectorial form,[38] some simple specific examples written in matrix form provide additional insight. Lesar of the DTNSRDC Structures Department has prepared such developments for simple examples that parallel two cases described for Lagrange multiplier friction in unpublished notes mentioned previously.

CONTACT CONSTRAINT/CONTINUUM ELEMENT COMPATIBILITY

Both the Lagrange multiplier contact "elements" of MARC and the hybrid Lagrange multiplier-penalty method contact "elements" of ABAQUS are kinematic constraints imposed at specified contact surface node pairs. Both are inherently compatible with all displacement-based continuum solid finite elements of low interpolation order. Such pointwise constraints are, however, incompatible with second-order solids. Additional constraints are needed to enforce compatibility.

The compatibility difficulty can be clarified by considering the simple solid element/contact element combinations shown in Figures 2a and 2b. In a finite element assembly, distributed pressure loads are transmitted from one solid element to another via equivalent nodal forces, which are calculated according to the element's displacement interpolation functions. Low-order elements (4-node axisymmetric,

8-node 3-D solid) will convert a uniform pressure load imposed on one face to a set of equal compressive nodal forces on the opposite face. In Figure 2a, the contact elements transfer these compressive forces to the rigid foundation. Second-order elements (8-node axisymmetric, 20-node 3-D solids) convert this same uniform pressure load to a set of both compressive and tensile nodal forces on the opposite face (Figure 2b, see also reference 39, p. 223). As a result, the contact elements at outer corners are forced to carry tensile load, an obviously unreasonable result that leads to false predictions of gapping at these corner nodes. Similar difficulties arise with tangential displacement degrees of freedom, resulting in invalid frictional force and slip predictions. The advantages offered by higher-order solid elements in modelling complex geometries are lost unless this compatibility problem is remedied.

The simplest cure is to convert the quadratic displacement interpolation functions for contact surface variables to linear functions. The equivalent nodal forces generated by these linear functions will always have the same algebraic sign. Linearization is accomplished by condensing all contact surface midside nodes out of the equilibrium equation system, i.e., by imposing constraints of the form shown in Figure 3:

$$U_z^b = 1/2\ (U_z^a - U_z^c) \tag{3A}$$
$$U_r^b = 1/2\ (U_r^a - U_r^c) \tag{3B}$$

for axi ymmetric elements and

$$U_x^b = 1/2\ (U_x^a - U_x^c) \tag{4A}$$
$$U_y^b = 1/2\ (U_y^a - U_y^c) \tag{4B}$$
$$U_z^b = 1/2\ (U_z^a - U_z^c) \tag{4C}$$

for three dimensional solids.

The MARC and ABAQUS programs contain features allowing easy input of such constraints. However, the local linearization remedy possesses two undesirable features. First, part of the advantage of high-order elements is lost. The removal of midside nodes reduces the number of contact node points. Loss of contact surface variables degrades the attainable accuracy. Second, linearization is

strictly valid only when the contact surface is initially composed of straight lines. In cases of curved geometry, the displacement linearization destroys the smoothness of predicted deflection distributions (Figure 4). This error worsens with greater element arc length and greater contact surface curvature.

The linearization constraint was the only compatibility remedy available when the analyses reported herein were carried out. Compatibility difficulties have been solved, however, through development of a new concept in contact and friction elements for the ABAQUS program. The basis for these new elements is a reformulation of contact and friction constraints into a continuously interpolated form, in much the same manner in which solid element properties are approximated. Fami'ies of first- and second-order "interface elements" for two- and three-dimensional analysis have been devised which interpolate contact and frictional forces with chosen functions that are inherently compatible with first- or second-order two- and three-dimensional solids. The new ABAQUS approach,[38,40] requires use of solid elements with variable numbers of nodes. The extra data preparation price for these special elements is well worth the much improved accuracy and generality which results.

ANALYSIS

VERIFICATION OF LAGRANGE MULTIPLIER METHOD FOR STATIC FRICTIONLESS CONTACT

The normal contact force, gapping, and friction capability of the Lagrange multiplier method has been partially verified in previous work.[22] The MARC program was used to analyze the Hertzian contact of two infinitely long cylinders of equal radius. The predicted contact pressure and internal stress distributions agreed reasonably well with the classical solution (reference 1, pp. 414-420). An interference fit contact of two cylinders with a friction coefficient of .30 was also analyzed. Frictional slip at all nodes resulted from imposition of a sufficient horizontal rigid body displacement on one cylinder.[22]

An elasticity solution of a similar fully slipped contact problem[41] results in an internal stress distribution that is nonsymmetric with respect to the center plane of the contact zone. MARC predicted stress contours which were very similar to the elasticity solution.[22]

Additional comparisons to elasticity solutions were thought necessary, mainly to clear up solid element/contact constraint compatibility issues but also to gain

a feel for the behavior of contact constraints in progressively more complex idealizations of mechanical systems. One such system of interest to the Navy's ship power transmission community is the shrinkfit of a finite length sleeve onto a long shaft. The principal focus of this study is on shaft and sleeve contact problems, the first step being evaluation of MARC solutions for stresses, contact forces, and displacements in two axisymmetric shrinkfit problems which have been treated by elasticity methods.

Axisymmetric Rigid Sleeve and Elastic Shaft Shrinkfit

Case 1. A rigid sleeve of finite length shrunk onto a long, hollow, elastic shaft is analyzed. The contact is frictionless and the shrinkfit is a uniform indentation over the entire contact zone. This elasticity solution[42] is more complete, in terms of calculated results, than many shrinkfit studies. The physical situation and important dimensions of the problem are shown in Figure 5. A schematic of the finite element representation appears in Figure 6. Second-order (8-node) axisymmetric solids were used with linearization of contact surface displacements. The shrinkfit interference is specified as a negative initial gap. A geometric symmetry plane through the center of the contact zone is used to advantage. The boundary conditions of the elasticity solution can only be approximated. The infinitely long shaft cannot be modelled without special "exponential decay" elements (reference 39, pp. 660-664) so a finite shaft half-length eight times the contact zone half-length was chosen. The end of the shaft is assumed to be free to expand; as will be seen, this was an inappropriate assumption. A rotation-free boundary cannot be directly specified at the symmetry plane since rotation degrees of freedom are not available for continuum elements. The standard "roller" boundary condition was used and this effectively eliminated almost all rotation. The finite element mesh is pictured in Figure 7; the finer discretization at the edge of the contact zone (an area of steep stress gradients) is evident.

It should be apparent that this problem could be solved without aid of contact elements - one may well have simply input the shrinkfit as a displacement load. This case served to resolve some side issues relevant to contact modelling. One main thrust of this effort was to see if MARC could produce reasonable stress predictions in a fairly simple shaft contact problem. A second objective was to evaluate the possibility of embedding layers of linear (4-node axisymmetric) elements

within the 8-node element mesh in the contact region. This seemed to be a viable way of achieving contact constraint/solid element compatibility. A third objective was to prove that contact surface linearizations are really needed in a practical problem.

The third issue was settled quite easily by an analysis without linearization, which produced a scalloped indentation pattern instead of the required straight line; an obvious consequence of the algebraic sign problem with equivalent nodal forces. A second analysis used a pure 8-node element mesh and a third analysis contained 4 layers of 4-node elements as shown in Figure 8. Element mixing turned out to be a poor option because linear elements cannot capture steep stress gradients; a typical result being the badly discontinuous integration point stresses shown in figure 9. The mixed mesh solution also resulted in higher computer charges. The element mixing option seemed to be a poor performer and was discarded.

The correlation of MARC results to the findings of Hill et al.[42] is judged to be fair despite two difficulties. First, Hill's numerical results are for an incompressible material with a Poisson's ratio of 1/2. This number can be used validly in finite element calculation only if special incompressible elements are used. Conventional elastic elements with $\upsilon = .49$ were used here. Second, the effect of infinite length may have been better represented with a fixed boundary at the end of the shaft; a boundary free of restraint was used instead. This choice may have produced some disagreement in radial (Figures 10a, 10b) and axial displacements (Figure 11). The predicted trends are, however, correct.

Computed variation of the four stress components with shaft length is compared, for several depths below the contact surface, to the Hill et al. solution in Figures 12-15. The stress curves are "by eye" interpretations of integration point values; no attempt was made to extrapolate and/or smooth them mathematically. The correlation appears fairly good, despite the Poisson's ratio approximation. Preliminary analyses with meshes coarser than the one pictured in Figure 8 showed severe overshoot and oscillation in radial, axial, and hoop stress beyong the edge of the rigid sleeve. This effect was minimized by the finer mesh used to obtain results shown in Figures 10-15.

It must be emphasized that the elasticity solution predicts singular radial and hoop stress at the edge of the contact zone, a typical feature of contact problems containing corner discontinuities. Finite element models require use of

special displacement functions (reference 39, pp. 664-673) when singular stress behavior needs to be accurately simulated. The sharp, finite peaks predicted by MARC are not physically real and there is little hope of predicting the actual stress state in the vicinity of a contact corner unless inelastic deformations are allowed. At this point, it is clear that a truly realistic finite element solution (in terms of stresses) for a contact problem with singularities involves many complicated side issues which were pursued to some extent in the next analysis.

An error in modelling was made but not identified until much later, in that contact elements were specified at both corner and midside node pairs. This should have resulted in a computational error since radial displacements at midside nodes are constrained out of the problem. Despite this, MARC reported compressive forces at all node pairs. A contact pressure distribution can be computed by dividing these forces by areas tributary to the node pairs. This can be done for all node pairs (both corner and midside) individually or by allocating midside node pair contact forces to corner nodes and using tributary areas that are twice as large as in the first case. Both options predict roughly the same pressure distribution. The only significant difference is that the individual node pair option leads to an edge pressure that is twice as large as the midside node pair allocation option. The pressure distribution shown in Figure 16 corresponds to the second (allocation) option. This is believed to be the proper way of interpreting the computed contact forces under the erroneous modelling conditions. Note that these pressures agree fairly closely with the radial stresses at integration points just below the surface (see Figure 12).

In summary, the MARC program proved itself capable of modelling the essential features of a fairly simple shrinkfit problem, although the predicted stress patterns are of questionable accuracy due to boundary condition errors, Poisson's ratio effects, and influence of a contact pressure singularity.

Axisymmetric Elastic Sleeve and Elastic Shaft Shrinkfit

Case 2. An elastic sleeve of finite length shrunk onto a long, solid elastic shaft is analyzed.[43] The contact is frictionless and the shrinkfit, as specified, is uniform; however, in reality it is nonuniform because of the elasticity of both members. The physical situation is shown in Figure 17, and a schematic of the finite element representation with dimensions appears in Figure 18. The modelling scheme, as far

as boundary conditions, shrinkfit loading, etc. are concerned, is exactly as in Case 1 except that dimensions are different and the sleeve must be modelled. The material is taken to be steel ($E = 30 \times 10^6$ psi, $\upsilon = .3$).

This problem is a stronger test of contact element performance. The dimensions chosen correspond to a shrinkfit assembly subjected to fretting tests at DTNSRDC.* This particular assembly was one of a series subjected to cyclic bending tests in an effort to identify key structural, material, and loading variables leading to fretting fatigue failure. (The relation of contact analysis to fretting is postponed to later discussion; the primary purpose here is to discuss contact modelling performance.) This geometry does not correspond to any set of proportions considered by Conway and Farnham[43] but the MARC results can be bracketed by two elasticity solutions. A more comprehensive mathematical shrinkfit study[44] produced results which correspond only to shorter sleeves but are helpful for qualitative comparison purposes.

The finite element mesh used here is shown in Figure 19. It became apparent in Case 1 that a mesh convergence study in conjunction with a smoothing/extrapolation scheme is necessary to get the best attainable estimate of stresses very close to or at the contact surface, subject to limitations implied by the inherent singularity. The mesh convergence issue, although important, seemed less worthy of attention than the stress smoothing question.

It is well known that the finite element procedure based on assumed displacement fields gives continuous and smooth displacement variations but yields stresses that are discontinuous between elements. This mathematical fact of life has been dealt with through many semi-empirical schemes (nodal averaging, extrapolation) for finding smoothed stress fields. Rational means of smoothing have, however, been devised;[45-47] one such method is used here. In second-order elements (8-node axisymmetric, 20-node solids) each stress component local to each element, when integrated exactly, follows a parabolic form. These parabolic forms are, under some situations, fairly continuous from element to element but tend to become badly behaved as stress gradients steepen (Figure 20). Use of "reduced integration"

*These tests were conducted by W. Werchniak of the Ship Materials Engineering Department of DTNSRDC. The results of the tests, herinafter called "DTNSRDC tests," have not been published.

elements (in which variables are integrated inexactly with fewer integration points) is equivalent to a least-squares smoothing of the local element stress field.[47] The smoothed local stresses follow a linear variation between integration points, and smoothed stresses can be found anywhere on an element edge by extrapolation. A fairly realistic estimate of nodal point stress can then be found after additional extrapolation concluded by averaging (Figure 21). This method cannot be claimed as the "best," but it proved both simple and expedient and produced reasonable results in this study.

The MARC displacement predictions are compared, in Figures 22-23, to solutions[43] that bracket the finite element results in terms of nondimensional contact zone size. Both the radial displacement and the percentage of the specified shrinkfit prevented by the shaft fall between the elasticity solutions and follow similar patterns. The nonuniform radial contact surface deflection predicted by MARC corresponds fairly well to the uniform plane strain prediction from the classical Lamé shrinkfit solution.[48] The shaft prevents 85-90 percent of the unrestrained sleeve shrinkage. The finite element results would fall halfway between the bracketing curves if the sleeve length-to-thickness parameter b/h corresponded to the b/h considered by Conway and Farnham. The slightly lower MARC b/h lowers the percentage shrinkfit restraint somewhat. The shaft restraint is greater at the end of the sleeve, so this effect is less pronounced there. Note that even though local displacement linearizations are in effect on the contact surface, the nodal displacements could still be faired into the smooth curves of Figures 22-23. The axial displacements on the shaft surface and inner sleeve bore are shown in Figure 24; this agrees qualitatively with previously cited results.[44] The sleeve bore moves in opposition to the shaft, the shaft expanding outward and the sleeve contracting inward.

The reduced integration/extrapolation smoothing method discussed earlier was used to obtain estimates of radial, hoop, and axial stress <u>on</u> the contact surface. The results of this effort are shown in Figures 25-27. Radial stress estimates are computed from integration points in the sleeve as well as integration points in the shaft. The estimates based on shaft data agree almost perfectly with the plane strain stress prediction[48] and also fall between existing bracketing cases.[43] The sleeve extrapolation is in lesser agreement because the stress gradients are much steeper there, and the mesh is not fine enough to model this gradient

accurately. Two-thirds of the contact zone is essentially in plane strain while interesting edge effects in the form of "wiggles" are evident (the Appendix contains a brief discussion of why these wiggles exist). The singular stress at the sleeve edge is evident. Although the singularity appears much less severe than in the rigid sleeve/elastic shaft case, the stress peaks at the sleeve edge cannot be construed as realistic predictions.

The axial stress behavior agrees qualitatively with other results.[44] The sleeve load causes shaft expansion, which is restrained somewhat by the long shaft beyond the sleeve edge. The resulting compression is counteracted by sleeve tension and shaft tension outside the contact zone. This effect is highly local to the edge, however. Finally, the shear stress extrapolated to the contact surface is essentially zero, as it should be for a frictionless contact.

An evaluation of contact element performance is shown in Figure 28. All contact elements reported a closed condition and bore compressive forces. Since this idealization also had contact elements at constrained midside node pairs, contact pressures were calculated from contact forces by allocating midside node pair forces to adjacent corner node pairs. As in Case 1, this does not seem to have seriously affected the results. The extrapolated radial stresses should approach these calculated contact element pressures in the limit. Figure 28 provides proof that contact element predictions are in good agreement with extrapolated stress, except at the edge of the contact zone. Here, contact elements show a tendency toward a sharp stress peak while extrapolated stresses do not. This is a fault of the solid elements rather than contact elements. The solids do not have the requisite enhancement for modelling singular stress fields.

In summary, the finite element method of contact modelling through Lagrange multipliers worked admirably well in two axisymmetric shrinkfit problems. Inter-element compatibility can be attained by linearizing contact surface displacements. Although many difficult side issues arise when accurate contact surface stresses are desired, the problem can be solved if enough effort is devoted to mesh convergence issues, and smoothing and extrapolation of predicted stresses. Calculated stresses near singularities must be viewed with great caution in such problems.

EVALUATION OF LAGRANGE MULTIPLIER METHOD
FOR 3-D STATIC FRICTIONLESS CONTACT

The methodology of contact modelling is now extended to three dimensions by reanalysis of the axisymmetric elastic shaft/elastic sleeve problem. The primary purposes here are to verify the linearization compatibility enforcement method for higher order 3-D (20-node) elements and to evaluate the effect of a coarser mesh. The modelling scheme, as far as boundary conditions, loads, and linearizations are concerned, is much like Case 2. The shrinkfit radial interference is .001 in. at all contact node pairs, and the material is again assumed to be steel. Reduced integration elements are again used, and contact suface stresses are obtained by the same extrapolation method. Two symmetry planes are utilized, as shown in Figure 29, with the X = 0, Y = 0, and Z = 0 planes fixed against X, Y, and Z displacement respectively. This mesh is very similar to that used in an earlier, independent attempt to analyze the DTNSRDC fretting fatigue test rig with the NASTRAN program.* The original intent was to study the response of this contact idealization to the .0005 in. radial shrinkfit and nonsymmetric loads considered in the NASTRAN analysis, but the MARC program appeared to be prohibitively expensive for this. The NASTRAN work did not consider the frictionless axisymmetric response so the analyses could not be compared, anyway.

The calculated results agree quite closely with those of the axisymmetric model considered previously. Radial displacements predicted by the axisymmetric and 3-D idealizations are compared in Figure 30. The linearizations did not cause any significant circumferential bias; that is, radial displacements at $\theta = 45^{\circ}$ are hardly different from those at $\theta = 90^{\circ}$. The details of edge effect on stresses and contact element pressures differed because of the coarser mesh near the outer part of the contact zone. This effect is seen in Figure 31, in which smoothed and extrapolated nodal averages of radial stress are compared for the axisymmetric and 3-D models. The stress curves shown have been faired through nodal averages based

*The nonlinear effects of contact and frictional slip were treated by successive linear analyses interrupted by analyst intervention. Contact node pairs were first constrained to move together. If contact surface stresses showed that separation or slip should be occurring, appropriate constraints were released and the analysis redone until gaps were eliminated and shear stresses were below or close to the frictional limit. This unpublished work was conducted by E. Schroeder of the Computation, Mathematics and Logistics Department of DTNSRDC.

on shaft integration point data. Although the stress decay beyond the edge of the contact zone is much slower for the coarser 3-D mesh, the essentials of the edge effect are captured and plane strain conditions are correctly approached. Radial stresses based on sleeve extrapolation are different, but it appears that better agreement could be obtained from sleeve mesh refinement; this is evident from Figure 32. Since contact elements were erroneously specified once again at constrained midside node pairs, a special scheme allocating these forces to corner nodes had to be devised (Figure 33). This adjustment resulted in a reasonable contact pressure distribution that agreed quite well with the pressure prediction of the axisymmetric idealization (Figure 34). Not surprisingly, the edge pressures differed substantially due to the different discretization levels. The mistake of retaining contact elements at midside nodes was corrected in later analyses.

In summary, the 3-D analysis results agreed with the axisymmetric idealization results, despite obvious discretization deficiencies. The contact elements performed acceptably well in a 3-D model with higher-order elements when contact surface displacement linearizations were used.

EVALUATION OF LAGRANGE MULTIPLIER METHOD FOR STATIC CONTACTS WITH FRICTION AND SLIP

The Lagrange multiplier method of MARC produced only limited success in modelling frictional contact behavior. Two attempts worked reasonably well; the axisymmetric elastic shaft/elastic sleeve shrinkfit with friction included, and a very coarsely discretized 3-D model of an asymmetrically loaded shrinkfit. MARC failed to produce convergent solutions to a plane stress contact, friction, and slip problem and a more elaborate model of the 3-D asymmetric shrinkfit. These four cases are discussed in the following section.

Axisymmetric Elastic Sleeve and Elastic Shaft Shrinkfit

Case 1. The elastic sleeve/elastic shaft model is reanalyzed with a friction coefficient of 0.15. The problem is completely linear because contact surface shear forces are not large enough to cause slip. As a consequence, all contact node pairs remain in adherence. The only variables affected to any discernible extent by friction were the contact surface axial displacements, the axial stresses, and the shear stresses. In Figures 35 and 36, results for the first two variables

are compared to the frictionless predictions. The relative slip, or difference between shaft and sleeve movement, is less than in the frictionless case, a physically reasonable result. Friction also converts axial stress from a localized edge effect to an effect over almost the entire plane strain zone, a natural consequence of frictional shear constraint on the contact interface. The smoothed integration point shear stresses were so drastically discontinuous from element to element that various efforts to further smooth the integration point data could not produce consistent results. Apparently, the shear stress gradient in the radial direction is so steep that only contact element shear forces are numerically significant. A frictional shear stress distribution was calculated from contact element shear forces in the same manner as for normal contact pressures, by reallocating midside node pairs (Figure 37). Although the trend toward zero shear at the symmetry plane and a peak at the sleeve edge is very rough, Figure 37 looks somewhat like the fully adhered frictional shear predictions for short sleeve/long shaft shrinkfits.[44] The lesson learned is that symmetry boundary contact node pairs should be assigned zero friction coefficient to suppress spurious frictional shear. This correction was made in subsequent analyses. In this case, the frictional shears are very small compared to contact pressures; their ratio is at most of order 1/100, much less than the specified Coulomb slip limit of 0.15. Interestingly, the result of Conway and Farnham's[49] plane strain punch/slab frictional contact study shows that the extent of slip in such a shrinkfit depends only on geometric ratios and not on material properties. It appears that slip would occur in this problem if the sleeve were much shorter.

2-D Friction and Slip Problem

Case 2. The previous case was particularly simple since no frictional slip occurred. In a more thorough test of Lagrange multiplier friction theory, approximate adherence and slip zones for a rigid flat-ended punch indenting a planar elastic slab are calculated by a combined elasticity/numerical method.[49] Conway and Farnham's calculation showed that the adherence/slip zone size depends only on the Coulomb friction coefficient and the punch half-width to slab depth ratio. Although the load in Figure 2 in Conways's work appears as a concentrated force, the unknown contact surface pressures and shears are determined by assuming a uniform indentation over the whole contact zone, a condition forced by the rigid punch. The MARC

solutions were carried out with a Young's Modulus of 30×10^6, Poisson's ratio of zero and a uniform contact surface indentation of .0005 in. The infinitely long slab is approximated by a finite slab with stress-free ends that are free to displace; the affect of a fixed end was found to be negligibly small. The finite element mesh is shown in Figure 38; eight-node reduced integration plane stress elements are used with the usual contact surface displacement linearizations. The Young's Modulus and indentation were varied in some test runs but these variables had no affect on adherence/slip predictions. The MARC calculations covered the friction coefficient range $.10 \leq \mu \leq .60$ for both a/h = 1/4 and a/h = 1/2. The solution strategy was the same as for all previous analyses:

(i) Impose shrinkage in increment "zero," assume zero friction, resolve contact/gapping by iteration, find normal contact forces.

(ii) Impose friction in increment "one," update normal contact forces retaining same shrinkage or indentation, resolve adherence/slip conditions, find tangential contact (friction) forces.

(iii) Repeat (ii) until MARC convergence criteria are satisfied.

The MARC results are summarized in Table 1. The only valid results agreeing with reference 49 were for complete adherence at the largest friction coefficients. None of the other solutions are valid; MARC either repeated a nonconvergent solution or ended up in a slowly convergent iteration loop which, for the lowest friction coefficients, approached a totally invalid result (full adherence where nearly complete slip is the correct answer). Efforts to locate a conceptual error or a modelling blunder were fruitless. This failed attempt led to further investigations of the MARC friction capability.

Primitive Model of 3-D Shaft and Sleeve Shrinkfit with Monotonic Bending

Case 3. The MARC friction capability is now tested in a very coarsely discretized shaft/sleeve shrinkfit subjected to nonsymmetric bending load. The shrinkfit assembly is the same as that treated in the elastic shaft/elastic sleeve problem considered earlier. The finite element idealization is shown, with boundary conditions, in Figure 39. Note that only two symmetry planes can be utilized. The radial shrinkfit interference is .005 in. and the bending load magnitiude is statically increased from zero to 1000 in-lb. A friction coefficient $\mu = .15$ is specified. The dimensions and load parameters pertained to a shrinkfit assembly in DTNSRDC

tests that suffered fretting corrosion damage when subjected to a cyclic 1000 in-lb bending load. This assembly is pictured in Figure 40. (The relation of contact analysis to the fretting experiments is deferred to a later section. It suffices to say at this point that adherence/slip predictions are important.)

Nodal forces equivalent to the bending load are calculated in a preliminary MARC analysis of the shaft alone. The axial deflections corresponding to a 1000 in-lb moment are calculated from a linear elastic beam equation analysis of the shaft. A MARC shaft model is fixed at one end with these axial displacements imposed at the free end. The axial reaction forces reported by MARC at the fixed end are equivalent to the desired moment. The maximum lateral deflection obtained is very close to the simple beam theory prediction. The sign of the moment is immaterial since the shaft is geometrically symmetric about the neutral plane of bending.

After bending moment nodal forces were identified, MARC solutions of shaft/sleeve interaction were carried out. A series of MARC analyses intended to find the load incrementation scheme necessary for convergence showed that nine equal bending moment increments were needed. Convergence could not be obtained for three or six increments. The finite element model is so coarse that calculated stresses have little meaning, but deflections and the frictional behavior of the contact surface are of interest. MARC predicted a maximum laterial shaft deflection of about .00221 in., which agreed closely with .00224 in. predicted by an approximate stepped beam deflection formula.[50] Deflections in the plane of bending showed that the assembly bends as a classical thick beam with noticable shear deflection in the sleeve.

The slip and adherence history is shown schematically in Figure 41. The shrinkfit is slightly relieved on one side and slightly increased on the diametrically opposed side in the plane of bending, a reasonable result. No gapping occurs for any load; the bending moment is not great enough to relieve the initial shrinkfit interference. The ratios of frictional force to normal force and the percentage of shrinkfit restrained by the shaft which are attained at each contact surface node pair are summarized in Table 2 for the equilibrated shrinkfit condition and various levels of bending moment. Frictional slip begins soon after bending load is applied, and the zone of slip spreads somewhat with further application of load. Slip is confined to the upper and lower edges of the contact zone in the plane of bending. This behavior is not unexpected and the MARC friction theory seems to have worked well in this particular case.

Improved Model of 3-D Shaft and Sleeve Shrinkfit
with Monotonic Bending

Case 4. The same modelling techniques used successfully in Case 3 are now applied to the same shaft/sleeve interaction problem with improved discretization in the radial and axial directions. The new finite element mesh is shown in Figure 42. All contact surface displacements are linearized, and contact elements link only the corner node pairs.

The idealization is well-behaved for zero friction and solution for normal contact force for the bending moment range 0-1000 in-lb was easily obtained. The friction analyses failed, however, to approach a reasonable result. All attempts to find load increments small enough for convergence failed due to slow convergence, divergence, or, more commonly, "ping-pong" divergence.* These problems arose when slip initiated at one or more contact surface node pairs. Load increments as small as 1/216 of maximum load (4.63 in-lb) managed to isolate the slip of one node pair at a time but did not eliminate "ping-ponging," which occurred for steps of 1/9, 1/18, 1/36 and 1/72 of maximum load as well. Apparently, at initial slip the first estimates of friction-force to current normal force ratio are so much greater than the coefficient of friction that convergence is impossible no matter how small the load increment. In one interesting analysis, for example, one node pair surpasses the Coulomb limit during a load increment of 4.63 in-lb (1/216 maximum load). MARC wound up in a "ping-pong" loop with the tangential-to-normal force ratio changing from .103 to .547 and back to .103, etc., never coming close enough to the actual limiting value of 0.15.

A thorough check of input by plotting and line-by-line scanning of input data failed to reveal errors or inconsistencies. Consultation with MARC users and developers did not reveal any faults in the problem definition. The unsatisfactory performance of MARC in this case and in the 2-D punch problem prompted consideration of an alternative computer code for frictional adherence/slip behavior. At this time, the ABAQUS code became available for in-house use. It appeared to be worthwhile to try the ABAQUS program, which contains a contact and friction capability.

---

*"Ping-Pong" divergence can occur when an iterative nonlinear equation solution process fails to home in on a unique equilbrium state at the end of a load increment. In the particular cases encountered here, the iterations bounced from one totally different "solution" to another, neither of which fully satisfied force equilibrium or contact constraints.

The contact algorithms of ABAQUS make use of the same Lagrange multiplier approach used successfully in MARC, and the friction agorithms are based on a stiffness method.

VERIFICATION AND EVALUATION OF FRICTIONAL STIFFNESS METHOD FOR STATIC FRICTIONAL ADHERENCE AND SLIP PROBLEMS

The ABAQUS program was applied to the 2-D mixed adherence/slip problem that MARC failed to handle and to the coarsely discretized shaft/sleeve shrinkfit, bending, and friction problem. It produced satisfactory solutions in both cases, which are described in the following section.

2-D Friction and Slip Problem

Case 1. The mixed adherence/slip contact problem[49] is modelled by ABAQUS in much the same way as in MARC. Only the a/h = 1/2 case is considered; the mesh is identical to that seen in Figure 38. The specified indentation, material properties, and dimensions are the same as used in MARC; the same elements (8-node reduced integration plane stress) are used along with the same contact surface displacement linearizations. The one new item of input is the "stiffness in stick" or "frictional stiffness," a parameter discussed earlier in the section on stiffness approaches to contact. This can be interpreted as the ratio of the local contact surface shear force to the local contact surface tangential displacement. However, because this parameter is problem dependent, the rationale for its estimation is not at first obvious. The friction theory's developer says that the proper stiffness to use is the highest number for which a convergent solution is possible.[51] The invalid MARC results for this problem provided ratios of friction force to tangential contact displacement and, with no other guidance available, sufficed as a basis for a parametric study. For $\mu = 0.35$ these ratios fell within the range $3 \times 10^6 < K_f < 5 \times 10^7$ when all contact node pairs are considered. The results of a successful ABAQUS parametric study based on these numbers is shown in Table 3 for $\mu = 0.35$ and Table 4 for $\mu = 0.80$. The upper limit on frictional stiffness K_f is very sharply defined by a convergence limit while the lowest stiffness results in a total adherence condition. Intermediate values produce mixed adherence/slip solutions. Total adherence is not reasonable for $\mu = 0.35$, hence the lower K_f can

be discarded. For $\mu = 0.80$, total adherence appears to be practically the only possible solution, which is somewhat consistent with previously cited findings.[49] Additional mesh refinement and trials are needed to obtain the optimum K_f, but this is hardly worth the effort. Note that for $\mu = 0.80$, the convergence limit is again sharply defined.

From the above two studies, it appears that $K_f = 1.1 \times 10^7$ is adequate; further ABAQUS simulations were carried out with this chosen stiffness parameter for other friction coefficients. Resulting ratios of contact forces are shown in Table 5, and the ABAQUS adherence zone predictions are compared to previously cited research[49] in Figure 43. Although the results are rather approximate because of discretization limitations and the inexactness of K_f, the correct trends are predicted quite adequately.

The stiffness approach to friction modelling requires a frictional stiffness K_f, which may be estimated if some guidance is already available. The difficulty in the stiffness method is to determine a physically reasonable K_f in a completely unique problem. This issue is addressed in the next case.

Primitive Model of 3-D Shaft and Sleeve
Shrinkfit with Monotonic Bending

Case 2. The ABAQUS friction capability is now applied to the coarsely discretized 3-D shaft/sleeve problem shown in Figure 39. The mesh, element type, material properties, and loading (.005 in. unrestrained sleeve shrinkage followed by 1000 in-lb bending load) are the same as before. All contact surface displacements are restricted to linear variations. The friction coefficient is fixed at $\mu = 0.15$, and frictional stiffness is varied in a parametric study to find reasonable K_f limits for this particular problem.

A preliminary analysis of frictionless axisymmetric contact without bending produced normal contact forces within 3.5% of the MARC predictions. The ABAQUS model's maximum lateral displacement was almost identical to the MARC value. Subsequent analysis focused on the frictional stiffness issue.

The behavior of this system with respect to differing K_f is much more complex than in the 2-D rigid punch/elastic slab problem. All contact nodes in the punch problem bear increasing normal forces as the indentation increases. In the 3-D problem, however, some contact node pairs carry increasing normal force while other

node pairs are relieved of load as bending proceeds. Friction forces tend to increase faster than normal forces at points bearing increasing normal load, and normal forces decrease more slowly than friction forces at points where normal load is shed. As a result, slip occurs at both locations. The friction response to this nonproportional loading is clearly sensitive to frictional stiffness choice in some unknown way.

A successful MARC solution to the 3-D problem was available as guidance for the K_f choice. "Frictional stiffnesses" were taken to be the ratio of friction force to relative tangential displacement from the MARC results for the frictional shrinkfit with no bending. All such computed "stiffnesses" fell in the range $1 \times 10^4 < K_f < 5 \times 10^4$. A series of ABAQUS analyses for this range of frictional stiffness at every contact node pair was compared to the MARC results for all loads up to the maximum bending load. A partial comparison of frictional/normal force ratios in Table 6 shows that the solutions compare well initially but diverge as bending load increases. Additional ABAQUS runs at higher K_f showed that the force ratios agreed with MARC results only at higher K_f's, and the K_f's necessary for good correspondence increased with the bending load. An example for one node pair is shown in Figure 44. The MARC approach effectively determines the changing contact surface frictional stiffnesses as load increases; this stiffness apparently changes over orders of magnitude in a highly nonlinear manner. The ABAQUS approach enforces a constant input stiffness. If the guess is too low, as in this case, frictional slip will not be predicted. If the stiffness is too high, slip will occur at too small a relative displacement. The results shown in Table 6 occurred because the initial MARC stiffnesses are too small to predict the slip behavior that occurs as the assembly is bent.

Several preliminary ABAQUS analyses for order(s) of magnitude variations in K_f were needed over the entire range of loads. The results of a lengthy parametric study are partially summarized in Figure 45. ABAQUS predicts practically all possible adherence/slip combinations within the range $1 \times 10^5 < K_f < 1 \times 10^7$. Again, the lower limit is a complete adherence solution. The higher extreme is certainly a convergence limit, as found in the 2-D punch/slab problem, but this particular limit was not determined.

The friction force response of selected contact node pairs for various choices of frictional stiffness is shown, for adherence conditions, in Figure 46 and for

mixed adherence/slip in Figure 47. The simultaneous loading and unloading of contact node pairs and the effect of slip on subsequent frictional response is clearly seen. The interaction of friction and contact forces is indeed an interesting and complex phenomenon.

The load versus calculated relative tangential displacement at an adhering contact node pair and a slipped node pair for $K_f = 2 \times 10^5$ is shown in Figure 48. The nonlinear response to monotonic load is easily explained if the correspondence of the stiffness friction formulation to the White-Besseling model of plasticity[52,53] is recognized. The stiffness theory characterizes the frictional response of an individual contact node pair by two fixed parameters; a "stiffness in stick," or frictional stiffness, and a coefficient of friction. The friction coefficient defines a normal force-dependent limit on frictional force at each node pair. The frictional stiffness is analagous to the elastic modulus and the limiting frictional force corresponds to the yield stress in the elastic-perfectly plastic model of metal plasticity. In the White-Besseling concept, a plastic material "element" exhibiting strain-hardening is characterized by a suitably chosen collection of elastic-perfectly plastic "subelements." The gross "element," composed of many subelements, will exhibit strain-hardening when subject to monotonically increasing load. In the ABAQUS friction theory, the contact surface is characterized by a suitably chosen collection of frictional node pairs, each with a force-deformation law analogous to an elastic-perfectly-plastic White-Besseling "subelement." The nonlinear hardening response seen in Figure 48 is, therefore, not surprising and can be interpreted to demonstrate a "contained plastic flow" of sorts, the "flow" being confined to the contact surface. An interesting, simple contact surface stiffness model explaining experimentally observed[54] dissipative behavior in monotonically and cyclically loaded contacts is found in a journal article by Burdekin, et al.[55] Although the authors utilize nonlinear normal and frictional stiffnesses, they mistakenly characterize the phenomena as being "elastic."

The friction theory is complicated by the fact that the Coulomb limit depends on the current normal force. It is clear, however, that the frictional response at any contact node pair depends on both the normal force and adherence/slip conditions existing elsewhere on the surface. The strong resemblance of this friction behavior under monotonic loading to contained plastic flow at small strains prompts

the question of whether ABAQUS can predict dissipative frictional behavior under fully reversed cyclic loading. This is the focus of further analyses.

The ABAQUS contact/friction model works fairly reliably and is capable of producing physically reasonable results. The calculations are, however, only as good as the chosen frictional stiffness. The above parametric study identified a reasonable K_f range which can only be justified by engineering judgment although one simple theory[55] implies that K_f reflects some measure of contact surface asperity roughness. The lowest K_f for which one node pair slipped in the entire range of loading is 2×10^5, and the lowest K_f for which three node pairs slipped during the shrinkfit is 6×10^5. The low stiffness is easily justifiable since it is quite near the full adherence limit. The high stiffness is more subjective since it is at least two orders of magnitude less than the limiting K_f for convergence, which was never determined here. These two limits were used in a subsequent study of this coarsely discretized system's reponse to cyclic bending loads.

APPLICATION OF FRICTIONAL STIFFNESS METHOD TO A COMPLEX 3-D FRETTING CORROSION AND FRETTING FATIGUE PROBLEM

The previously discussed MARC analyses have verified the Lagrange multiplier method for contact problems, and the ABAQUS analyses have verified the stiffness approach for friction and slip. These contact analysis capabilities have been extended to 3-D problems, and the calculation of stresses near contact surfaces has been proven possible, with some limitations due to stress singularities. The verified and extended ABAQUS finite element capability is now applied to fretting corrosion and fretting fatigue, a complex and difficult class of mechanical engineering problems.

Fretting corrosion is a type of surface damage that results from small periodic relative motions between metal parts that are held together by clamping pressure. Such conditions exist in many machine components that are not intended to undergo relative movement, e.g. bolted or riveted connections, and shrinkfitted shaft/sleeve assemblies. Fretting corrosion can drastically reduce the fatigue strength of machine parts. If it is severe enough, fretting corrosion leads to surface and/or near-surface fatigue crack formation, which can ultimately result in crack propagation into the bulk material and subsequent failure by fracture. Fretting corrosion

damage mechanisms, from a metallurgical and tribological point of view, is fully discussed by Duquette.[56] Both this source[56] and Nishioka, et al.[57] include lists of references on fretting corrosion tests made over the past 40 years.

The study of tribological and material influences on fretting fatigue is very important and constitutes the bulk of related work to date. Experimental evidence shows, however, that fretting fatigue in machine components also depends on macroscopic factors, some of which can be quantified by continuum (structural) analysis. The relative slip amplitude at the edge of the contact surface in pressfitted hub/axle assemblies loaded in periodic (rotating) bending was measured experimentally and reported upon.[57] These experiments showed that the degree of relative slip depends on geometric characteristics (axle diameter vs. hub diameter, hub overhang vs. no overhang). Relative slip increased with increasing shear force and nominal bending stress, implying a dependence on external loads. Relative slip quickly assumed a steady-state variation which persisted for perhaps 1000 cycles but then slowly decreased in amplitude as wear processes began. The slip was found to be independent of the rapidity of cycling and the material's surface hardness. The relation between nominal bending stress and relative slip took the form of a hysteresis loop, indicating the dissipative nature of the friction process. The dissipated energy is partly conducted and/or radiated away from the contact surface as heat. The remaining energy is dissipated in plastic deformation and crack formation local to the contact surface.

The DTNSRDC experiments attempted to define the effects of contact interference, sleeve diameter, bending load amplitude, and number of bending cycles on fretting corrosion damage and fretting fatigue failure in shrunkfit shaft/sleeve assemblies loaded in rotating bending. Fretting damage, when it occurred, was localized to the edge of the shaft/sleeve contact zone. Fretting corrosion showed very little dependence on duration of test or degree of shrinkfit interference. Although fretting damage tended to increase somewhat for larger-diameter sleeves, the extent of damage depended more strongly on bending moment amplitude than any other variable; fretting damage increasing with greater bending moment. The most highly loaded specimens eventually failed by fracture.

Both the DTNSRDC tests and the study of Nishioka et al.[57] indicate, to varying degrees, that fretting damage and relative slip are dependent upon geometry and external loads. These variables can be easily accomodated in a continuum structural

analysis, particularly a finite element method that handles contact and friction. Quasistatic analysis is appropriate since relative slips appear to be insensitive to the rapidity of loading, and the extent of fretting damage depends only slightly on the number of load cycles. The previously observed[57] change of relative slip with cycles is due to wear effects which cannot yet be modelled by finite elements.

The dependence of fretting on loads and geometry implies that the stresses on the contact surface are influential variables. This study has shown that finite element contact analysis methods can be used to determine these stresses. However, sharp contact zone edges cause mathematical singularities which complicate the stress field considerably. If the location of contact surface cracking is known (as it is here) and the degree of initial crack can be characterized, linear elastic fracture mechanics concepts can be used to determine stress intensity factors. These factors can, in turn, be correlated to crack growth rate. Such an approach has been taken in a simple analysis where the stressing is caused by both general structural loading and by local shearing contact stresses.[58] A similar approach is taken for a cracked sheet subjected to predefined normal and shearing "fretting forces."[59] In any case a suitable means of stress singularity representation is required to model the singular stress field due to special corner geometries or existing cracks. The difficulties with singularities detracts somewhat from the utility of correlating calculated contact surface stresses to fretting fatigue failure.

Additional analytical refinements beyond the scope of this study are required to predict fretting fatigue failure; however, the contact analysis method may be useful in predicting fretting corrosion damage. The finite element method is capable of predicting both the location and extent of frictional slip in a monotonically loaded static contact. The method should also be capable of predicting the tangential contact force vs. slip response in cyclic loading. If such dissipative behavior (the referenced hysteresis loops[57]) can be predicted, then the energy converted into plastic deformation and heat generation local to the contact surface can be calculated. The damaging energy is that which cannot be conducted and/or radiated away as heat. Since experimental evidence shows that the fretting process is time-independent (not accounting for wear effects on slip amplitude), a quasistatic analysis seems feasible. Two series of shaft/sleeve analyses under cyclic bending conditions have been completed. It is important to realize that

cyclic bending is not the same mode of loading as the rotating bending conditions in the DTNSRDC tests; this fact is clarified in Figure 49. The finite element predictions quoted in the following sections do not correspond to the real case because load is removed from all points simultaneously in cyclic bending. A zero-loading condition does not exist in the actual experimental mode of rotating bending. Rotating bending requires a full three dimensional analysis, however, without symmetry planes of any kind. This was judged to involve too much sophistication and expense at this point since the effects of mesh refinement and the validity of an assumed frictional stiffness with respect to load level were not sufficiently clear. For these reasons, efforts were confined to the simpler cyclic bending case. All ABAQUS analyses discussed in the remainder of this report concern steel shrink-fit assemblies ($E = 30 \times 10^6$ psi, $\upsilon = .3$) with an assumed friction coefficient of 0.15.

Primitive Model of 3-D Shaft and Sleeve Shrinkfit with Cyclic Bending

Case 1. The response of the coarsely discretized 3-D shrinkfit model to cyclic bending is briefly discussed. Although the predictions for a more finely discretized model are more important, these results demonstrate that the choice of frictional stiffness is important in cyclic friction analysis by the ABAQUS program.

The ABAQUS shrinkfit and bending idealizations for frictional stiffnesses $K_f = 2 \times 10^5$ and 6×10^5 were subjected to several fully reversed bending load cycles using the restart features of ABAQUS. The bending load amplitude was 1000 in-lb. A steady-state condition was reached for both stiffnesses after only a few cycles. The predicted sequence of slip events, normal stress vs. friction stress, friction stress vs. relative tangential displacement, and relative tangential displacement vs. bending load are shown, at the most crucial node pairs, for $K_f = 2 \times 10^5$ in Figures 50-53. Corresponding predictions for the $K_f = 6 \times 10^5$ appear in Figures 54-57.

A fully linear limit cycle is approached for the lower frictional stiffness. All slip eventually ceases and the assembly shakes down to a fully adhered state within just two cycles. The contact surface "hardens" very quickly with this particular combination of variables. The behavior of the higher stiffness system is fundamentally different in that a steady-state slipping cycle is reached after an initial transient. The contact surface does not harden sufficiently to prevent

a steady-state hysteresis loop in which the work done on the system by the bending is dissipated partially by repeated frictional slipping. The behavior for the higher stiffness is much more interesting and probably more representative of freting conditions. The higher K_f behavior is more fully investigated in a shrinkfit model with improved discretization.

Improved Model of 3-D Shaft and Sleeve Shrinkfit with Cyclic Bending

Case 2. ABAQUS analysis of the more finely discretized 3-D shrinkfit model in Figure 43 showed that the major differences in steady-state slip predictions observed in the coarsely discretized model (fully adhered vs. mixed adherence/slip limit cycles) are due more to finite element discretization than to the frictional stiffness. This point is clarified in Figure 58. This figure shows that the frictional stiffnesses producing steady-state, fully adhered and partially adhered conditions in the coarse model (2×10^5 and 6×10^5, respectively) do not predict fundamentally different slip behaviors when the finite element mesh is made finer in the radial and axial directions. Clearly then, when the frictional stiffness is applied to analyze these complex frictional systems, simultaneous mesh convergence and parametric frictional stiffness studies are needed.

The steady-state mixed adherence/slip conditions depend heavily on the bending moment, as shown in Figure 59. In all cases frictional slip was principally confined to the three percent of contact zone length closest to the sleeve edge; however, the results for 1000 in-lb., 666-2/3 in-lb. and 333-1/3 in-lb. maximum bending moment magnitudes indicate that frictional slip becomes more severe and widespread as bending moment increases, a result qualitatively in agreement with the DTNSRDC tests. A rough quantitative comparison of theory and experiment in Table 7 shows that the combination of discretization (36 3-D elements, 15 contact node pairs), frictional stiffness ($K_f = 6 \times 10^5$), and frictional coefficient ($\mu = 0.15$) used in the analyses may have produced pessimistic slip predictions. This illustrates the not unsurmountable difficulty in predicting complex frictional behavior in mechanical systems by a method that requires knowledge of a contact surface stiffness measure that only grossly represents many influential tribological variables.

Figures 60-62 show the relation of frictional shear stress to normal contact stress at the two most highly loaded node pairs for the three bending load levels. The stress behavior at these two points approaches steady-state loops that are identical to each other but 180 deg out of phase. The loops trace progressively smaller excursions in the normal force direction as bending load decreases. In all cases, the steady state is quickly reached after a brief transient period. The decrease in cycle duration spent under slip conditions with decrease in bending load is clearly evident.

The predicted relative tangential contact surface displacements vs. frictional shear stress are shown for 1000 in-lb, 666 2/3 in-lb, and 333 1/3 in-lb moments in Figures 63-65. The displacement vs. stress behavior at the two most highly loaded node pairs approaches hysteresis loops that are identical in shape but 180 deg out of phase. The steady-state loops are quickly approached after brief transients and enclose a larger "area" as bending moment increases. Not unexpectedly, the frictional energy dissipation represented by this hysteretic behavior becomes much more pronounced as bending load increases. The energy dissipated at one node pair per cycle can be determined easily. The shear stress axis can be converted to a force axis by a simple multiplicative factor, and the area enclosed by a single steady-state hysteresis loop can then be calculated. The total energy dissipated on the contact surface per cycle is found by adding the steady-state hysteresis loop areas for all slipping node pairs.

A side issue not explored in this analysis is the effect of shrinkfitting stage analysis method on subsequent response to mechanical loading. All analyses have treated the shrinkfitting as a purely mechanical loading, while in reality the process is both mechanical and thermal. (The sleeve is heated to high temperature and is slipped onto the shaft while thermally expanded. The sleeve shrinks tightly onto the shaft as it cools). This thermal process can be simulated with ABAQUS and will certainly produce initial shrinkfitting and transient cycling response that differs from that presented here. It is believed, however, that the thermomechanical option of shrinkfit modelling and the purely mechanical approach used here will produce similar steady-state frictional behavior.

APPLICATION OF LAGRANGE MULTIPLIER METHOD TO CONTACT/GAP PROBLEMS

The mixed contact/gap analysis capability of ABAQUS has not been exercised in this work. It is currently being applied, in a separate project, to analysis of the interaction of controllable pitch propeller blade components. The ABAQUS results obtained to date seem reasonable and are computed quite straightforwardly as long as contact surface linearization constraints are used. The results of these efforts will be published in a separate DTNSRDC technical memorandum.

POSSIBLE IMPROVEMENTS

IMPROVED CONTACT ELEMENTS

The aforementioned experiences in contact analysis revealed a need for contact restraints that are mathematically compatible with higher-order finite elements. Although this difficulty was circumvented here by contact surface displacement linearizations, such a mathematical artifice detracts from solution accuracy. This problem can be solved once and for all by "interface elements" based on assumed contact pressure and contact surface displacement interpolations that are mathematically compatible with 2-D and 3-D higher-order solids.

A family of such elements has been derived for use in conjunction with first- and second-order solids.[40] These interface elements are based on the concept that the contact surface is a 2-D, geometrically continuous "sheet" of sorts over which pressures and displacements also vary continuously. The conventional isoparametric interpolation method (reference 39, Chapter 8) is used in conjunction with trapezoidal integration over the surface in the first-order case and Simpson Rule integration in the second-order case. In the conventional direct stiffness equation assembly approach, the interpolated interface elements possess elemental contact force vectors that combine to form the global contact force vector. In contrast, pointwise contact node pair constraints possess individual contact force components. Unlike the independent forces of the pointwise contact element approach, the elemental contact force vectors are inherently compatible with both first- and second-order solids. Interface element "strains" are defined as the relative displacements between contact node pairs. These displacements are monitored for contact and gapping. The active node pairs in contact are imposed via the Lagrange multiplier technique while inactive (gapping) node pairs are determined by iteration.

In summary, the definition of the global contact force vector is the one major difference between this new interface approach and the pointwise contact element method used herein. Additional details on the interpolated interface theory and results produced in some simple test cases with the ABAQUS code are given in reference 38. The interpolated interface method performs quite well in simple 2-D and 3-D Hertzian contact test problems.

IMPROVED FRICTION MODELLING

These experiences in friction analysis have shown that the frictional stiffness method is computationally useful and is capable of producing reasonable results. It is not always easy to choose a proper frictional stiffness. The widely varying results produced by different finite element discretizations with the same frictional stiffness suggest that frictional stiffness is a problem-dependent parameter as much as a material property parameter. In addition, the relation of this stiffness to tribological conditions is vague and has physical meaning only in the sense of the resistance of surface asperities in shear. An effort has been made to identify a promising new approach for metallic friction based on experimentally definable variables that better reflect the resistance of contact surfaces to deformation. One such method[38] is briefly described in the following paragraphs.

This new approach to contact is called "Critical State Theory" (CST) which refers to a mathematical model for soil mechanics from which it borrows some concepts. CST abandons the mathematically convenient Lagrange multiplier artifice for normal contact in favor of a nonlinear normal pressure-normal strain relation. This relation produces experimentally observed "hardening" and "softening" behavior through a pressure-dependent nonlinear stiffness. The gradual approach of contact surface asperities during loading and the gradual separation of asperities in unloading is well represented by the mathematical "hardening" and "softening" behavior. The stiffness in shear is represented by a conventional shear modulus which utilizes the nonlinear normal pressure-normal strain relationship instead of the usual elastic modulus. The shear behavior is thus coupled to the normal behavior and reflects a hardening shear stiffness with increasing normal pressure. This relation represents, in a gross way, the increasing asperity resistance to shear loading that occurs with increasing clamping pressure. Since they are valid in the sub-slip

range, where all strains are recoverable, the normal and shear stiffnesses just discussed are nonlinear but elastic. Both of these stiffness formulations are thus meaningful in a tribological sense and are explicitly defined in terms of experimentally obtainable variables.

The CST approach for frictional slip strongly resembles classical strain-hardening flow theories of plasticity. Some features of plasticity theories are assumed in the definition of slip displacements; namely, strain rate decomposition, associated flow, normality rule, and the yield surface concept. The hardening rule is a form of combined isotropic and kinematic hardening in which the size and orientation of the "yield" (in this case, slip) surface depends on the current relative tangential strain. The slip surface represents a critical intensity of contact surface shear and normal forces at which slip initiates and continues. The extent to which the classical Coulomb friction limit (analagous to perfectly plastic flow) is reached depends on the hardening parameters. The "plastic strain" components, calculated by conventional normality and associated flow assumptions, represent nonrecoverable contact surface displacements that occur under slipping conditions. These "plastic strains" are, in a sense, tribologically real because slip occurs when contact asperities are grossly (plastically) deformed and forced over one another by shear loads. The geometric scale of this predicted frictional plasticity is correctly confined to the contact surface. The CST frictional slip formulation is also capable of producing the energy dissipation by hysteresis observed in cyclically loaded frictional systems.

In summary, the CST concept[38] defines contact surface behavior in meaningful tribological terms rather than relying on mathematical conveniences. This theory is one step toward a rational description of interface behavior in "constitutive equation" terms and shows promise as a basis for further generalization toward certain kinds of lubricated contacts.

SUMMARY AND CONCLUSIONS

This work has verified, extended, and improved finite element methods for solution of several classes of dry contact problems in solid mechanics. The class of problems treated can be categorized as follows:

(1) Dry contact, no lubrication

(2) Static contact, no dynamic impact effects

(3) Monotonically and quasi-static cyclically loaded contacts

(4) Elastic material behavior

(5) Small displacements and strains

(6) Frictionless contacts and contacts with Coulomb friction under both adherence and mixed slip adherence conditions

(7) Full contact (Mixed contact gapping has been treated in a separate effort)

The contact analysis capabilities of the MARC and ABAQUS programs have been verified by comparison of elasticity solutions to computed responses of contacts with and without friction. The Lagrange multiplier method of MARC and ABAQUS handles the normal contact problem quite satisfactorily. The stiffness method is best suited to the friction problem. Because the ABAQUS program follows these two approaches, it is recommended as an analytical tool for unlubricated contacts.

The existing ABAQUS capability has been extended to modelling with higher-order elements and has been applied to problems that must be posed in three dimensions. The current method of modelling with higher-order elements is somewhat deficient because of limitations imposed by necessary compatibility restraints. The new contact modelling concept of reference 41 could not be evaluated in this work, but preliminary tests have shown that it will effectively eliminate contact constraint/higher-order solid compatibility difficulties.

ABAQUS has been applied to a 3-D contact problem which represents most features of a fretting corrosion and fretting fatigue test apparatus. The results obtained for this study demonstrate that the complex contact and friction interaction occurring under fretting conditions can be modelled mathematically. The contact surface energy dissipation and the portion of dissipated energy leading to surface damage can be calculated by finite element methods.

Despite its limitations, this work has verified advanced methods for analyzing unlubricated mechanical contacts and has extended the analysis capability to a level that is useful in complex practical problems.

TOPICS FOR FUTURE WORK

This experience has demonstrated that there are many "side issues" peculiar to certain dry contact problems which can only be resolved after prolonged effort.

These side issues were not thoroughly treated in this work, but they can be considered as open topics worthy of further research.

(1) If singular points exist in the stress field due to sharp corners or cracks, computed stresses will not be realistic in the vicinity of the corner or crack unless the singularity is explicitly modelled. Such stress concentrations may also cause material nonlinearities in the form of plasticity. All of this will have some effect on contact surface behavior.

(2) The effect of element size and disposition on the convergence of displacement and stress predictions toward some "actual" result should always be examined in finite element treatments of nonlinear problems. This issue could not be fully treated in the many test and evaluation cases of this study. Although 20-node solids are monotonically convergent in themselves, convergence of an entire solid element-contact element system in the presence of singularities (if any), contact surface constraints (if any), and plasticity (if any) is not guaranteed and should be checked.

(3) Matters are not simple if stresses very near the contact surface are of interest. Extrapolation of integration point stresses proved useful in this study, but there is no single foolproof way to interpret the discontinuous stress fields that naturally occur in displacement-based finite elements. Alternate means of calculating surface stress should be evaluated. One useful alternative may be hybrid finite elements, which are mathematically constructed to predict continuous stress fields. Hybrid elements also converge faster than displacement-based elements in zones adjacent to a singularity.[60] Some very recent contact analysis work in this direction has been accomplished.[61]

A more fundamental problem involves unlubricated interface modelling. The contact and friction behavior of interfaces has been simulated by necessarily simple mathematical conveniences (Lagrange multipliers and/or constraint equations), but such models are somewhat artificial. In many cases, such approximate models can capture the essentials of contact interface behavior, but this holds true only in cases where friction stresses are limited by the Coulomb theory. In particular, although the stiffness approach to friction is computationally successful, a frictional stiffness characteristic that in some way reflects surface roughness is required. The computed results will depend on the chosen stiffness, and there seems to be no clear way of correlating this number to actual surface characteristics.

There is a need for experimentally definable contact surface friction models, expressed in terms of finite element constitutive equations, that more directly account for surface roughness. Some possible first steps in this direction have been discussed.[38,62]

The finite element method is a very powerful analytical tool and offers promise for treatment of even more complex interface problems in machines and machine components. An example of some advanced dry contact work is a finite element simulation of transient thermoelastic contact with wear effects.[63] Lubricated contacts are another important class of problem; much work has been done in developing finite element methods to determine pressure distributions and load capacities for complex bearings operating in fully lubricated conditions.[64-68] For highly loaded bearings or certain bearing pad materials, the bearing pad deformations are as important an effect as the lubricant behavior. Finite element methods have been used to calculate pressures, film thickness distributions, and maximum load capacities of bearings under elastohydrodynamic conditions.[69-71] Finally, finite elements have been applied to lubricated contacts in which thermal effects are important.[72] It appears that well-defined numerical methods exist for analysis of geometrically complex, fully lubricated contacts for a variety of conditions. Although lubricated contacts are very important in naval machinery applications, such problems require analytical approaches which in no way resemble those considered herein for dry contact. Finite element treatment of such problems would require completely new efforts.

Finally, the problem of partially lubricated contacts (boundary lubrication) is much more complex than dry or fully lubricated cases. None of the dry contact methods considered here or the lubricated contact approaches listed above are appropriate. Application of finite elements to boundary lubrication first requires a statement of the problem in fundamental mathematical terms. Such mathematical statements must reflect observed relationships among important variables, which can only be defined through experimental effort. Even so, finite elements may not be the most effective technique for analyzing boundary lubrication problems.

ACKNOWLEDGMENTS

The author acknowledges the efforts of Dr. Paris Genalis, formerly of DTNSRDC, who conceived this project and provided guidance in the early stages, and Dr. Dave

Hibbitt and colleagues, of Hibbitt and Karlsson Inc., who modified the ABAQUS program for easier and rationalized contact and friction modelling. Dr. Hibbitt has also provided instructive insight into the frictional behavior of mechanical systems.

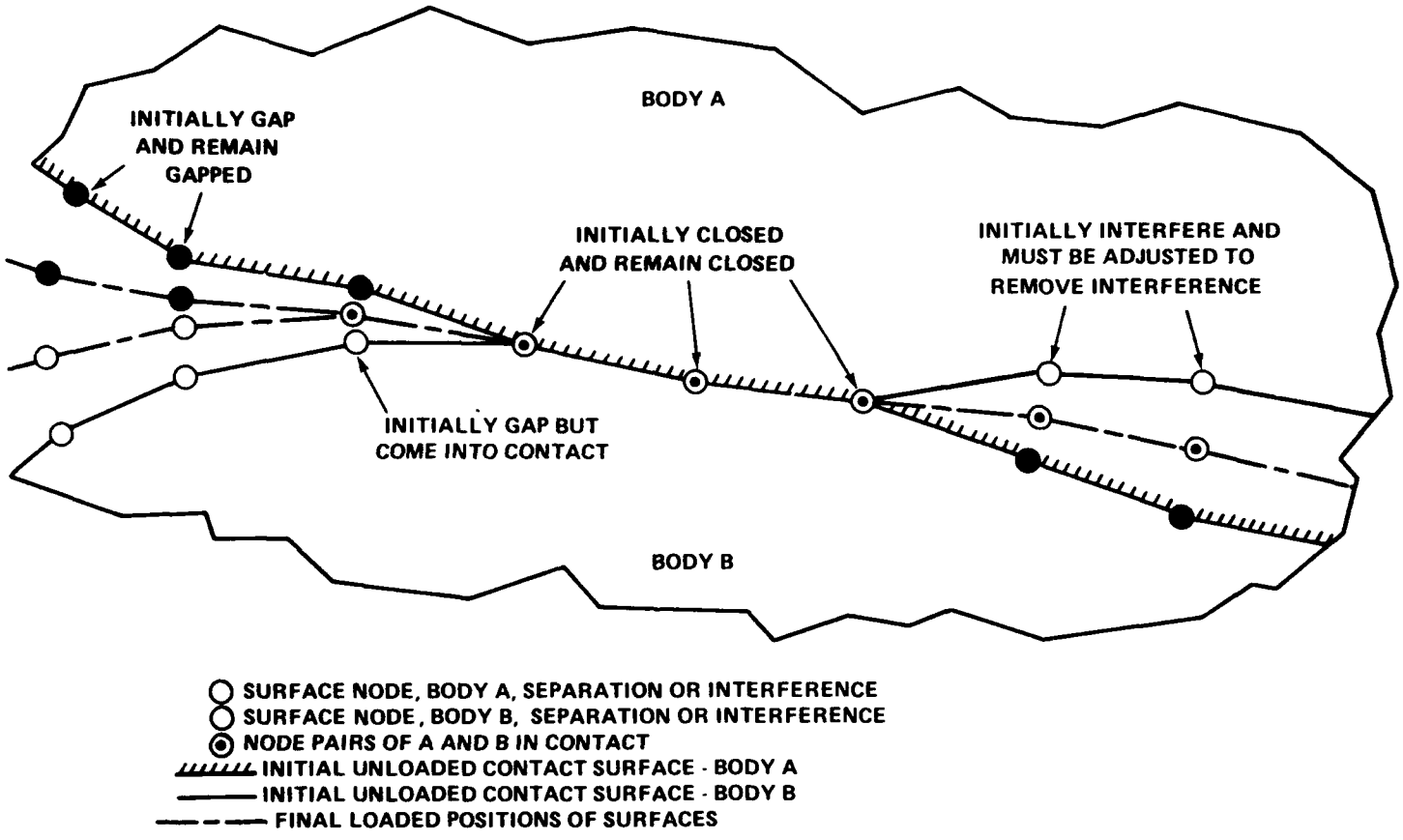

Figure 1 - Contact Surface Node Pair Configurations

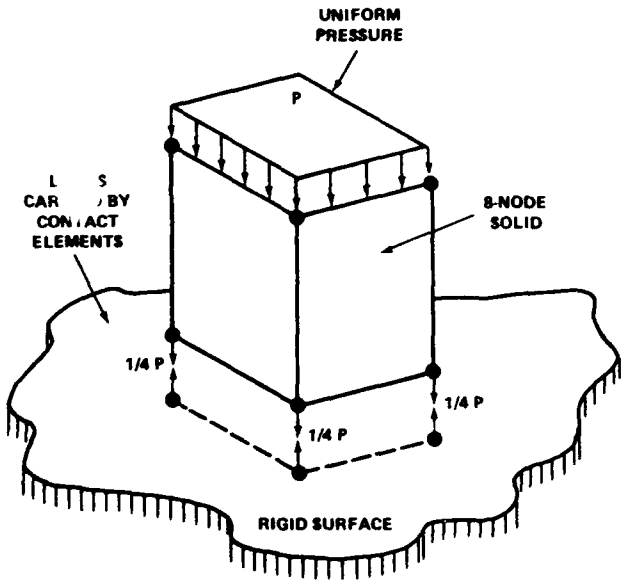

Figure 2a - 8-Node Solid

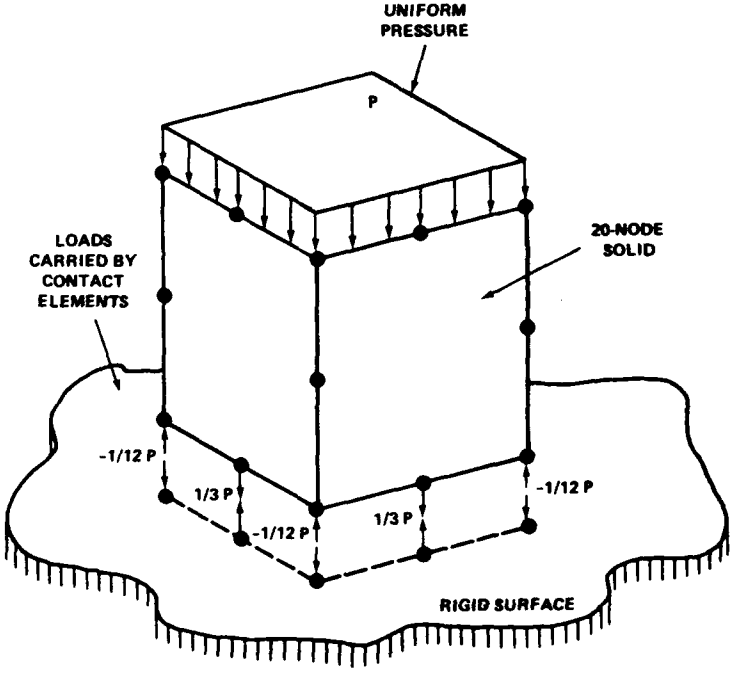

Figure 2b - 20-Node Solid

Figure 2 - Contact Forces Resulting from Uniform Pressure on One Face of Rectangular 3-D Solids

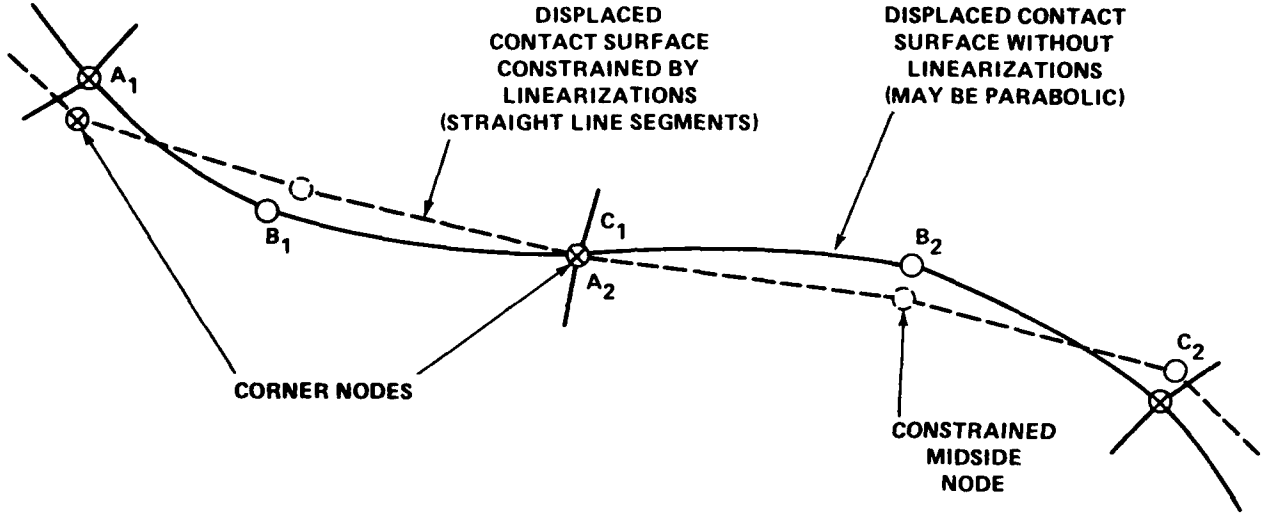

Figure 3 - Contact Surface Compatibility Linearizations

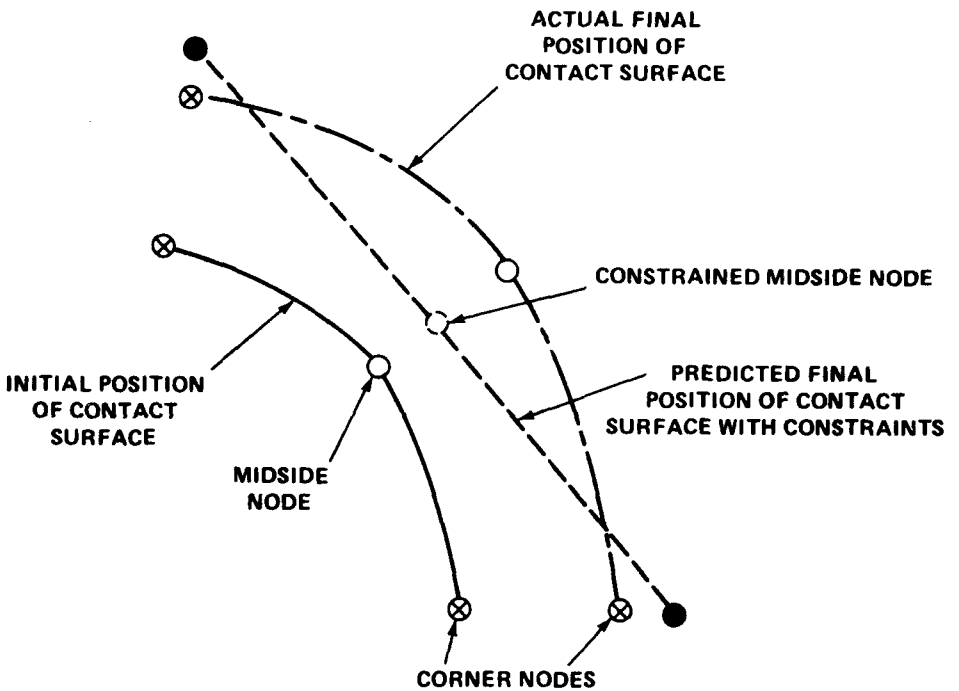

Figure 4 - Distortion of Predicted Contact Boundary Due to Compatibility Linearization

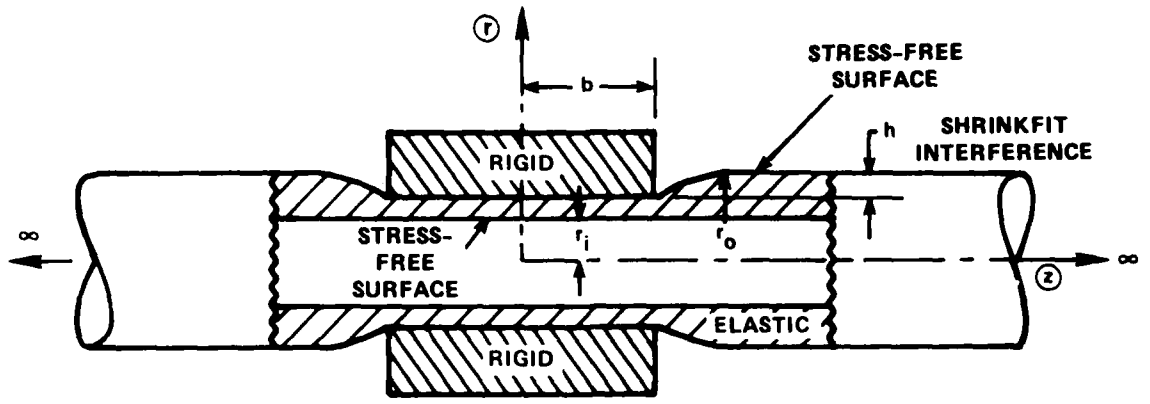

Figure 5 - Elastic Shaft/Rigid Sleeve Contact

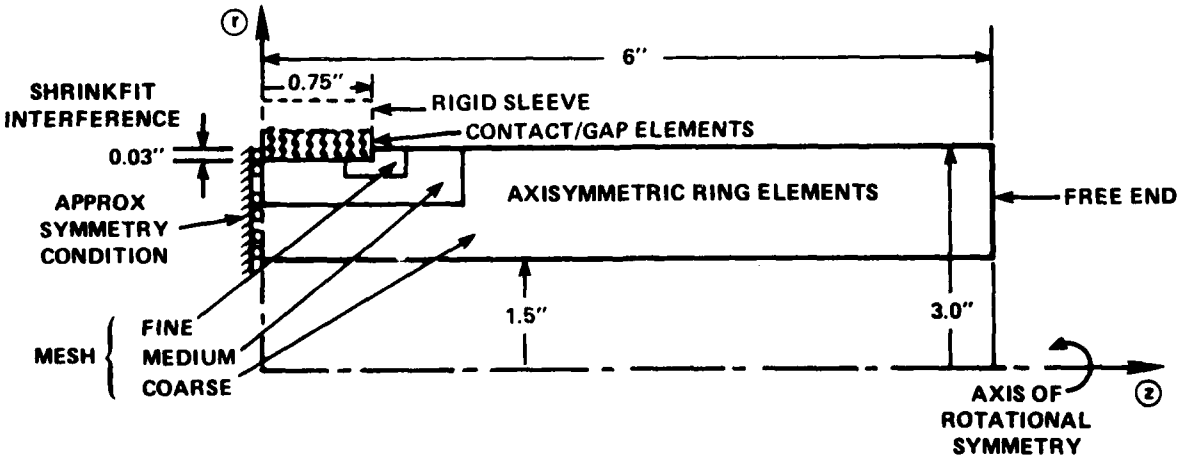

Figure 6 - Finite Element Representation of Elastic Shaft/Rigid Sleeve Contact

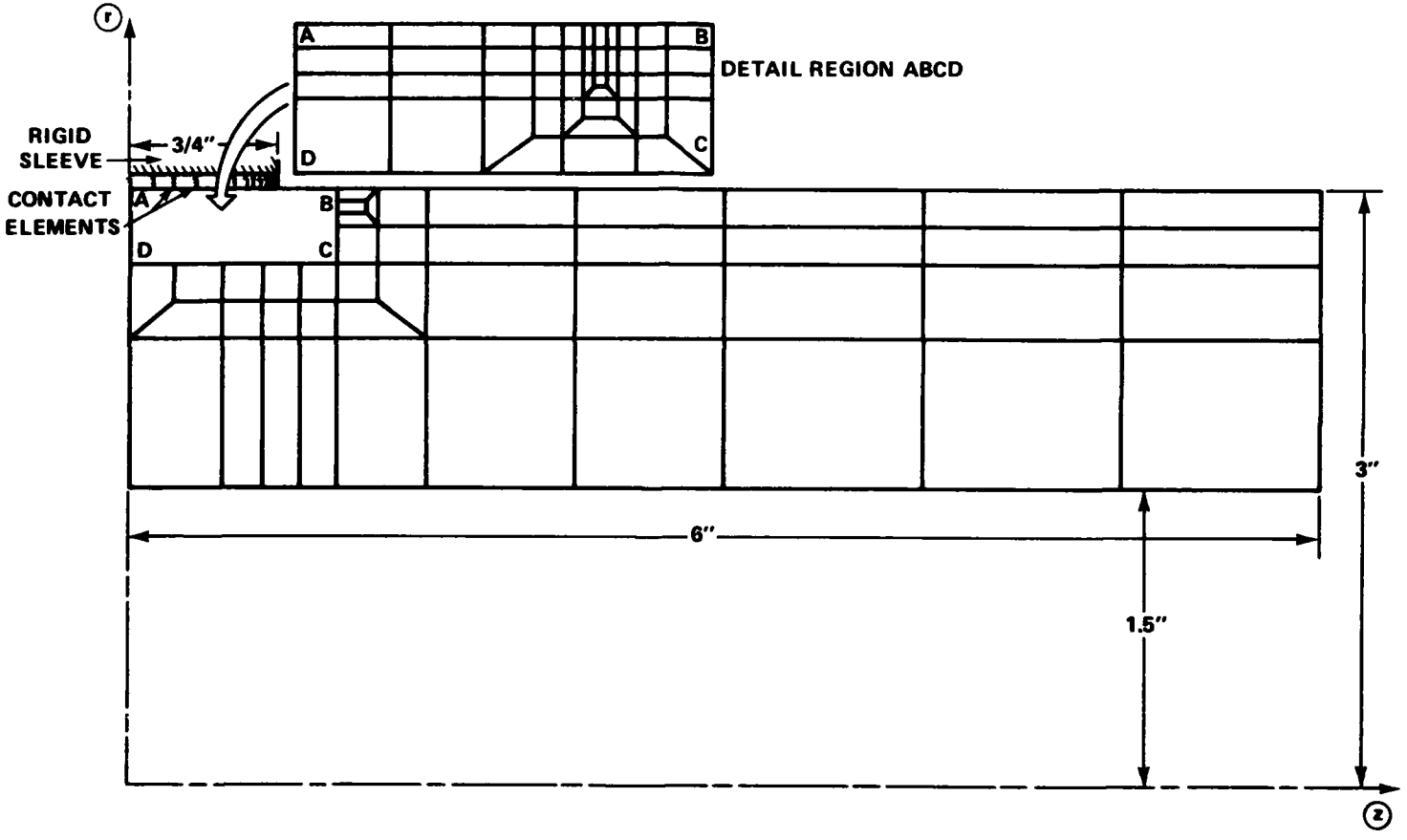

Figure 7 - Finite Element Mesh for Axisymmetric Elastic Shaft/Rigid Sleeve Contact Problem

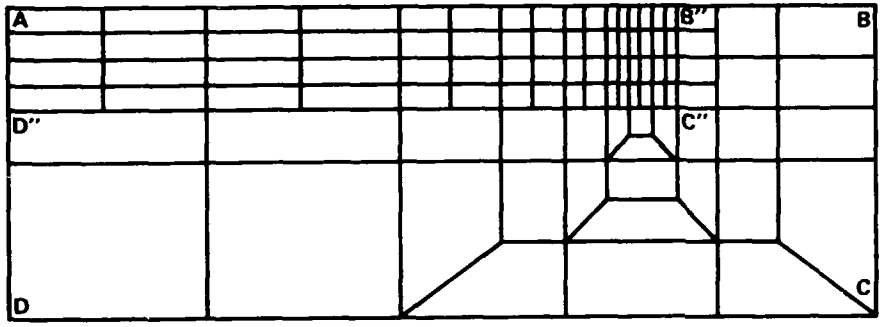

ONLY DETAIL OF REGION ABCD OF
FIGURE 7 SHOWN
TYING CONSTRAINTS ON BOUNDARY $\overline{A\ B''C''D''}$
8-NODE RINGS IN REGION A B''C''D''

Figure 8 - Mixed 8-Node and 4-Node Finite Element Mesh for Axisymmetric Rigid Sleeve/Elastic Shaft Problem

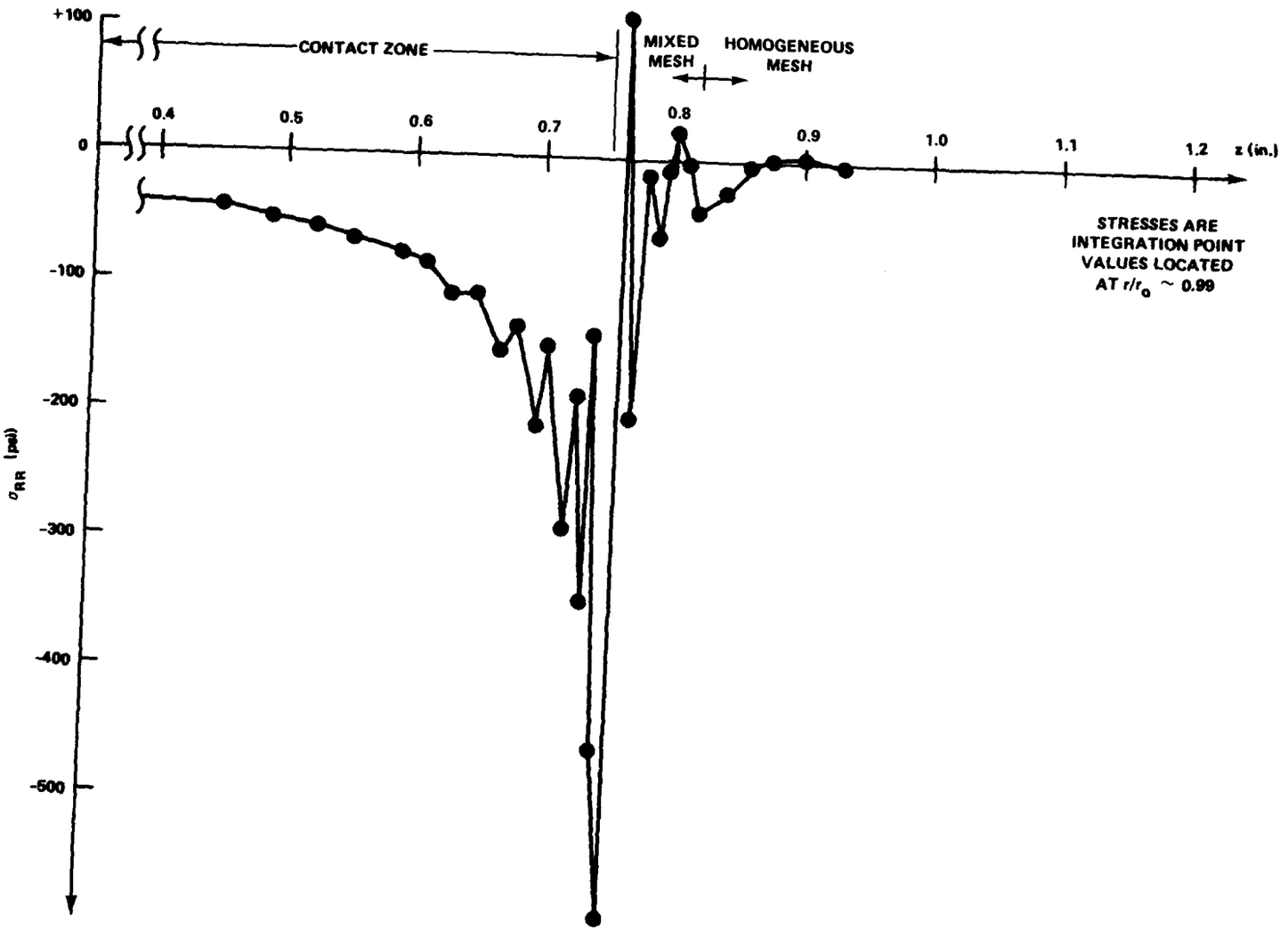

Figure 9 - Radial Stress Near Shaft Surface, Mixed 8-Node and 4-Node Element Mesh

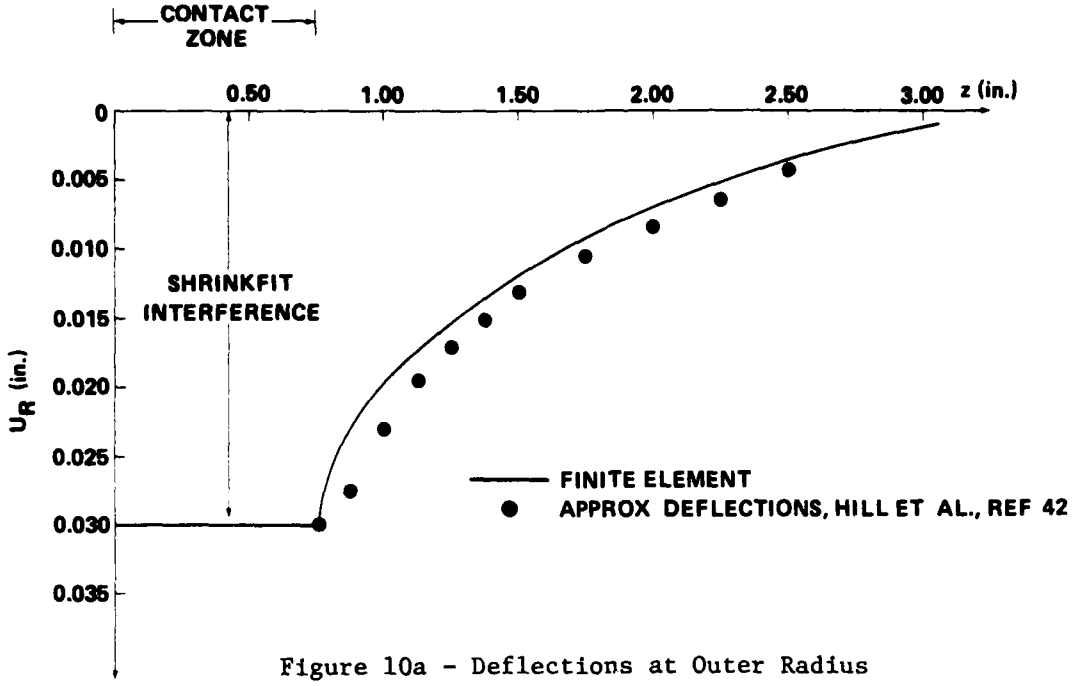

Figure 10a - Deflections at Outer Radius

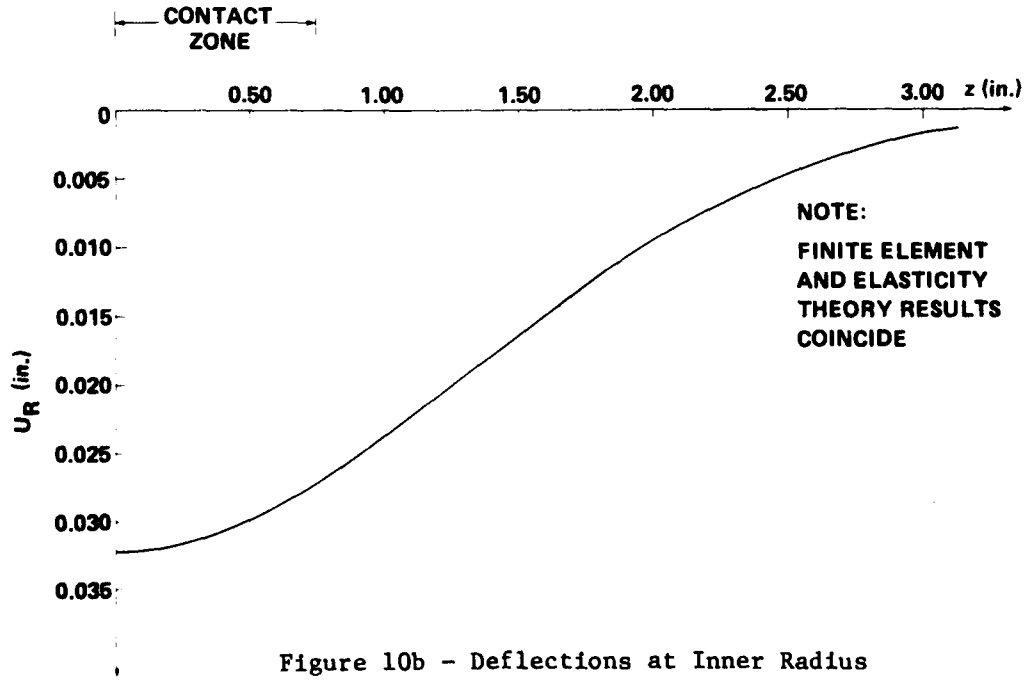

Figure 10b - Deflections at Inner Radius

Figure 10 - Elastic Shaft/Rigid Sleeve, Radial Shaft Deflection Predictions

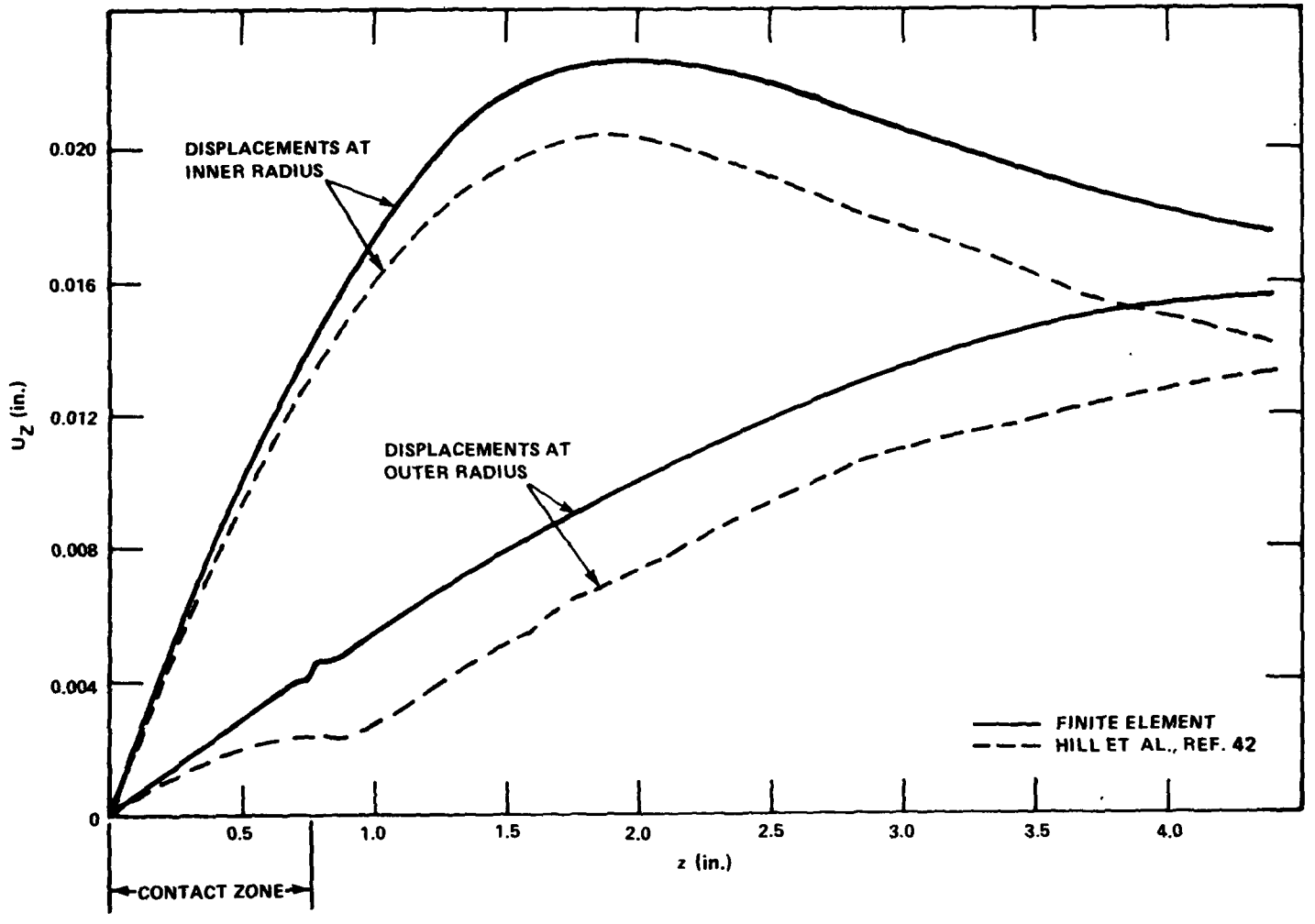

Figure 11 - Elastic Shaft/Rigid Sleeve, Axial Shaft Deflections at Inner and Outer Radii

Figure 12 - Elastic Shaft/Rigid Sleeve, Radial Stresses Near Contact Surface/ and in Shaft Interior

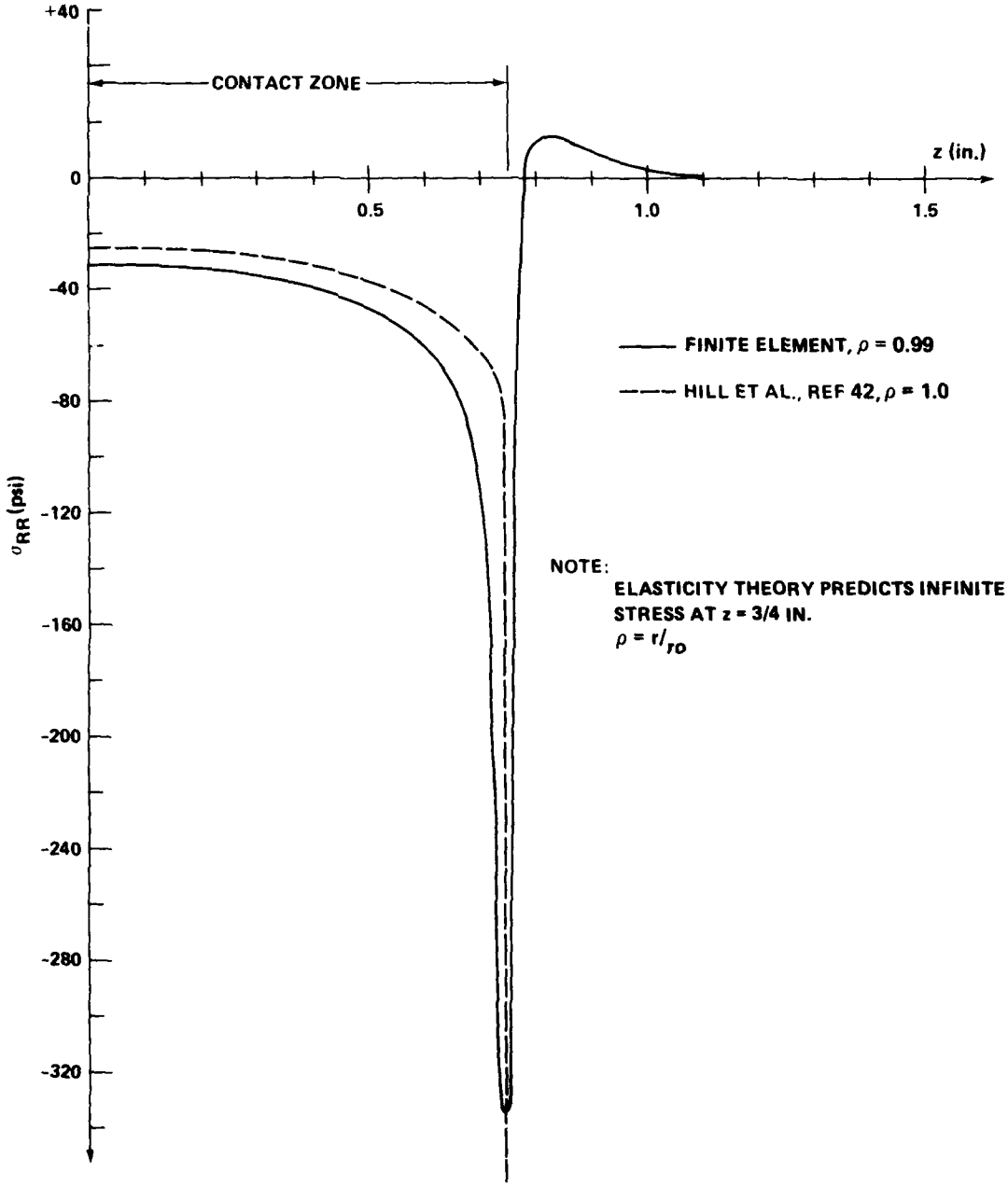

Figure 12a - Radial Stresses Near Contact Surface

Figure 12 (Continued)

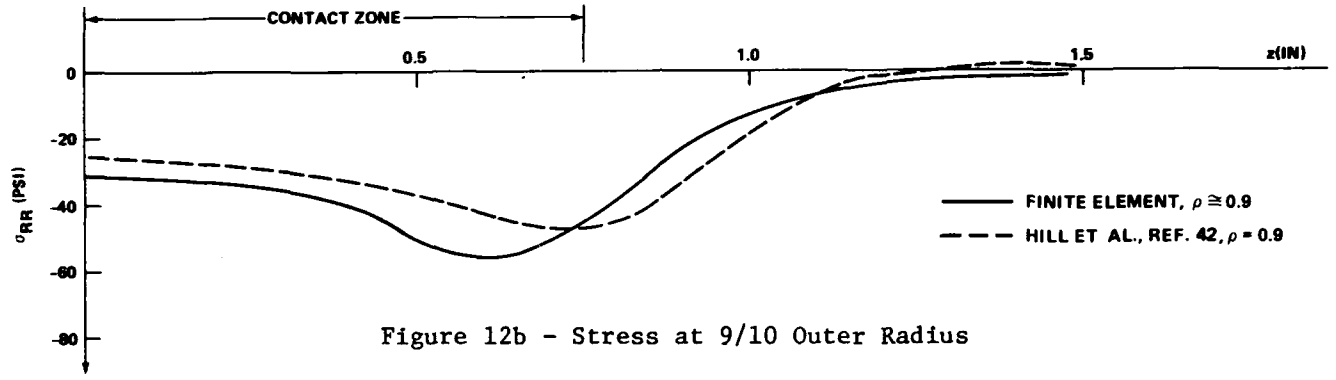

Figure 12b - Stress at 9/10 Outer Radius

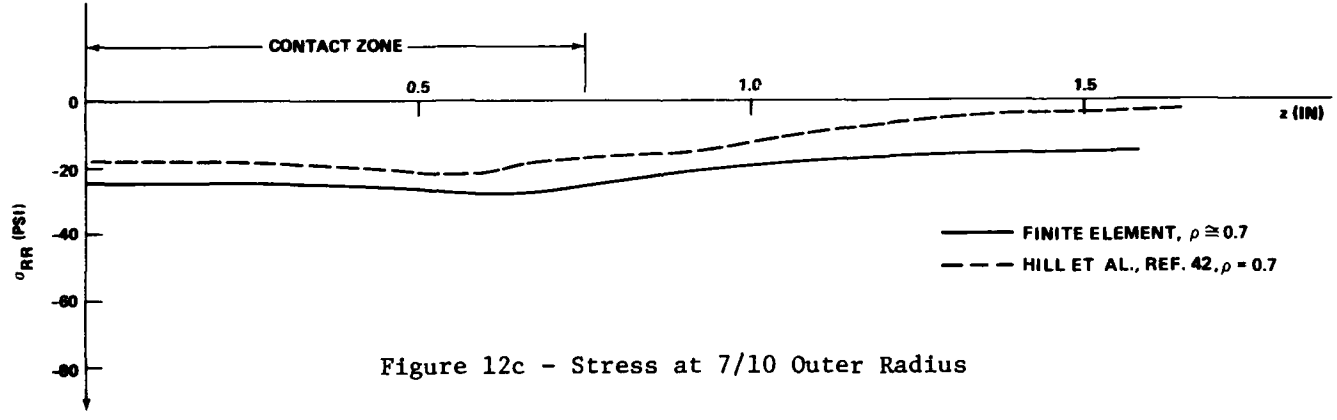

Figure 12c - Stress at 7/10 Outer Radius

Figure 13 - Elastic Shaft/Rigid Sleeve, Hoop Stresses Near Contact Surface and in Shaft Interior

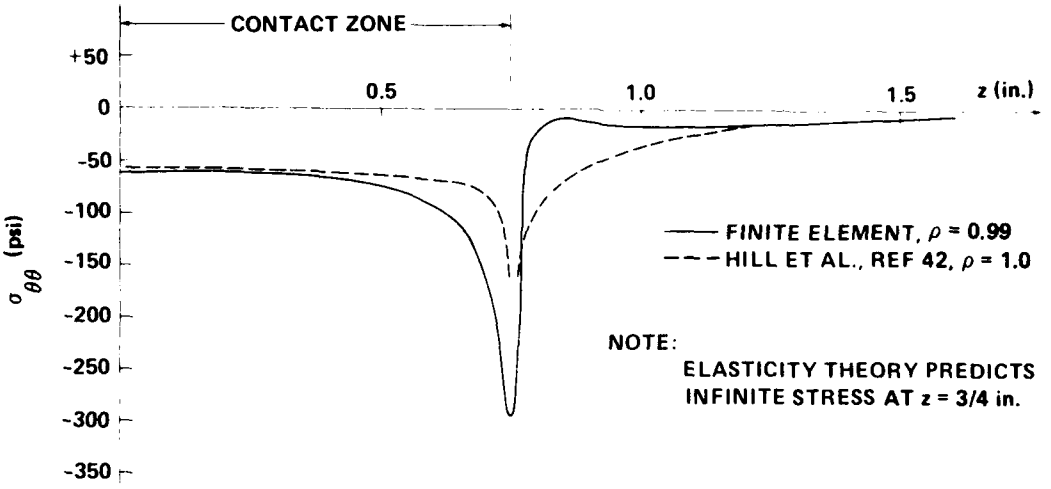

Figure 13a - Hoop Stress Near Contact Surface

Figure 13 (Continued)

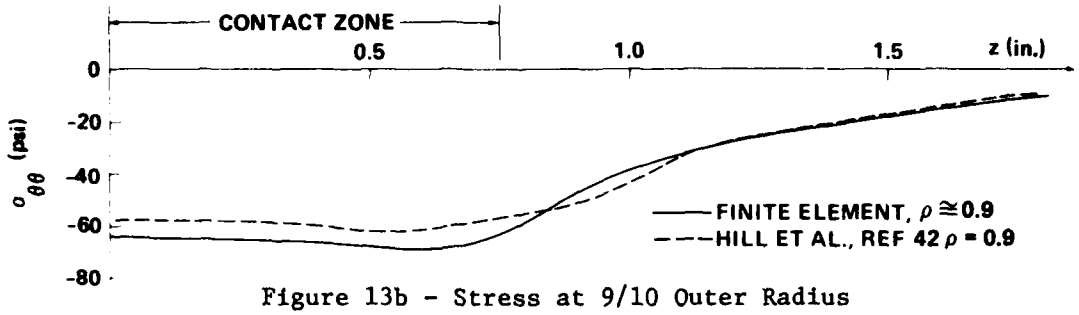

Figure 13b - Stress at 9/10 Outer Radius

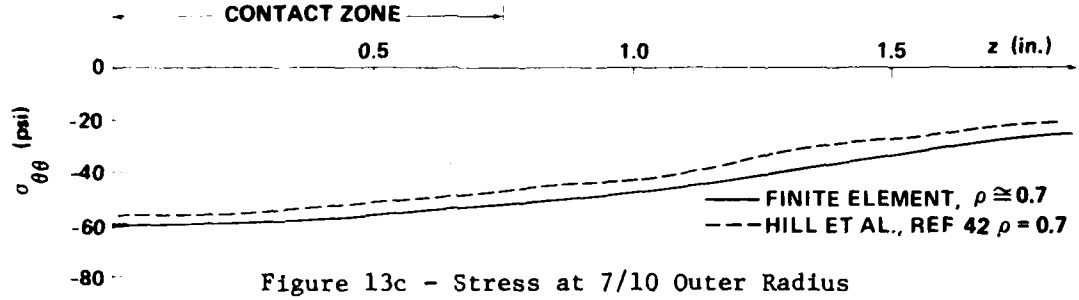

Figure 13c - Stress at 7/10 Outer Radius

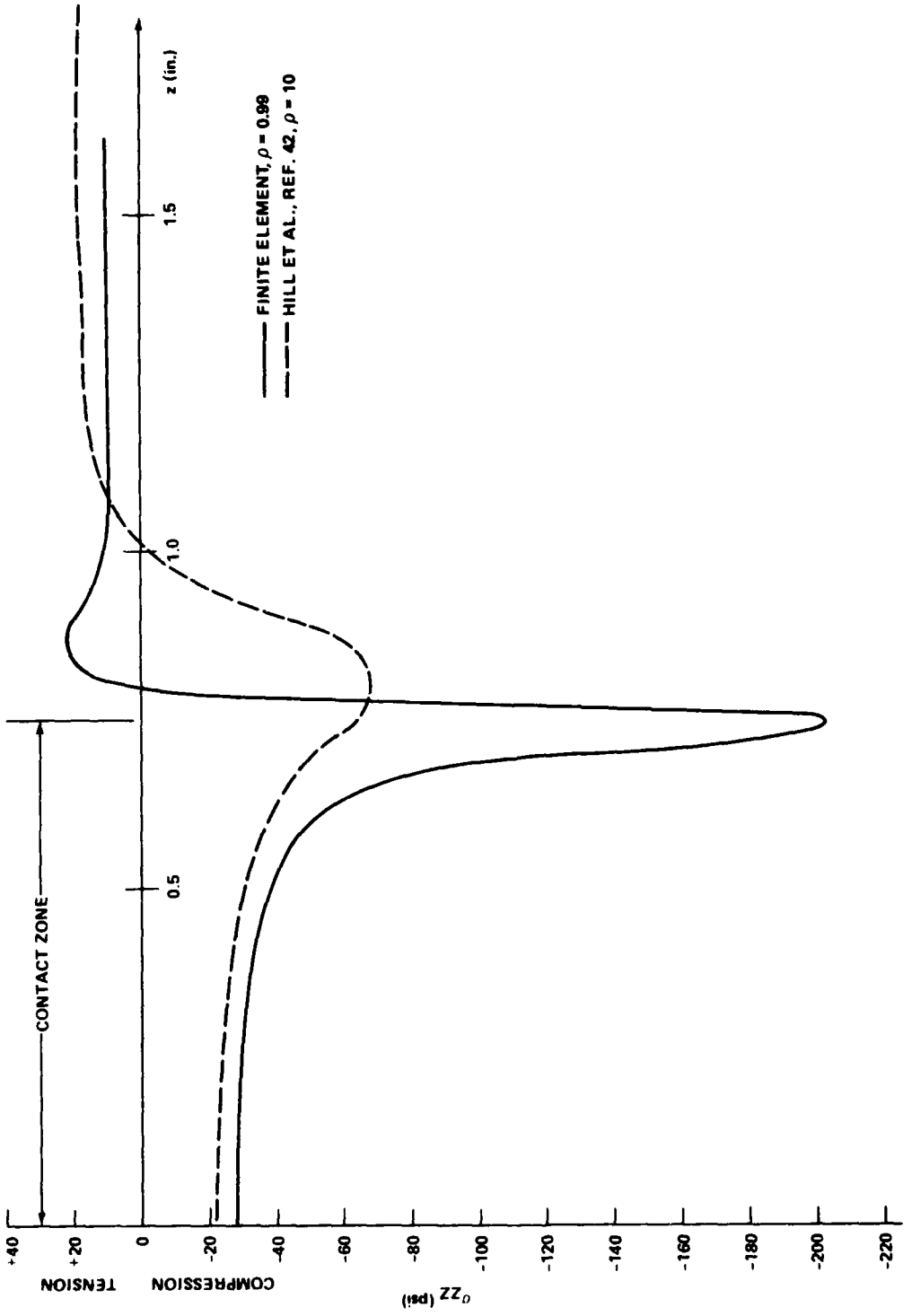

Figure 14 - Elastic Shaft/Rigid Sleeve, Axial Stress Near Shaft Surface

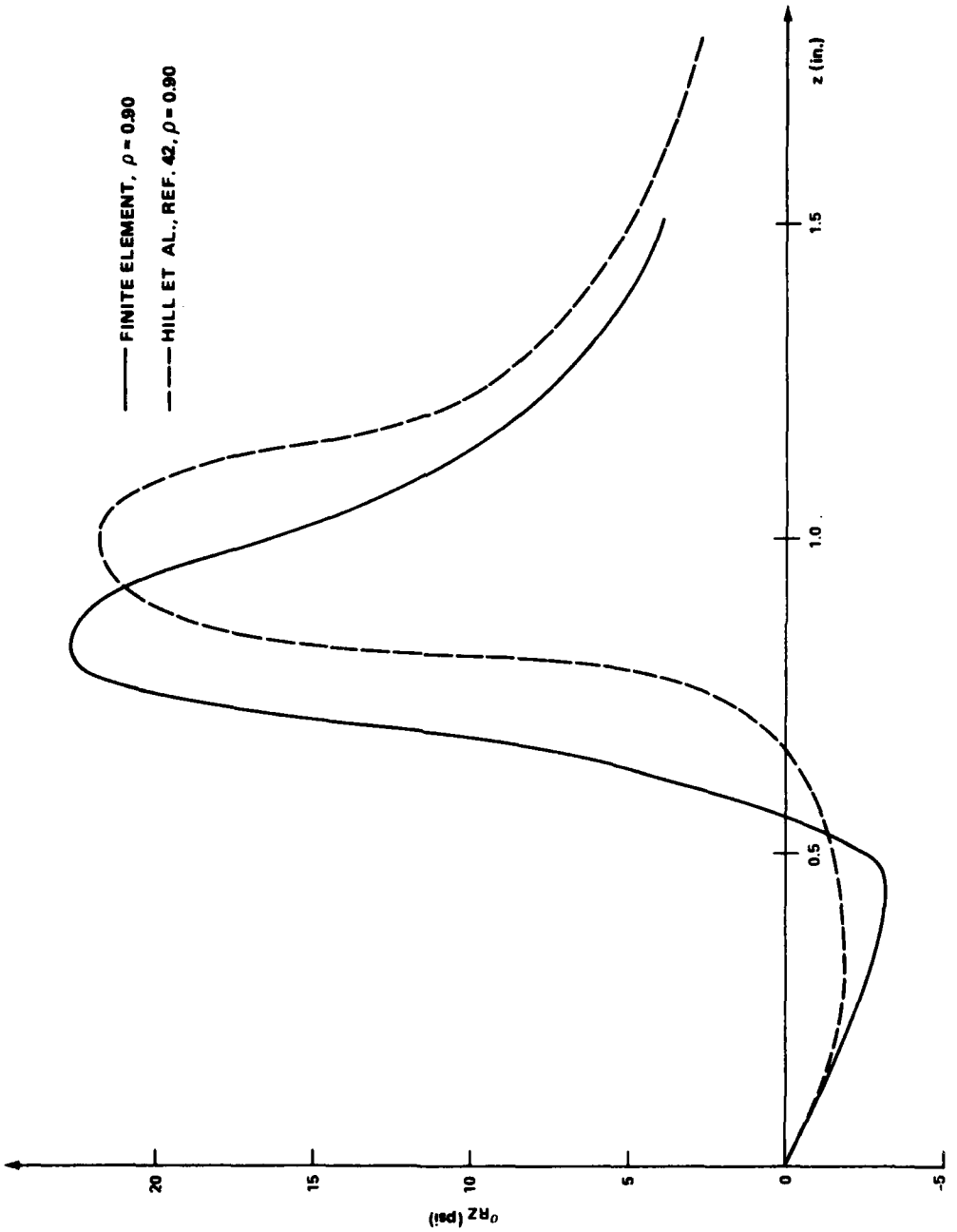

Figure 15 - Elastic Shaft/Rigid Sleeve, Shear Stress in Shaft Interior

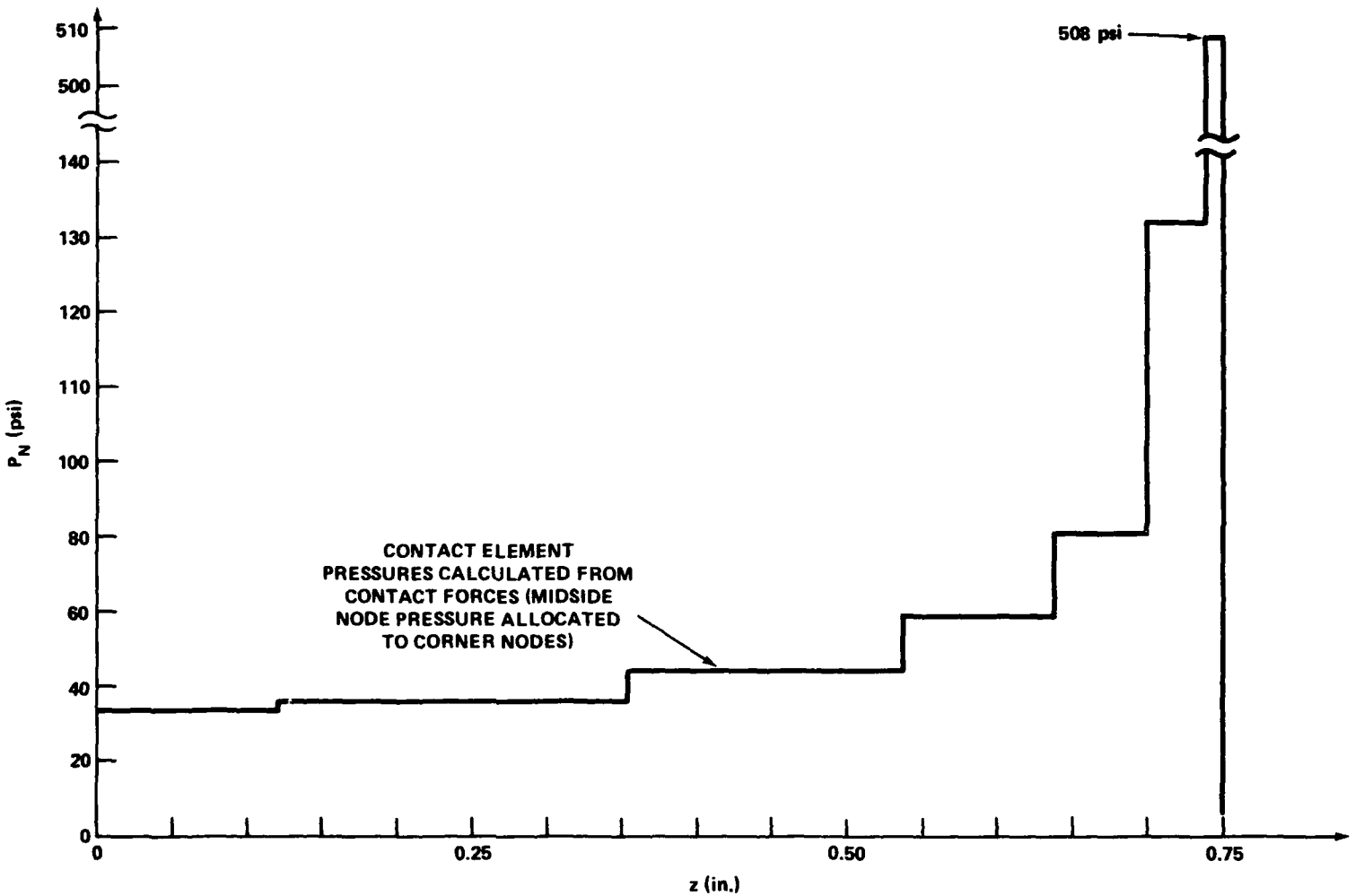

Figure 16 - Elastic Shaft/Rigid Sleeve, Contact Element Pressures

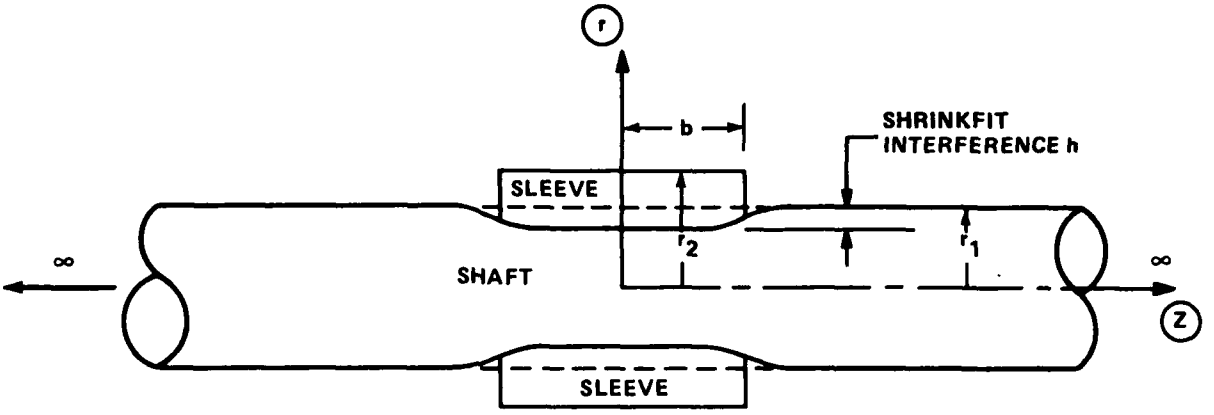

Figure 17 - Elastic Shaft/Elastic Sleeve Contact

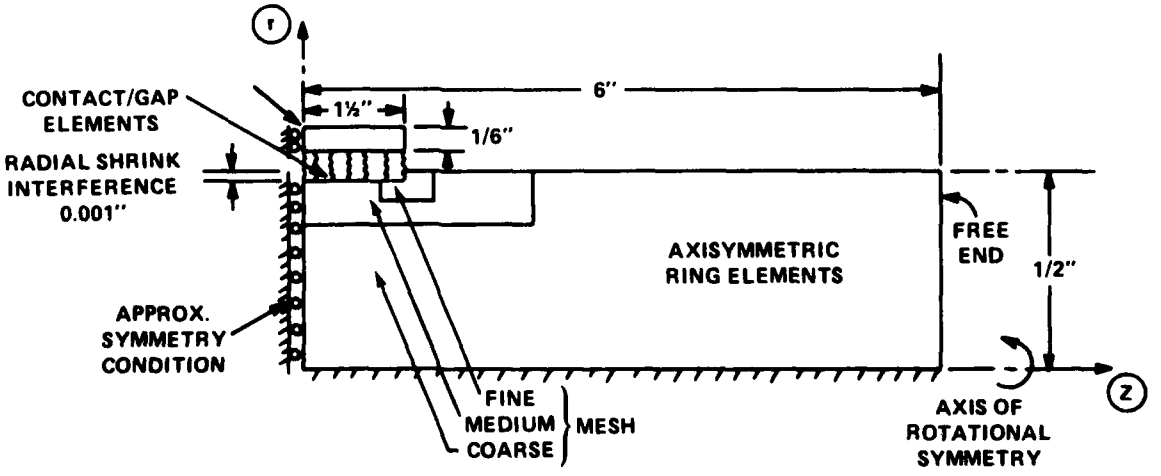

Figure 18 - Finite Element Representation of Elastic Shaft/Elastic Sleeve Contact

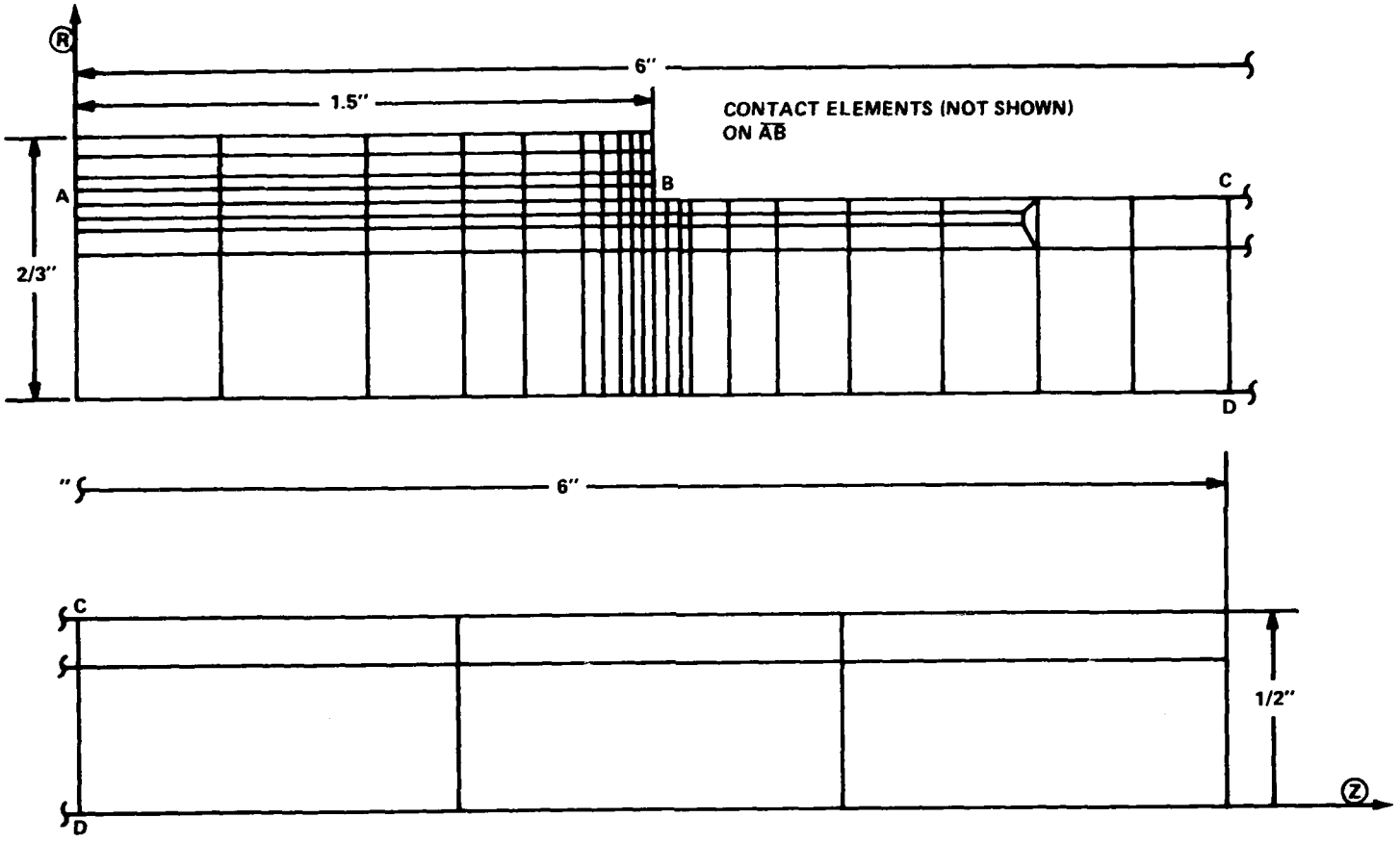

Figure 19 - Finite Element Mesh for Axisymmetric Elastic Shaft/Elastic Sleeve Contact Problem.

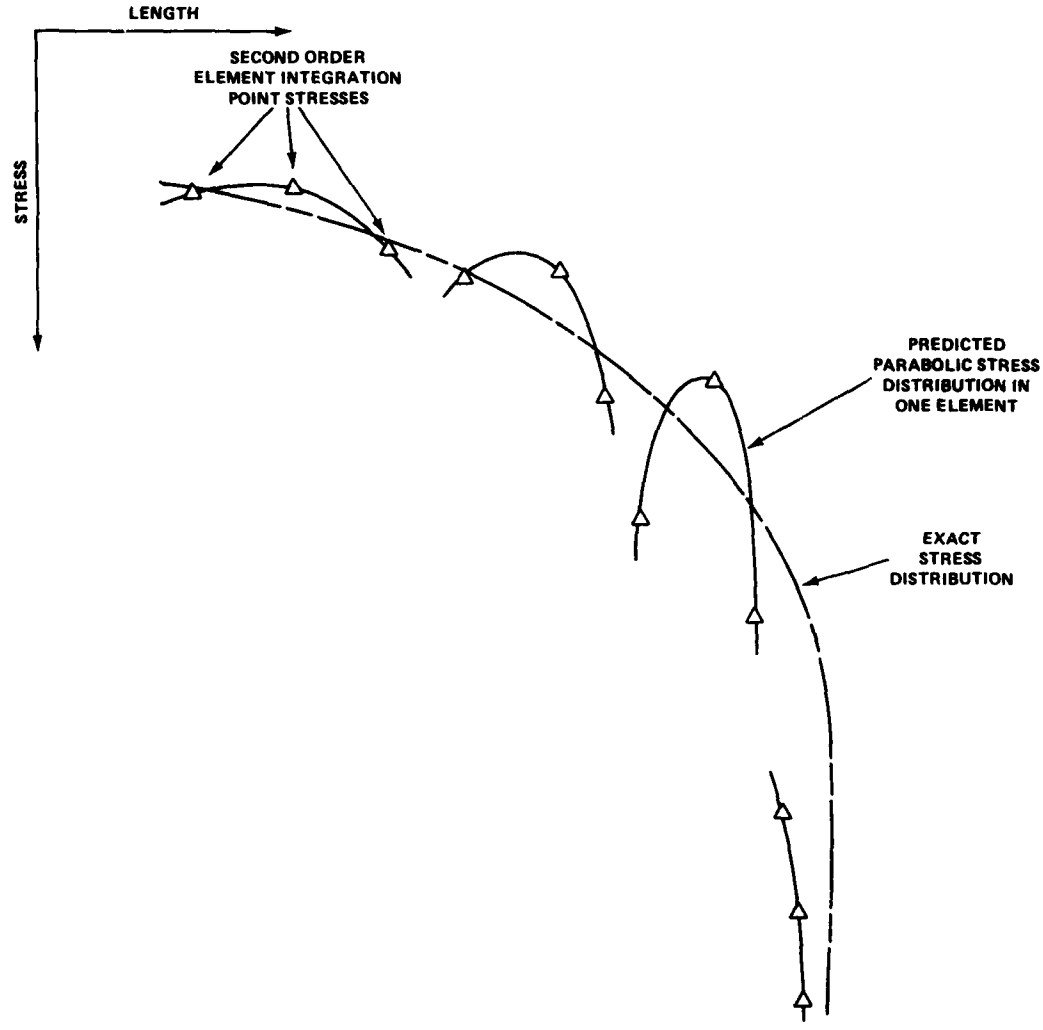

Figure 20 - Typical Stress Prediction of Fully Integrated Higher Order Solids Near a Steep Stress Gradient

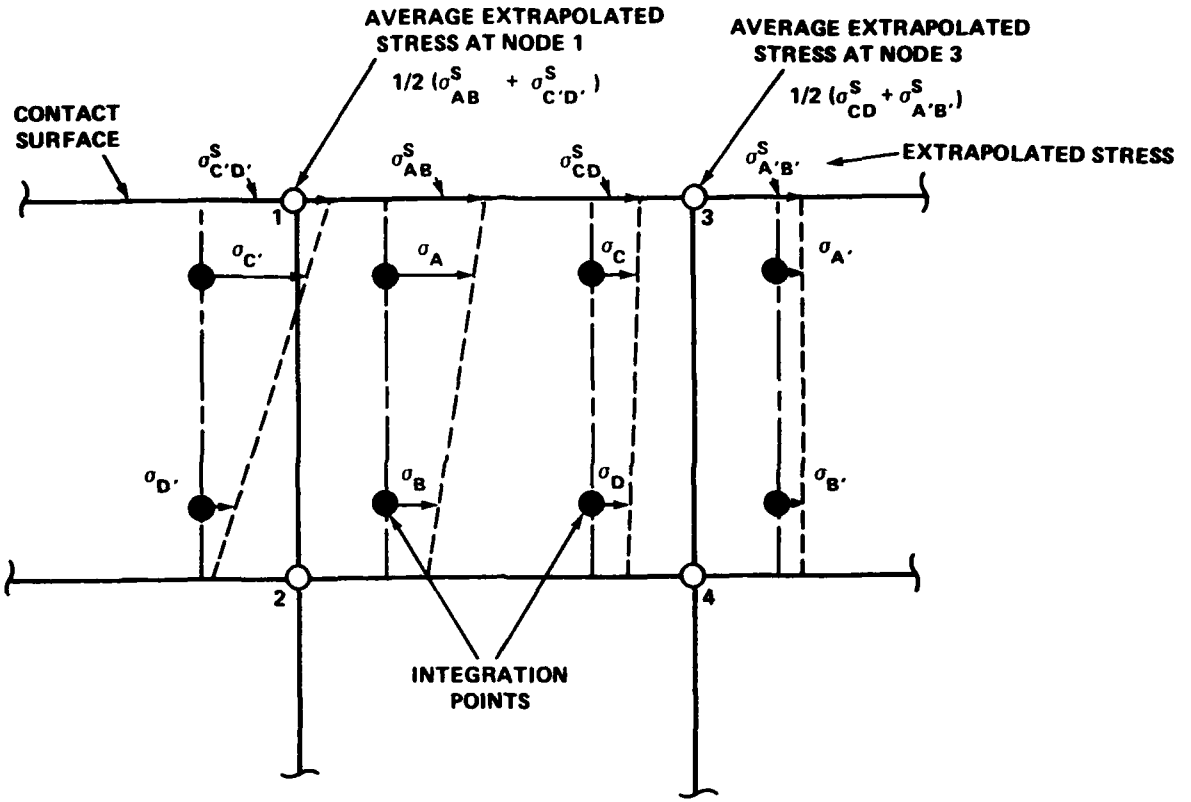

Figure 21 - Calculation of Contact Surface Nodal Stress by Extrapolation and Averaging

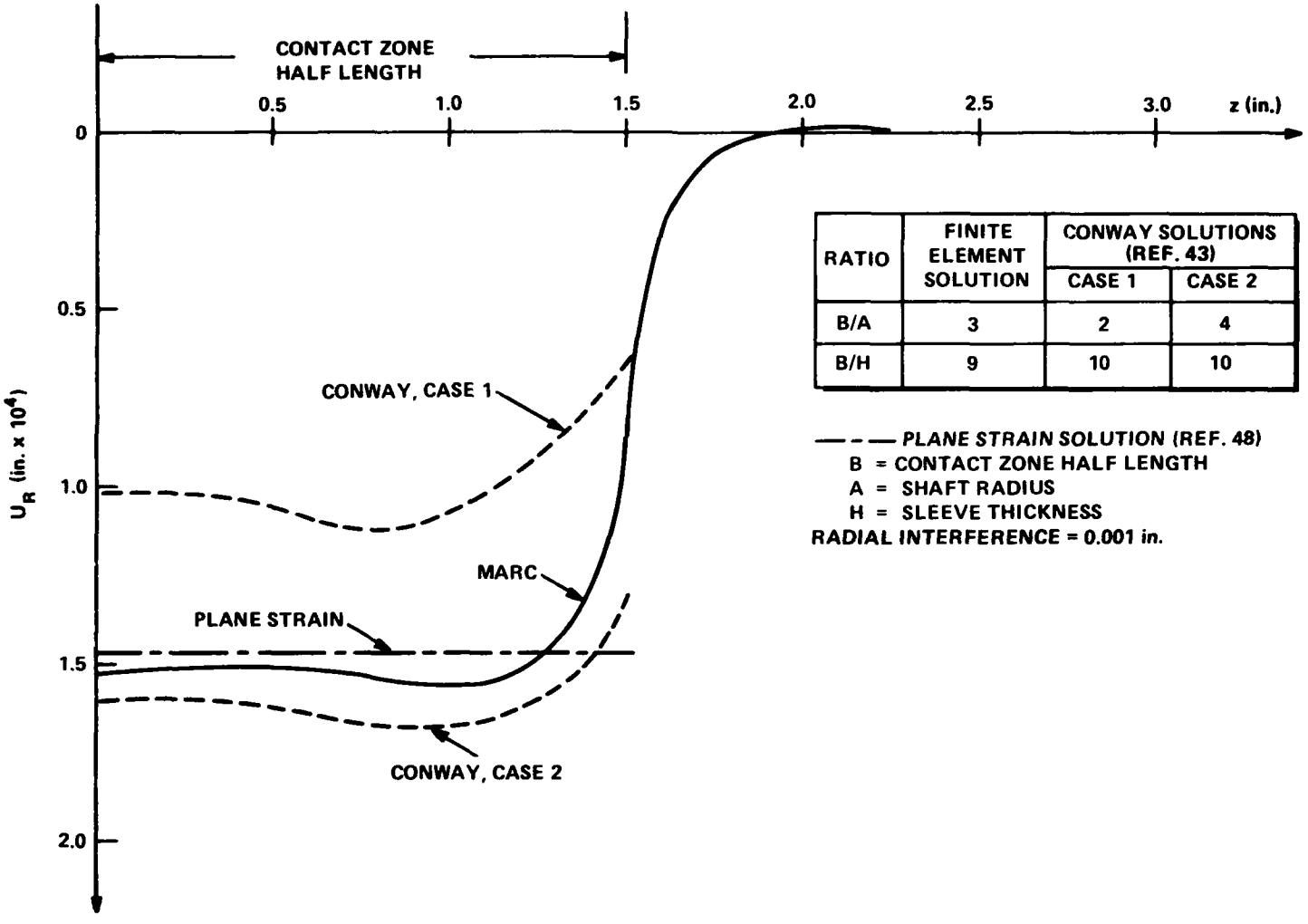

RATIO	FINITE ELEMENT SOLUTION	CONWAY SOLUTIONS (REF. 43)	
		CASE 1	CASE 2
B/A	3	2	4
B/H	9	10	10

— — — PLANE STRAIN SOLUTION (REF. 48)
B = CONTACT ZONE HALF LENGTH
A = SHAFT RADIUS
H = SLEEVE THICKNESS
RADIAL INTERFERENCE = 0.001 in.

Figure 22 - Elastic Shaft/Elastic Sleeve, Radial Displacements at Outer Shaft Radius

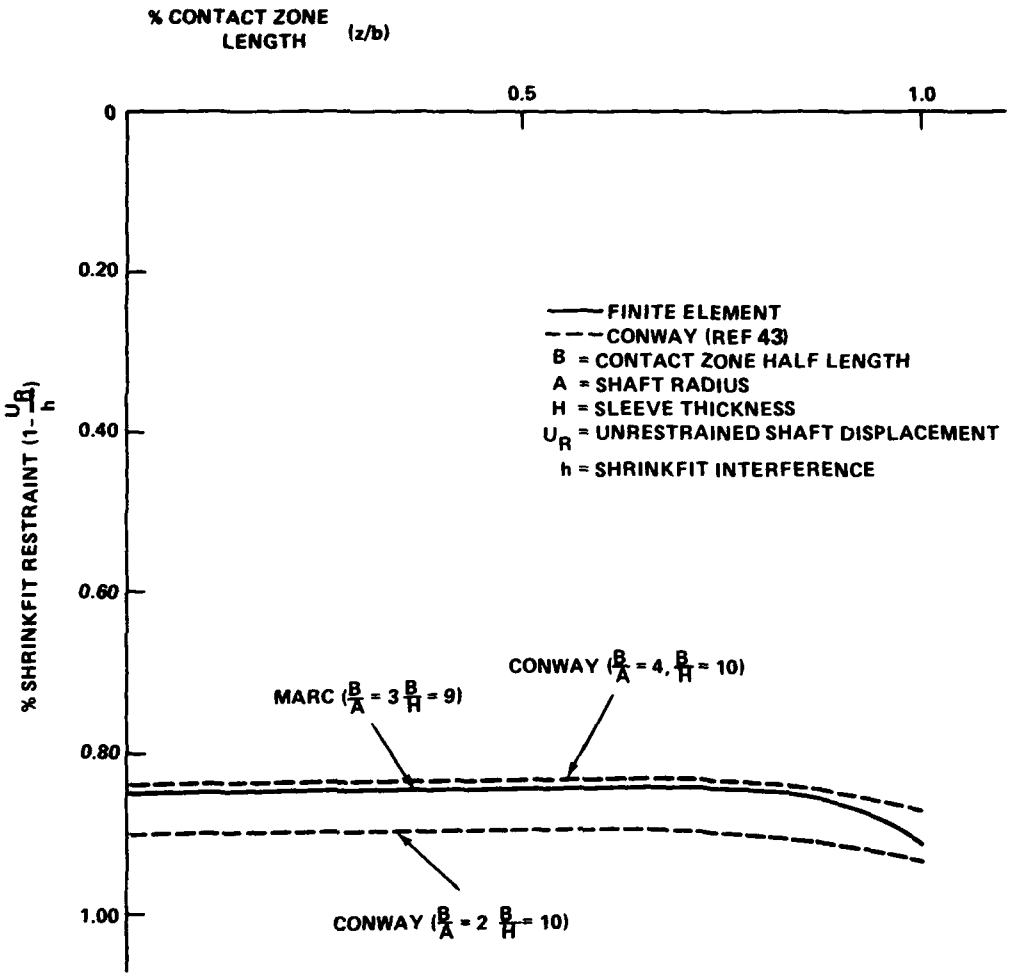

Figure 23 - Elastic Shaft/Elastic Sleeve, Radial Displacement Restraint Comparison

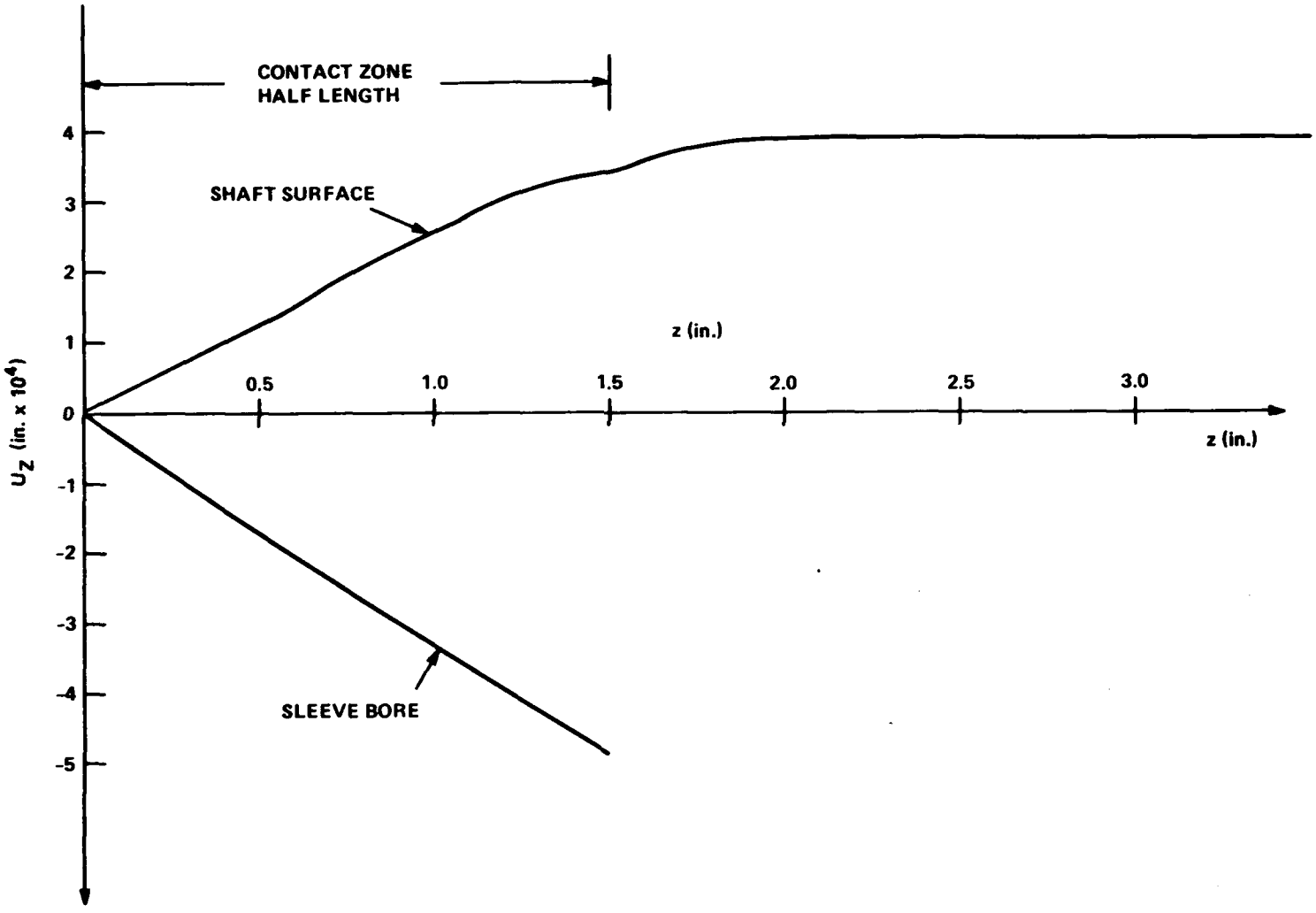

Figure 24 - Elastic Shaft/Elastic Sleeve, Axial Displacements at Contact Surface

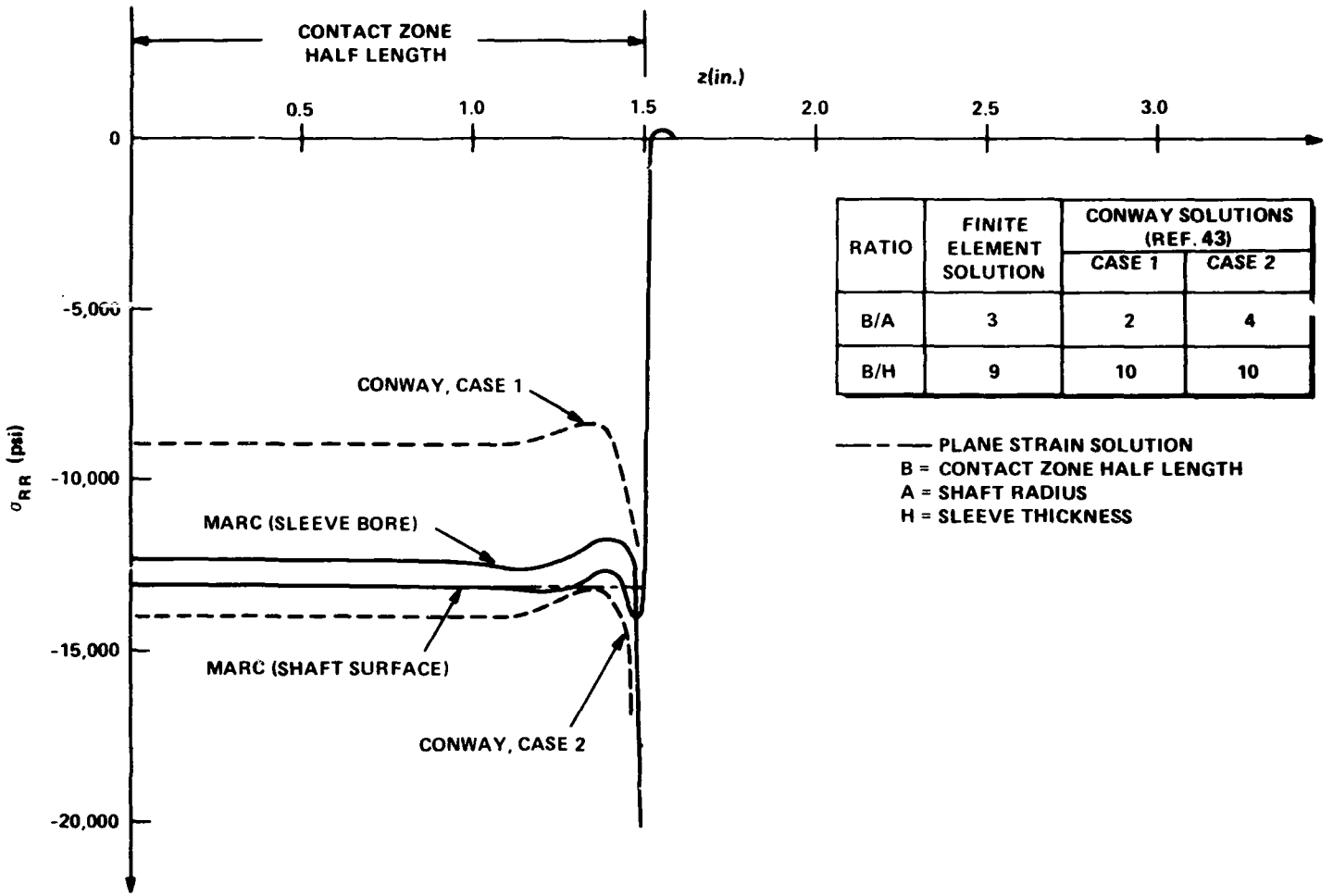

RATIO	FINITE ELEMENT SOLUTION	CONWAY SOLUTIONS (REF. 43)	
		CASE 1	CASE 2
B/A	3	2	4
B/H	9	10	10

Figure 25 - Elastic Shaft/Elastic Sleeve, Radial Stresses Extrapolated to Contact Surface

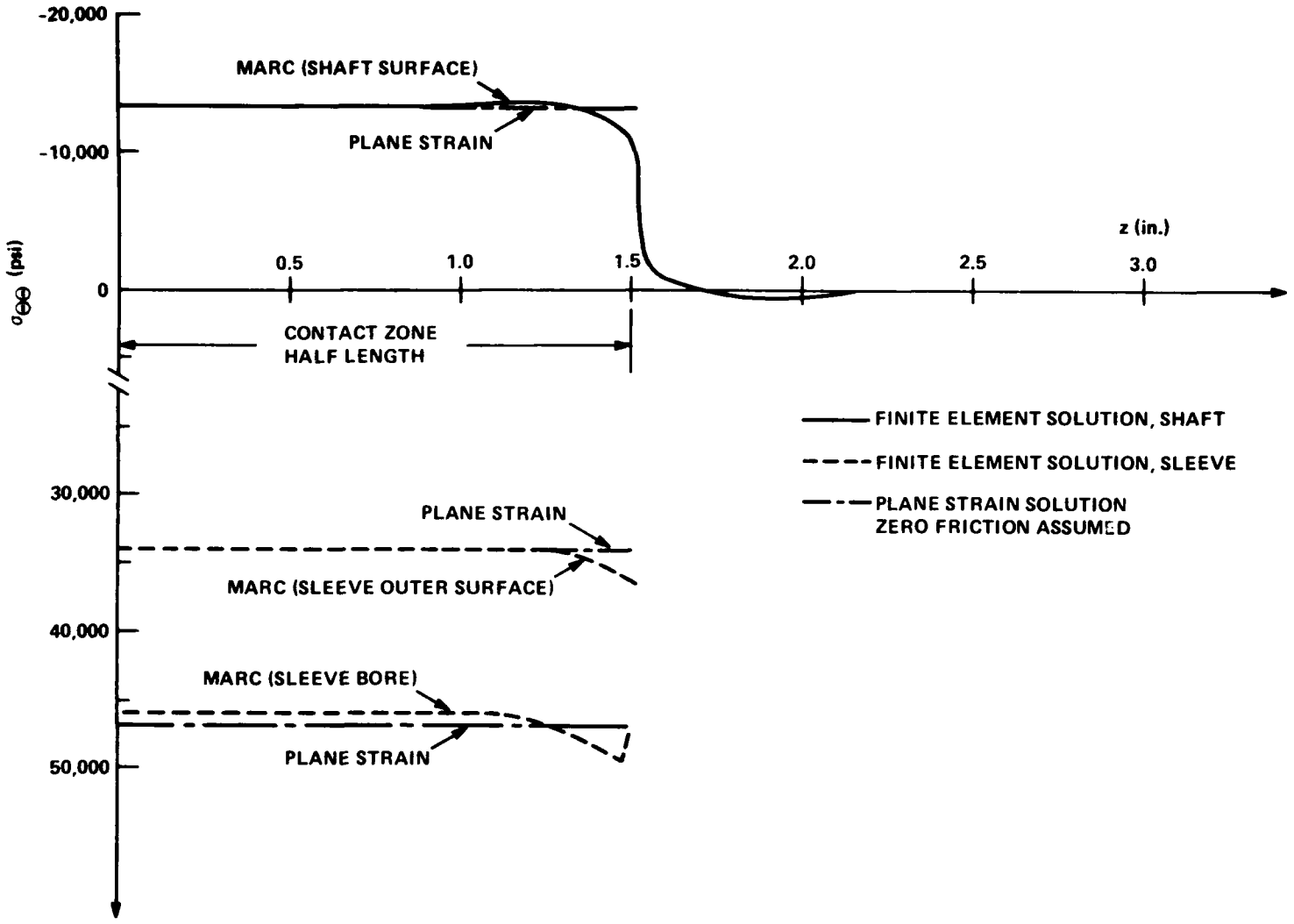

Figure 26 - Elastic Shaft/Elastic Sleeve, Hoop Stresses Extrapolated to Shaft and Sleeve Surfaces

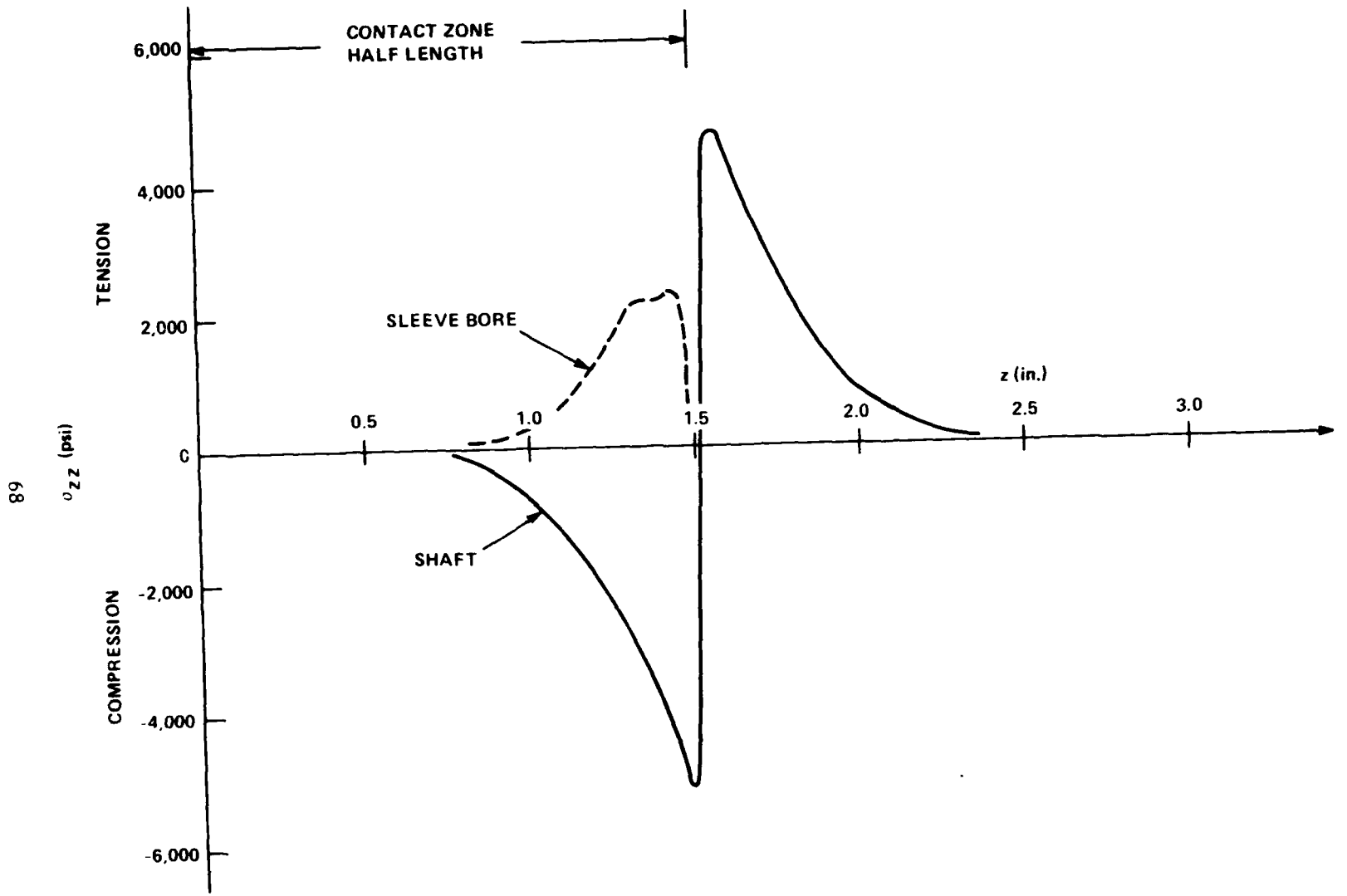

Figure 27 - Elastic Shaft/Elastic Sleeve, Axial Stress Extrapolated to Contact Surface

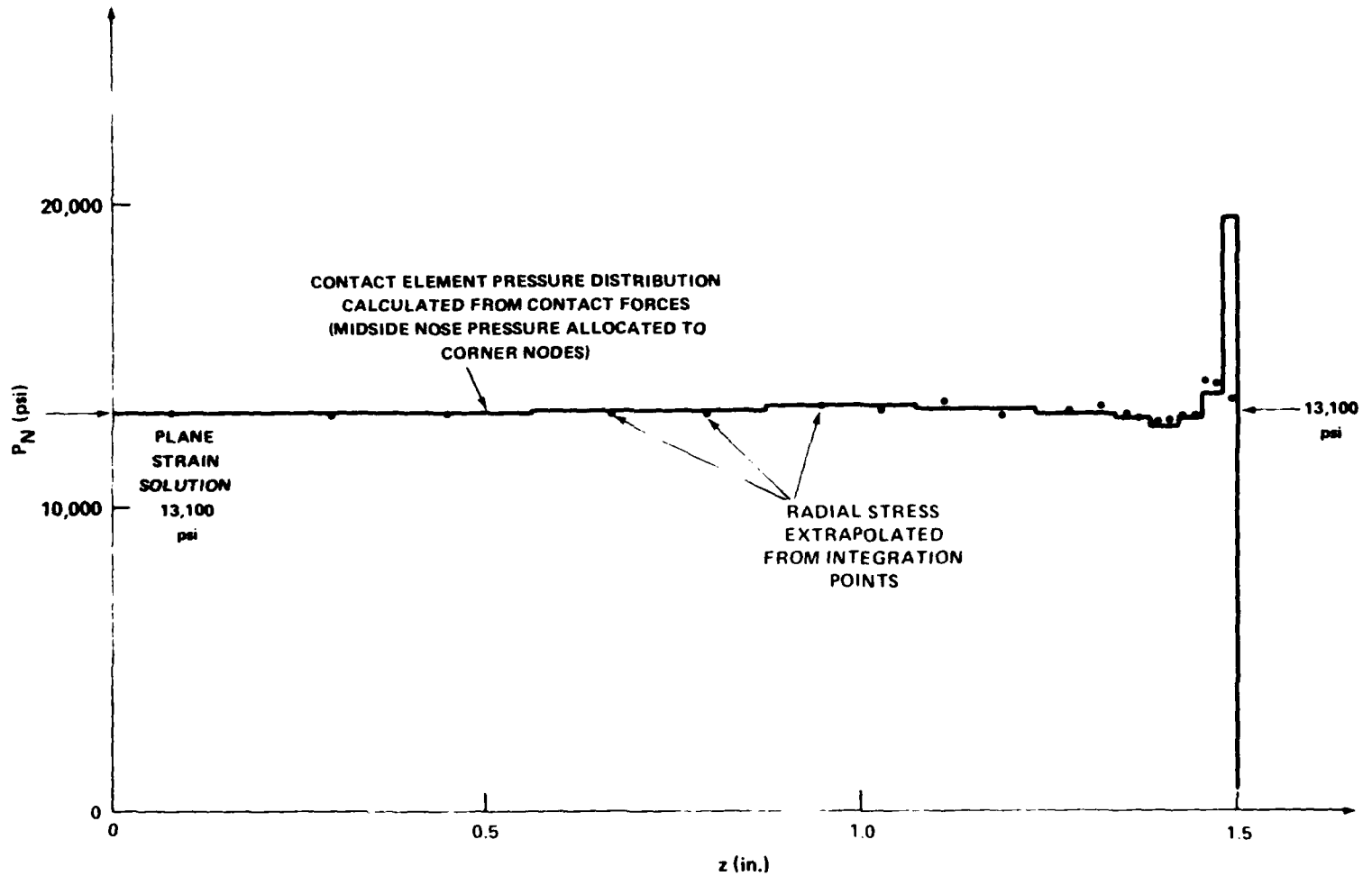

Figure 28 - Elastic Shaft/Elastic Sleeve, Contact Element Pressure Compared to Extrapolated Radial Stress

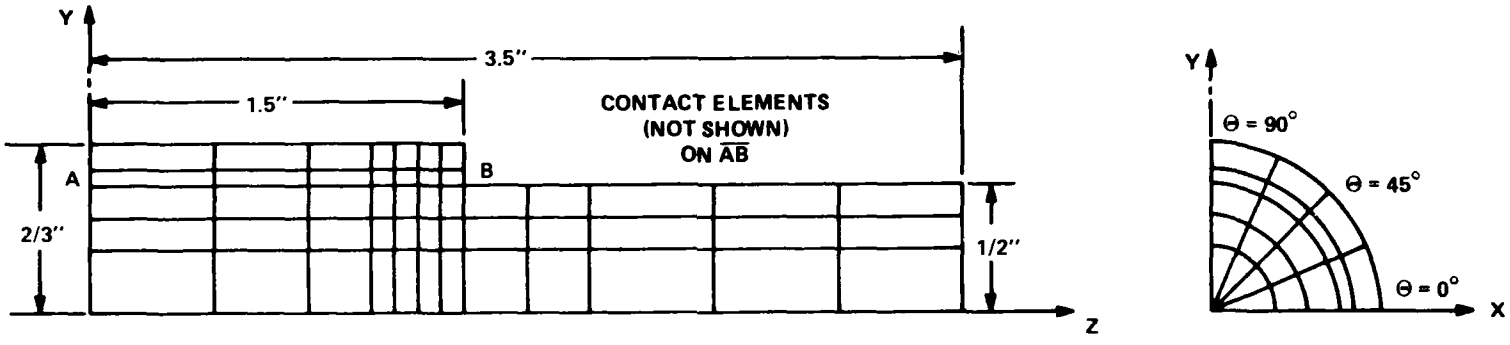

Figure 29 - 3-D Finite Element Mesh for Elastic Shaft/Elastic Sleeve Shrinkfit

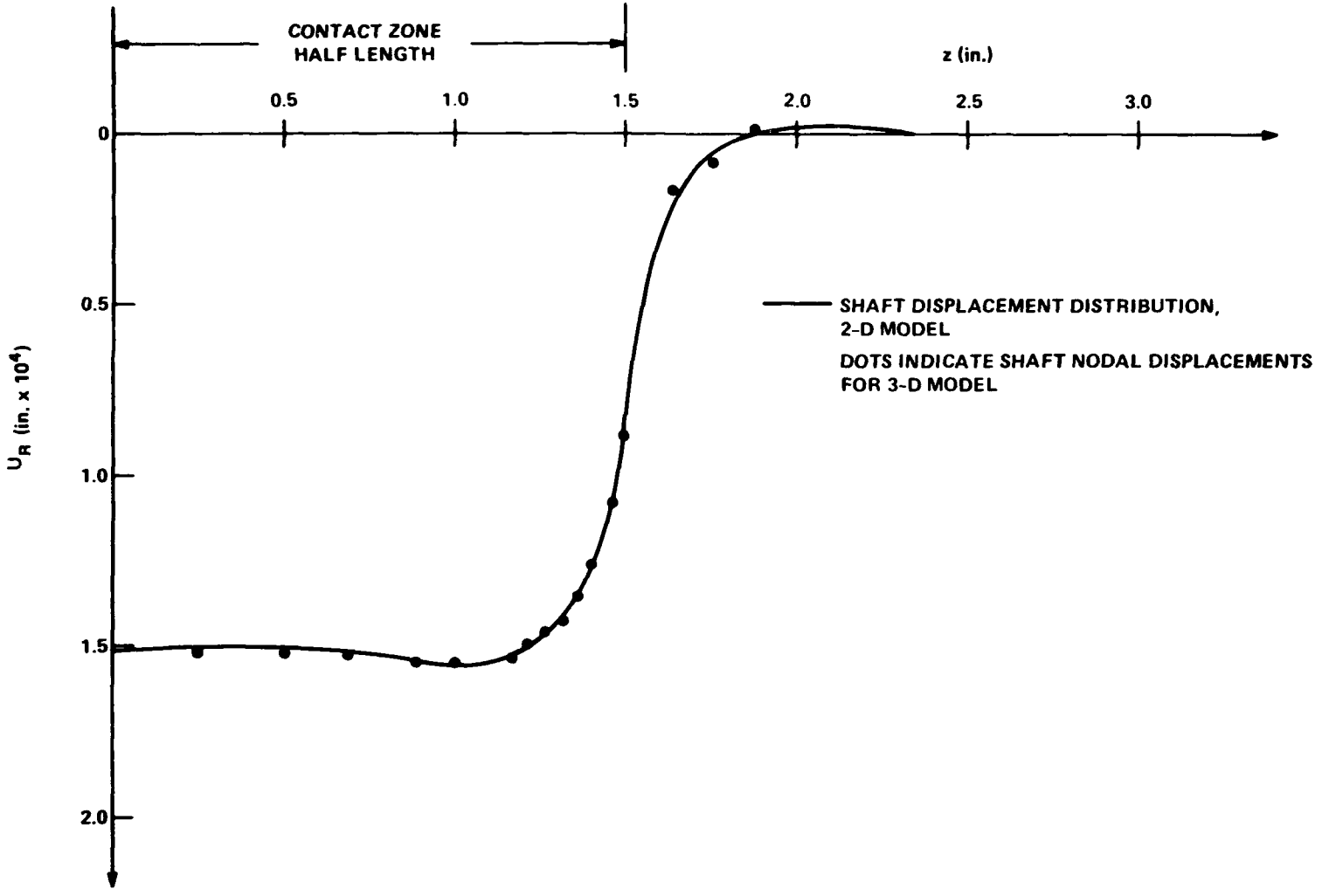

Figure 30 - Elastic Shaft/Elastic Sleeve, Comparison of Radial Deflection Predictions for Axisymmetric and 3-D Models

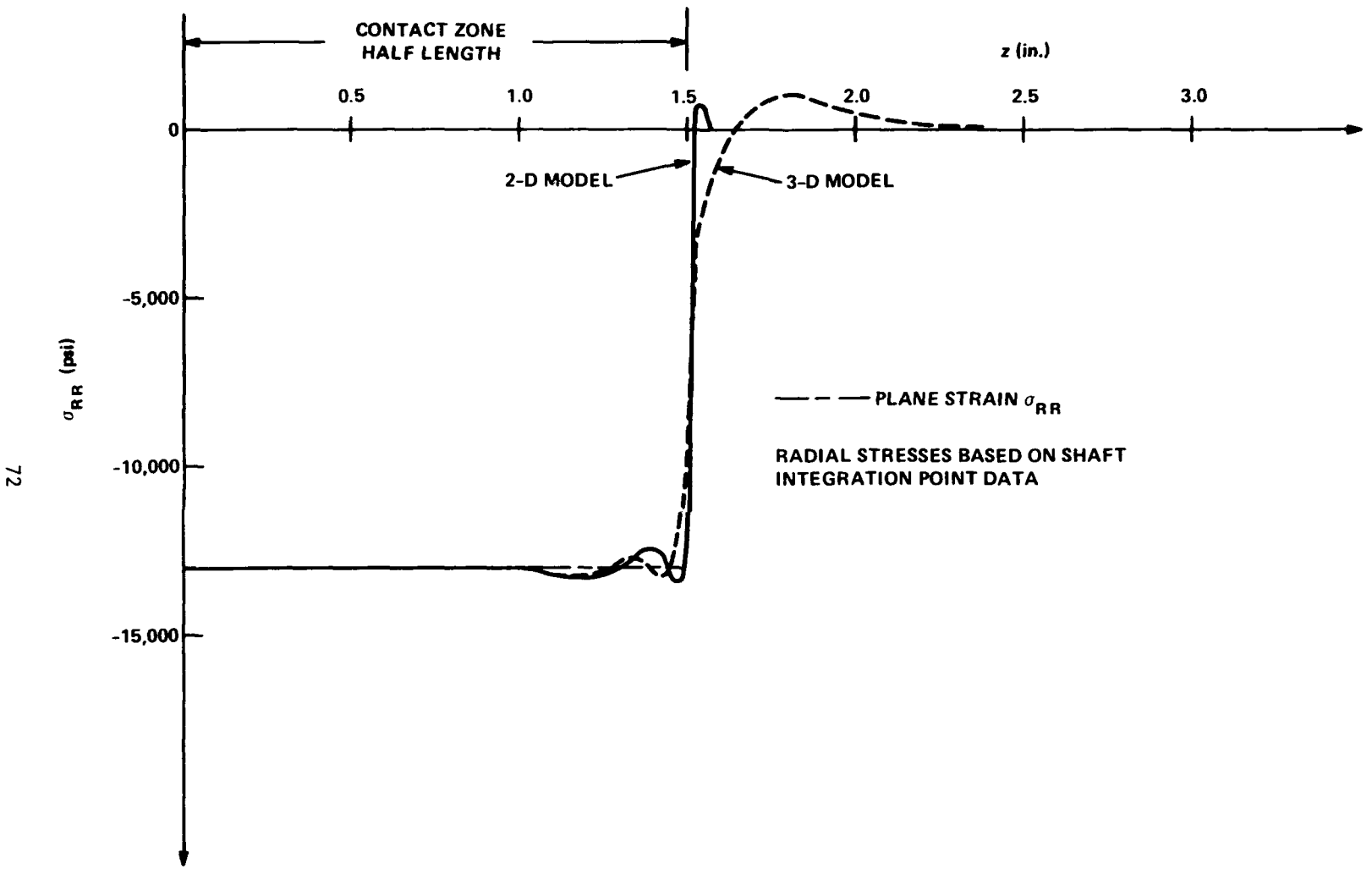

Figure 31 - Elastic Shaft/Elastic Sleeve, Comparison of Contact Surface Radial Stress for Axisymmetric and 3-D models

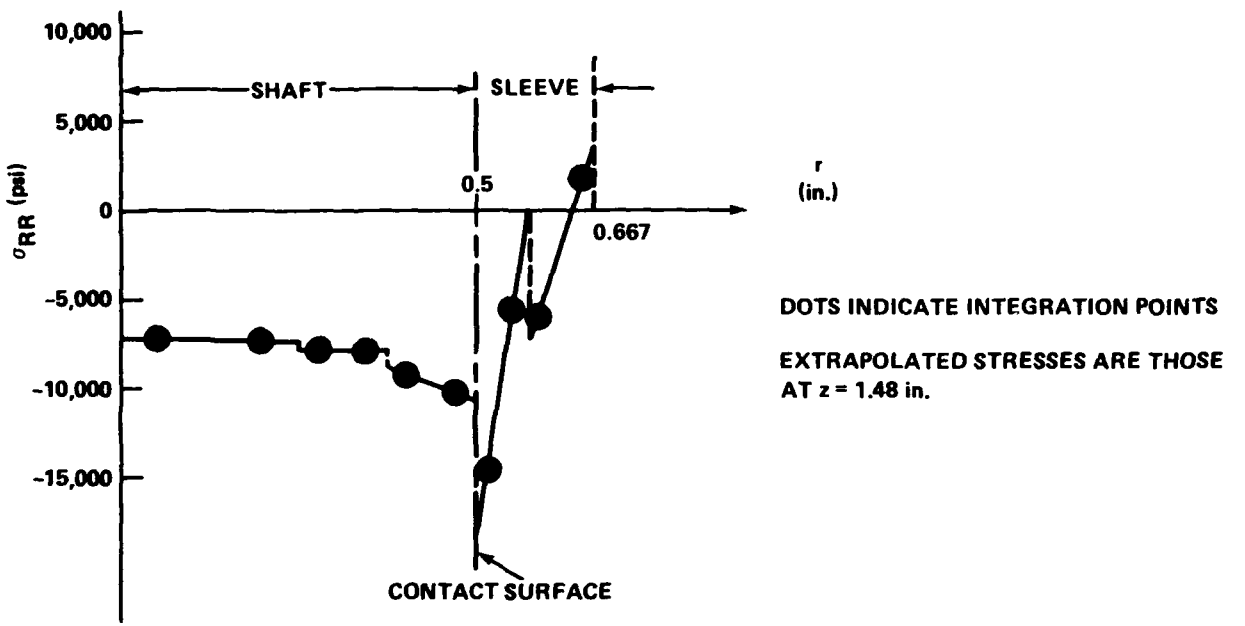

Figure 32 - 3-D Shrinkfit, Radial Stress Distributions in Shaft and Sleeve Near Edge of Contact Zone

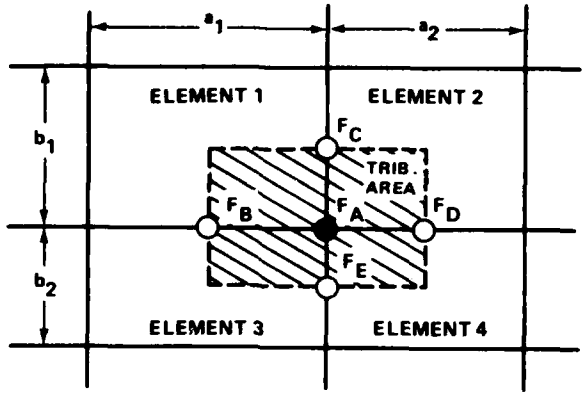

Figure 33a - Near an Interior Corner Node

● CORNER NODE
○ MIDSIDE NODE

CORNER NODE CONTACT FORCE

$F_A' = F_A + 1/2\ (F_B + F_C + F_D + F_E)$

CORNER NODE CONTACT PRESSURE

$P_A' = F_A'/\sum_{i=1}^{4} a_i b_i$

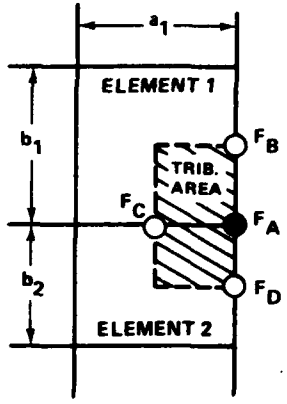

CORNER NODE CONTACT FORCE

$F_A' = F_A + 1/2\ (F_B + F_C + F_D)$

CORNER NODE CONTACT PRESSURE

$P_A' = F_A'/(a_1 b_1 + a_1 b_2)$

Figure 33b - Near an Edge Corner Node

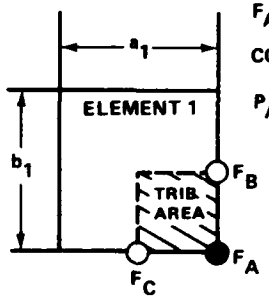

CORNER NODE CONTACT FORCE

$F_A' = F_A + 1/2\ (F_B + F_C)$

CORNER NODE CONTACT PRESSURE

$P_A' = F_A'/a_1 b_1$

Figure 33c - Near a Corner Node

Figure 33 - Contact Pressures Calculated from Contact Forces

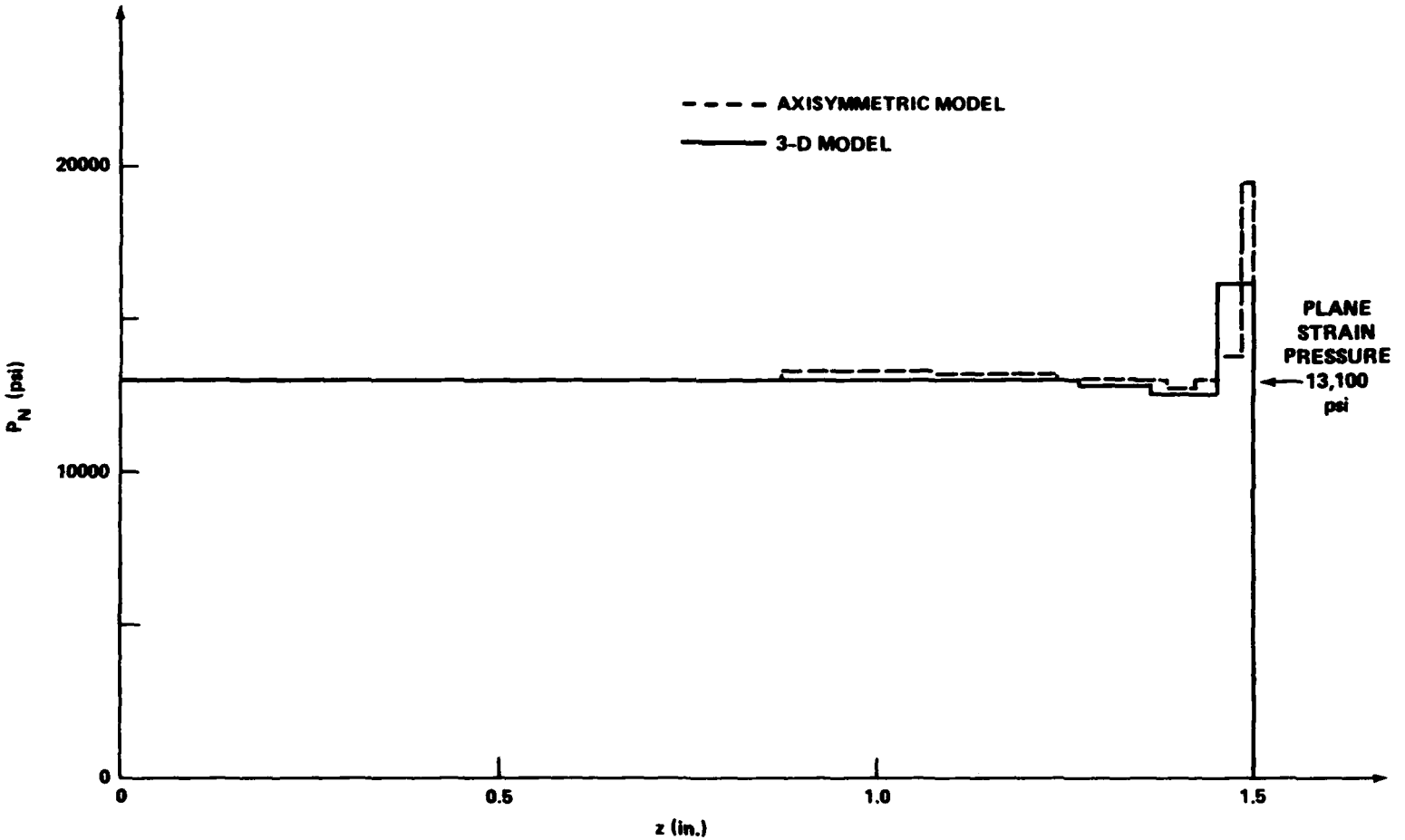

Figure 34 - Elastic Shaft/Elastic Sleeve, Comparison of Contact Element Pressure for Axisymmetric and 3-D Models

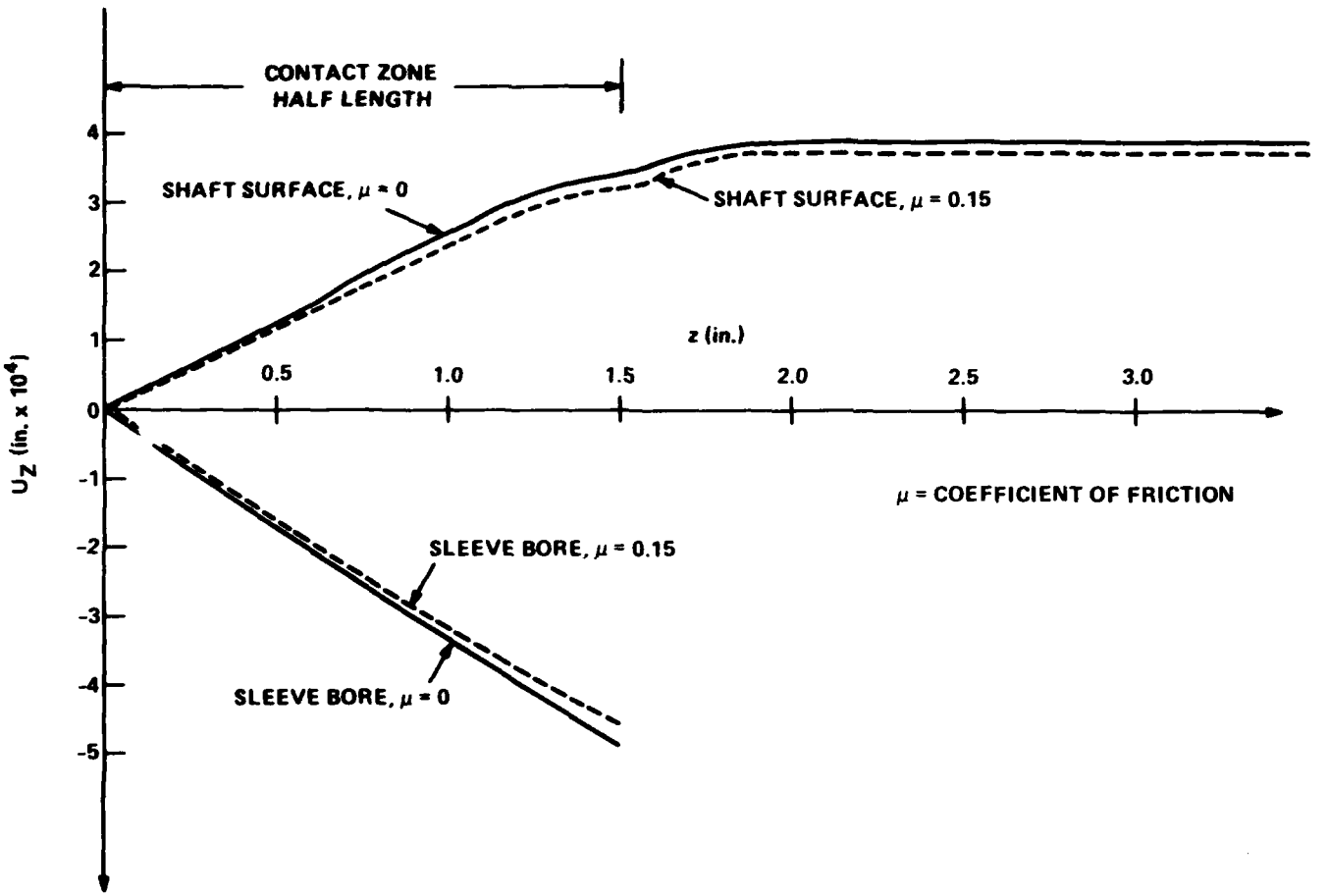

Figure 35 - Elastic Shaft/Elastic Sleeve Shrinkfit with Friction, Comparison of Predicted Axial Displacements to Frictionless Result

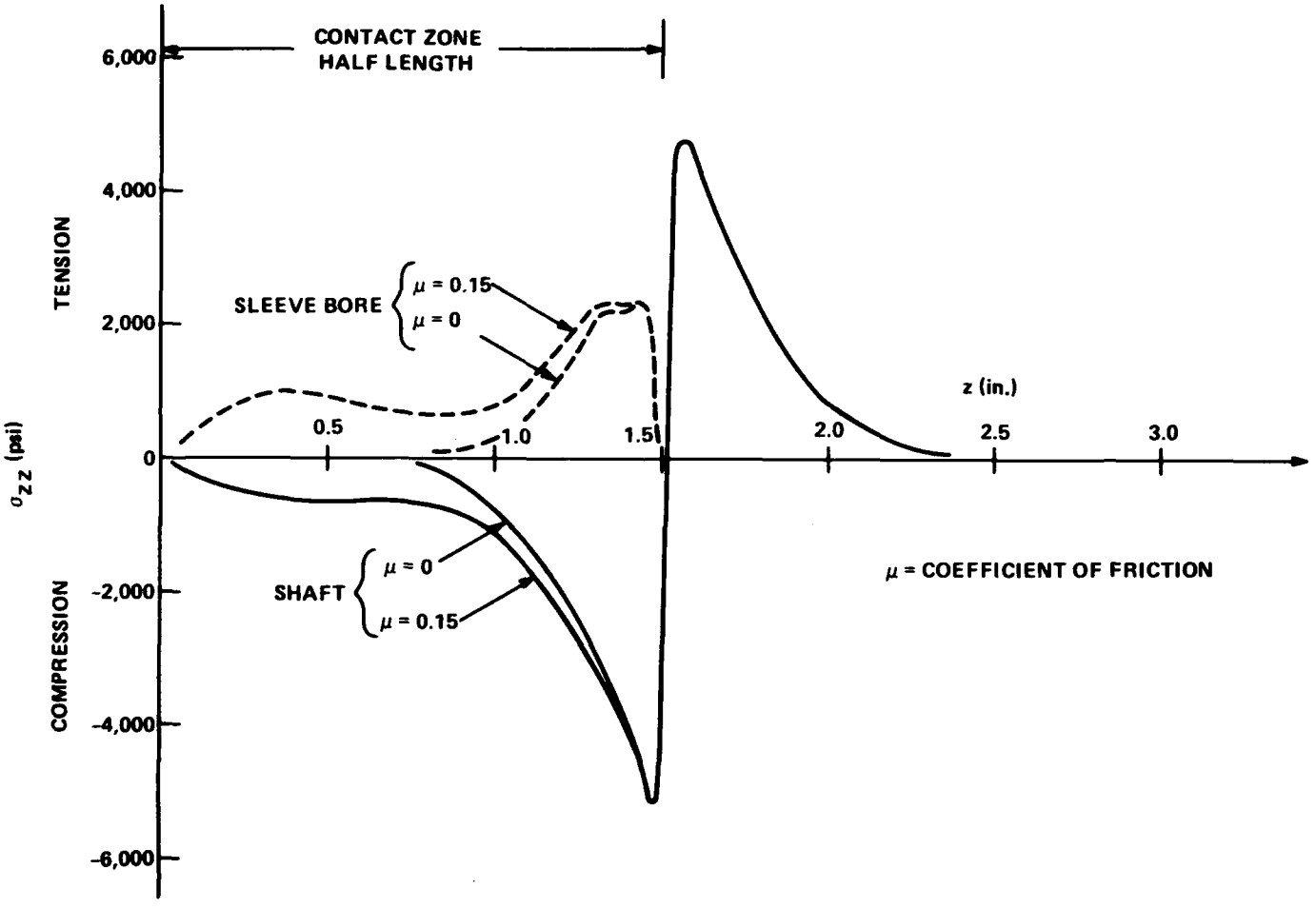

Figure 36 - Elastic Shaft/Elastic Sleeve Shrinkfit with Friction, Comparison of Predicted Axial Stresses to Frictionless Result

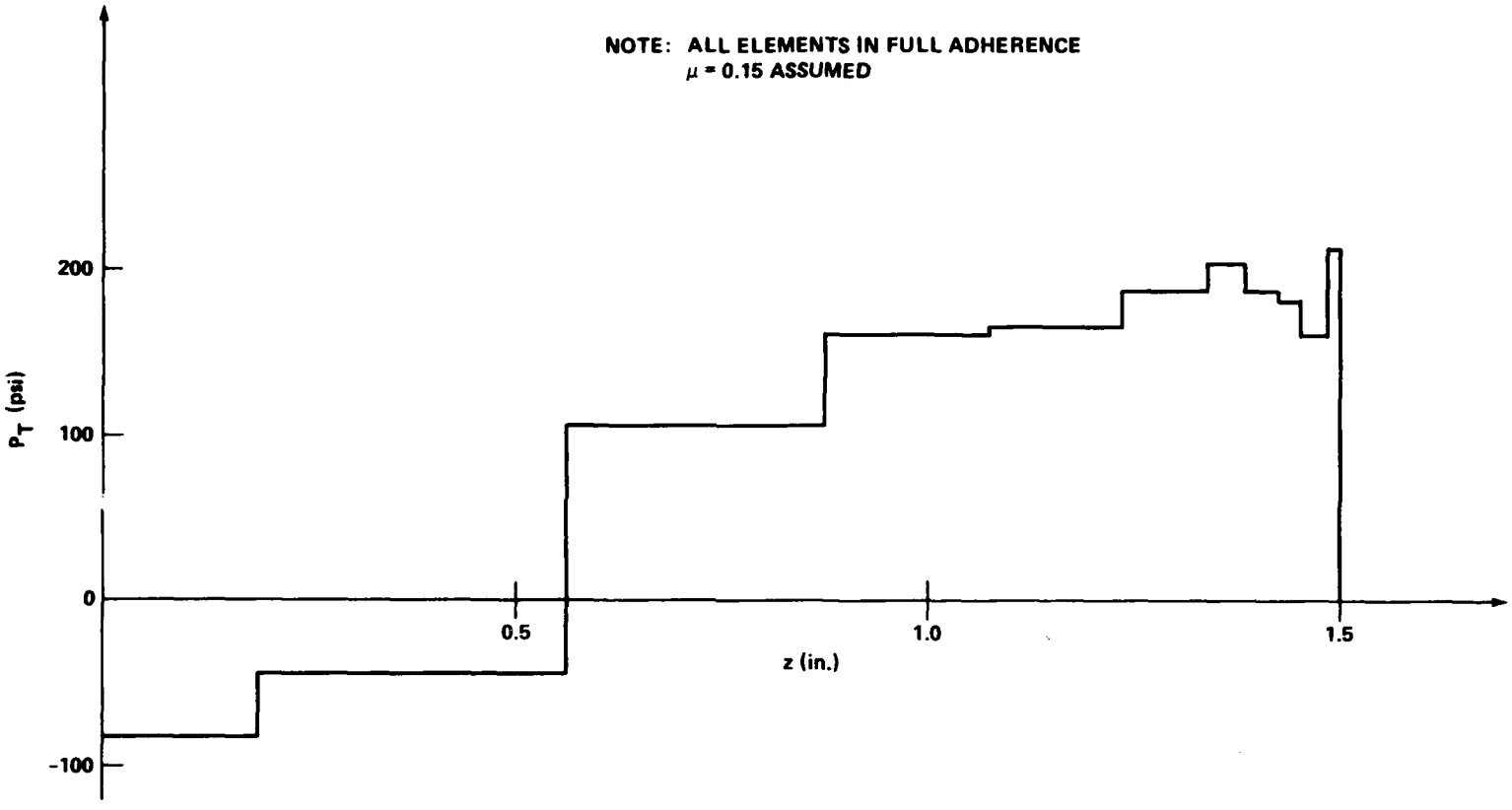

Figure 37 - Elastic Shaft/Elastic Sleeve Shrinkfit with Friction, Contact Surface Tangential Shear Based on Contact Element Forces

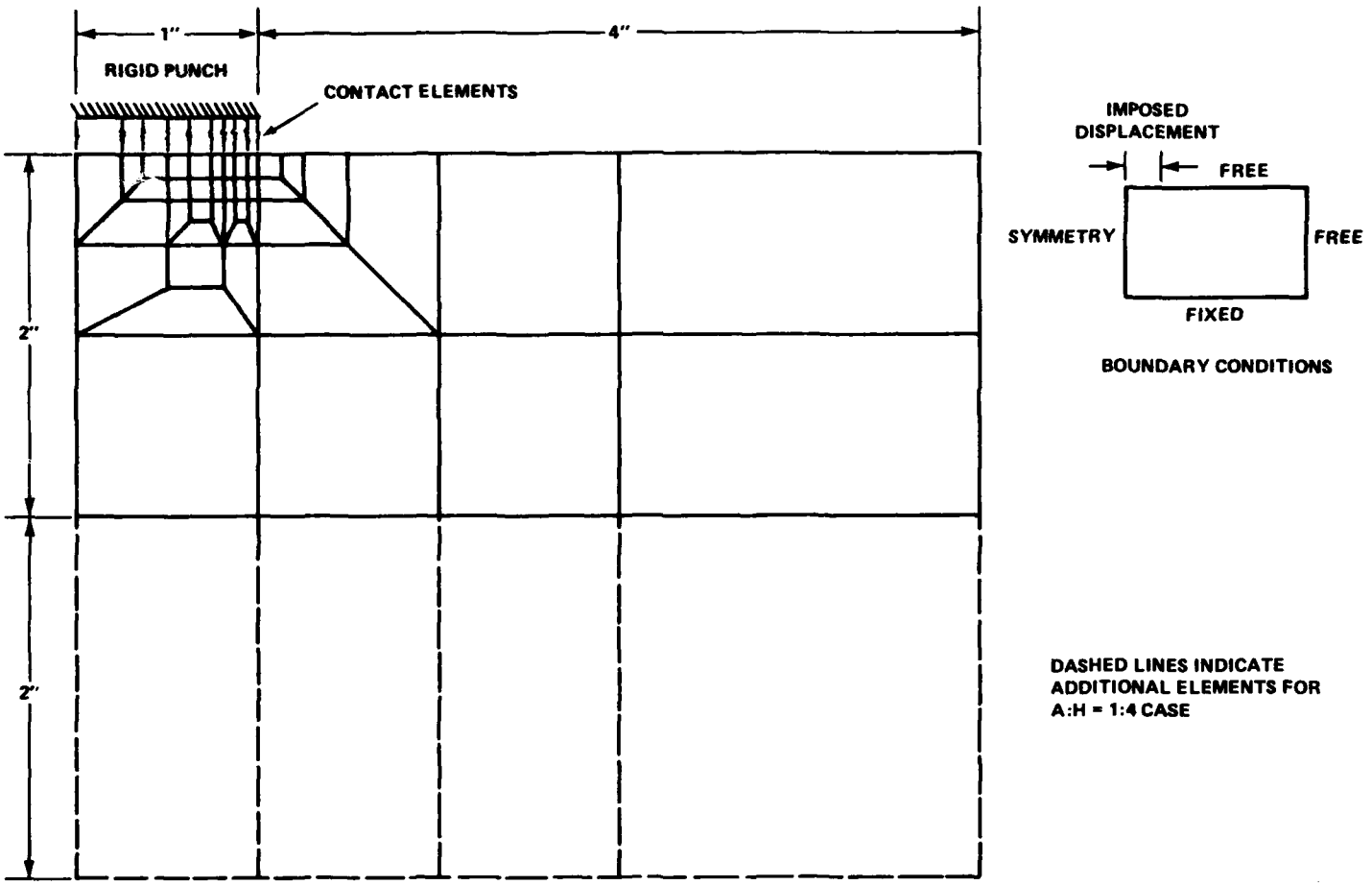

Figure 38 - Finite Element Mesh for Flat Rigid Punch/Elastic Slab Contact with Friction

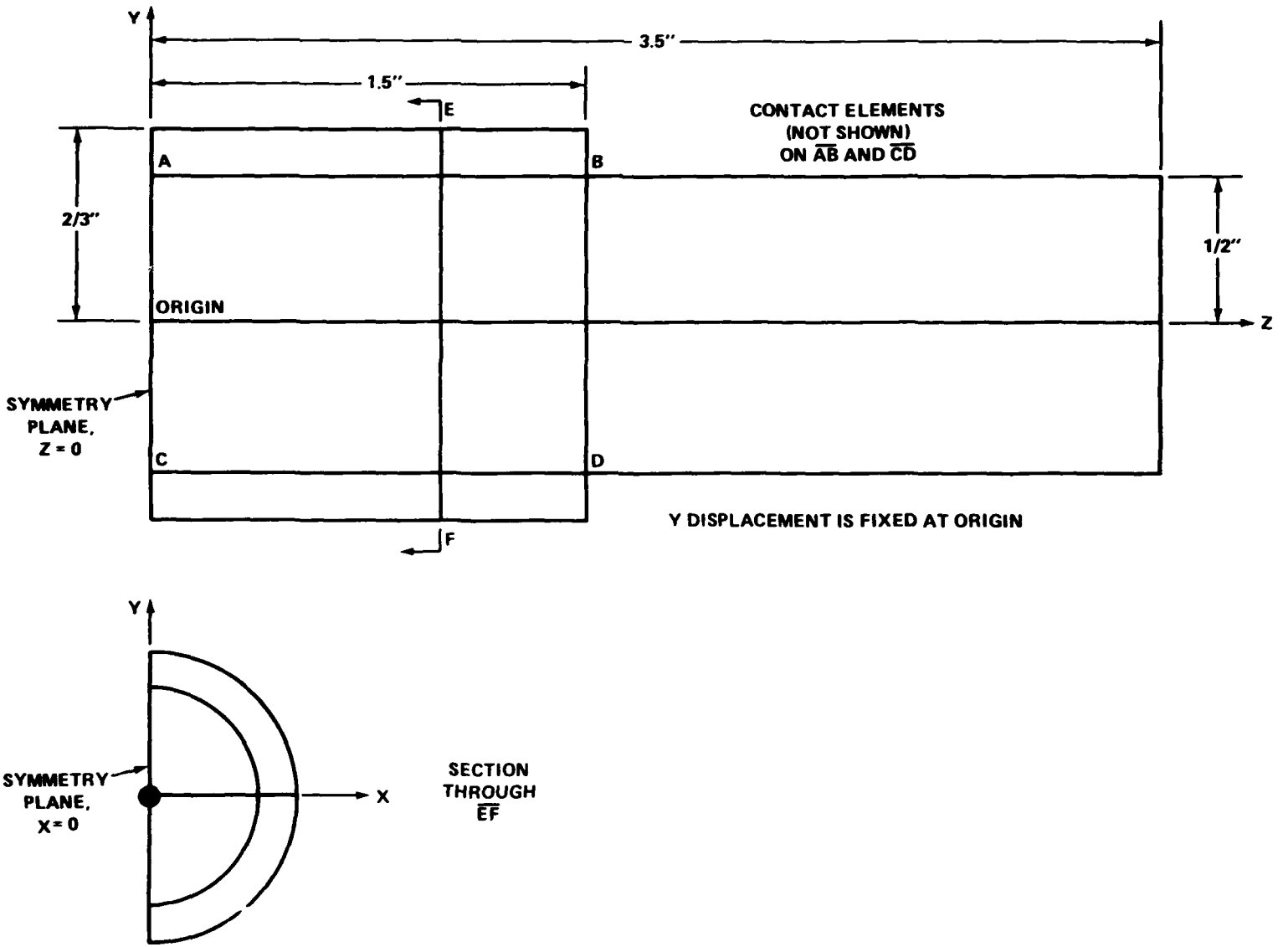

Figure 39 - Coarse Finite Element Mesh for 3-D Elastic Shaft/Elastic Sleeve Shrinkfit with Bending and Friction

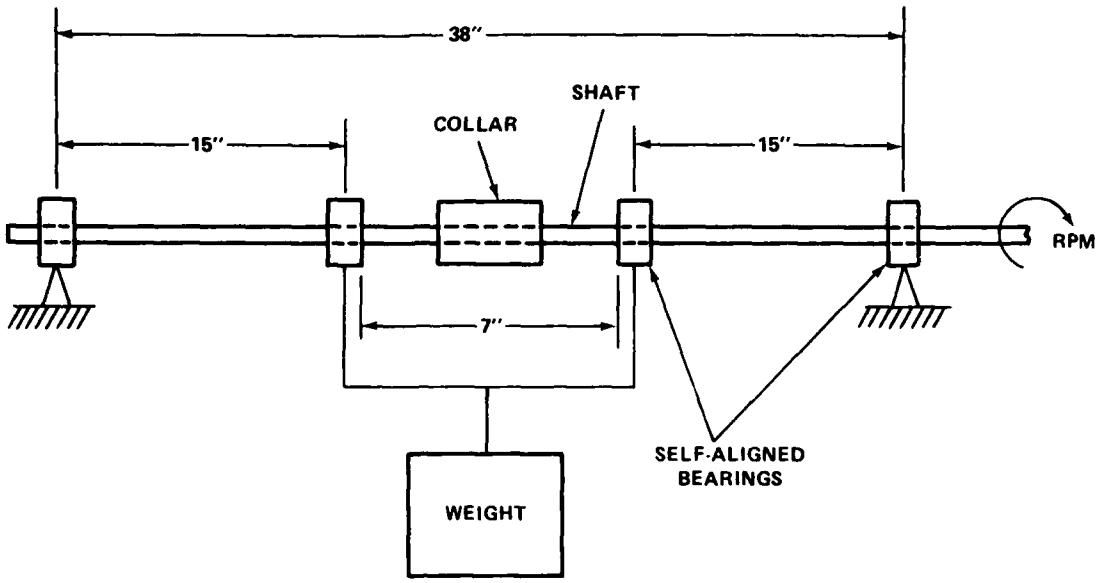

FRETTING TEST SETUP

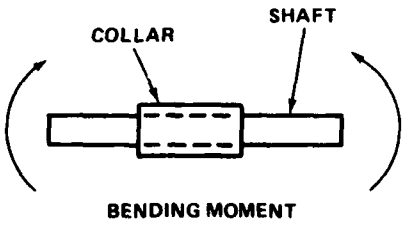

EQUIVALENT STRUCTURAL MODEL

Figure 40 - Experimental Fretting Corrosion Test Machine

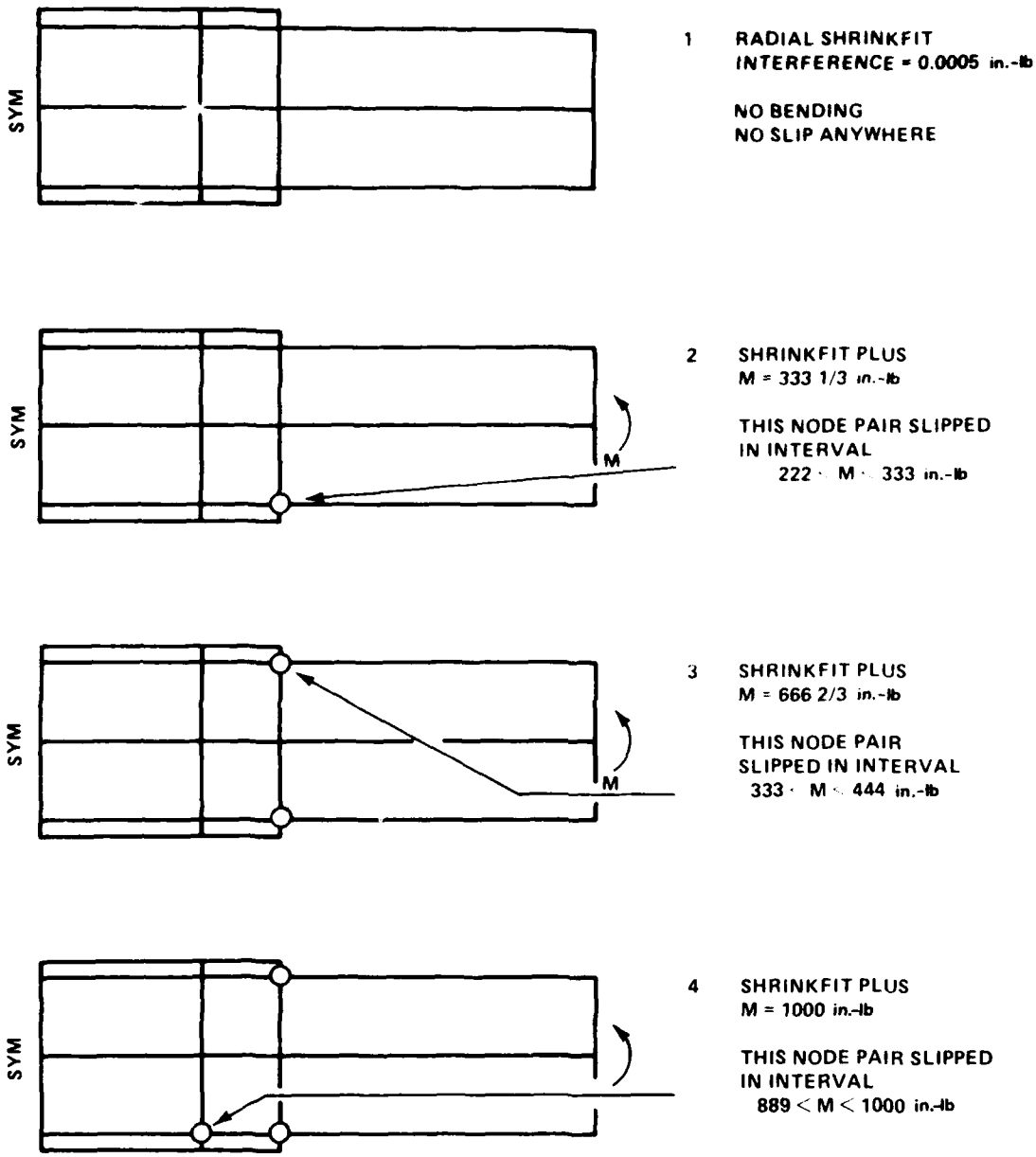

Figure 41 - 3-D Elastic Shaft/Elastic Sleeve Shrinkfit with Bending and Friction, Frictional Slip Development in Plane of Bending with Increasing Bending Load

AD-A118 583 DAVID W TAYLOR NAVAL SHIP RESEARCH AND DEVELOPMENT CE--ETC F/G 12/1
CALCULATION OF CONTACT PRESSURES AND FRICTIONAL EFFECTS ON MECH--ETC(U)
AUG 82 D E LESAR
UNCLASSIFIED DTNSRDC-82/033 NL

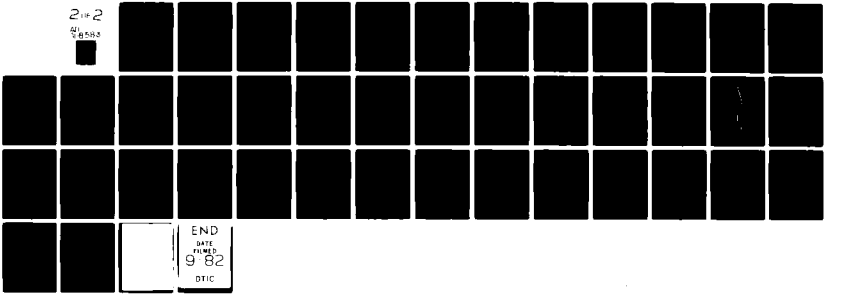

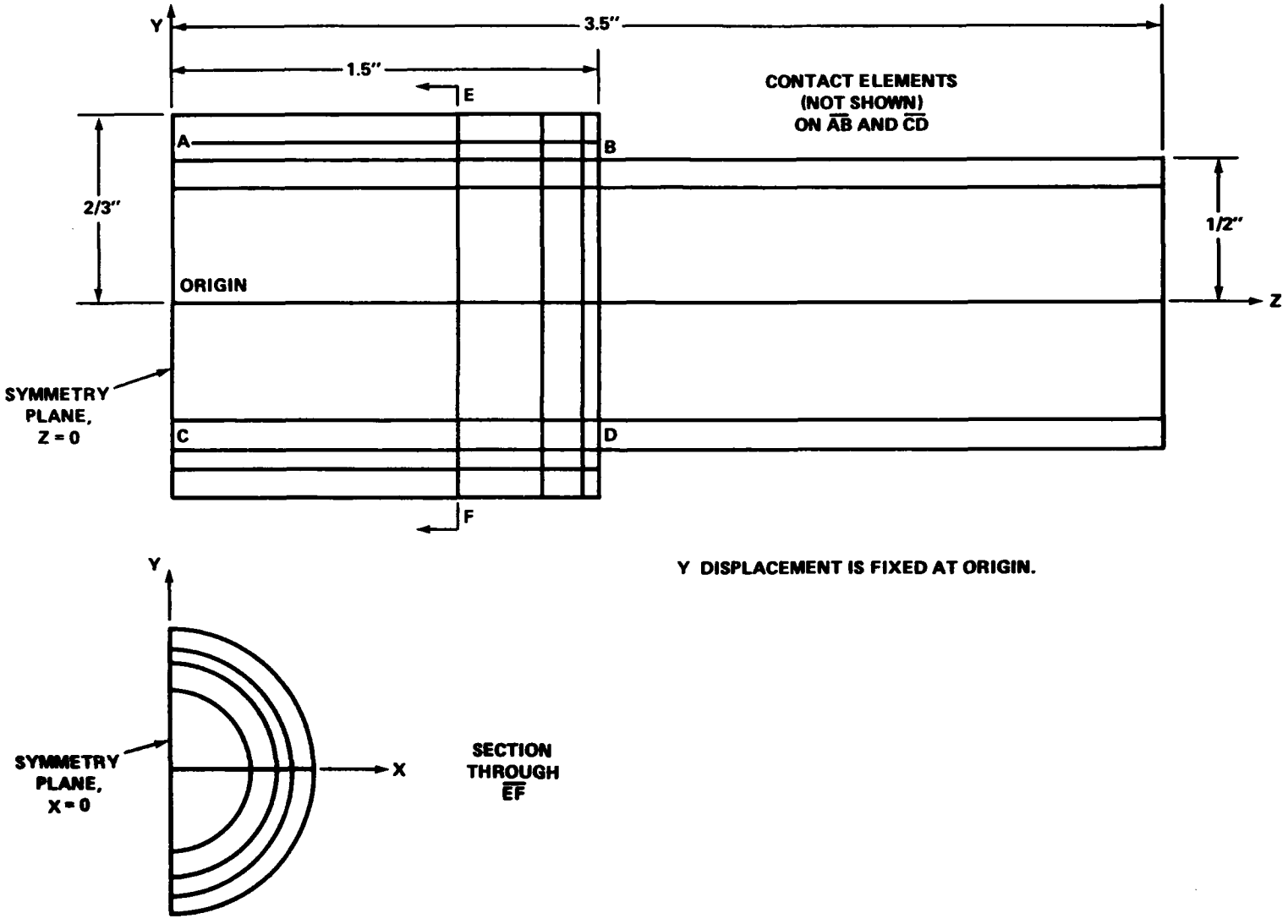

Figure 42 - Improved Finite Element Mesh for Three Dimensional Elastic Shaft/Elastic Sleeve Shrinkfit with Bending and Friction

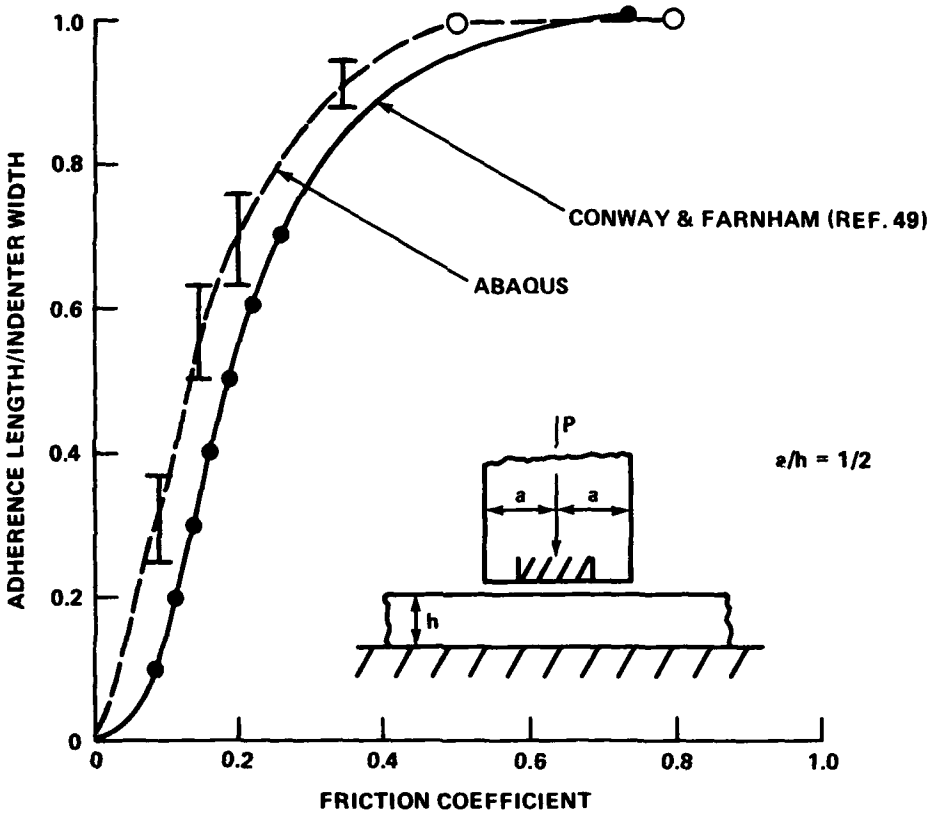

Figure 43 - Flat Rigid Punch/Elastic Slab Contact with Friction, Comparison of ABAQUS Results to Conway et al. Solution

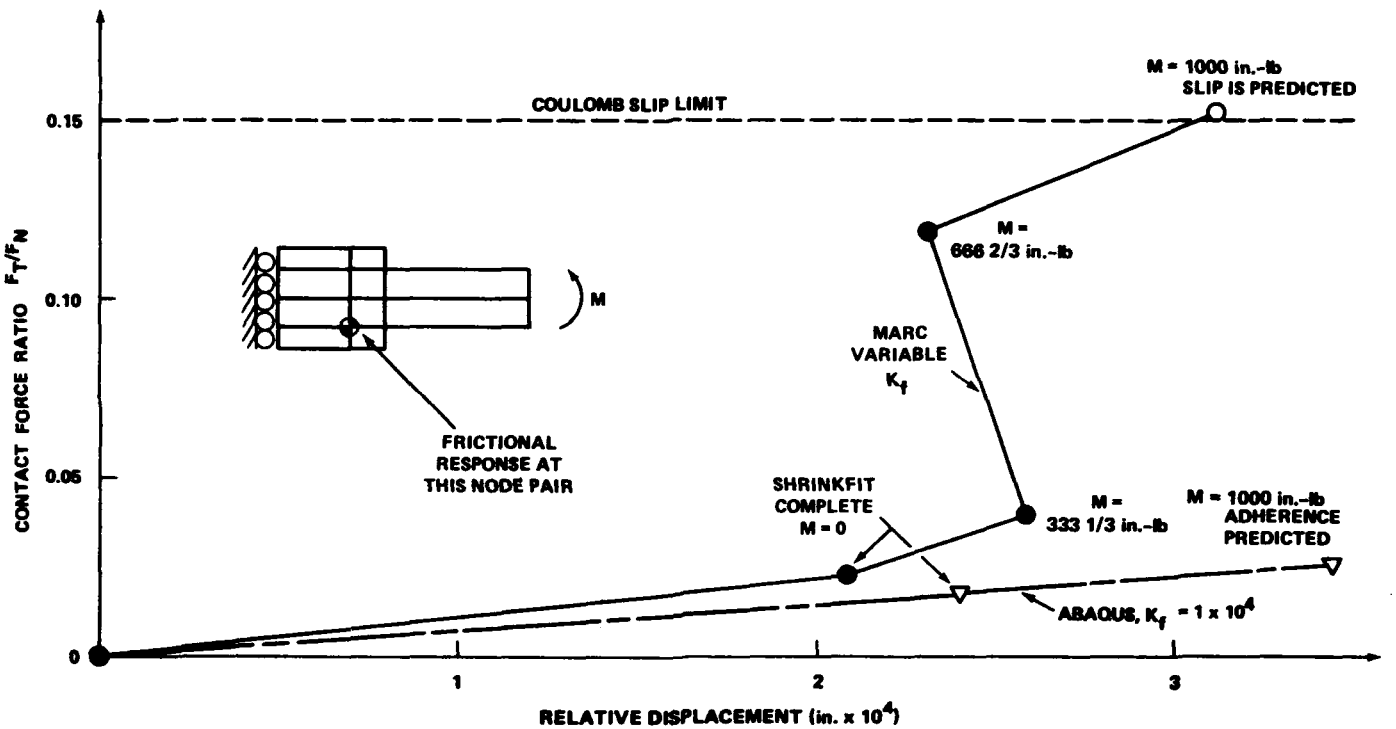

Figure 44 - Failure of ABAQUS Program to Predict Slip Due to Low Frictional Stiffness

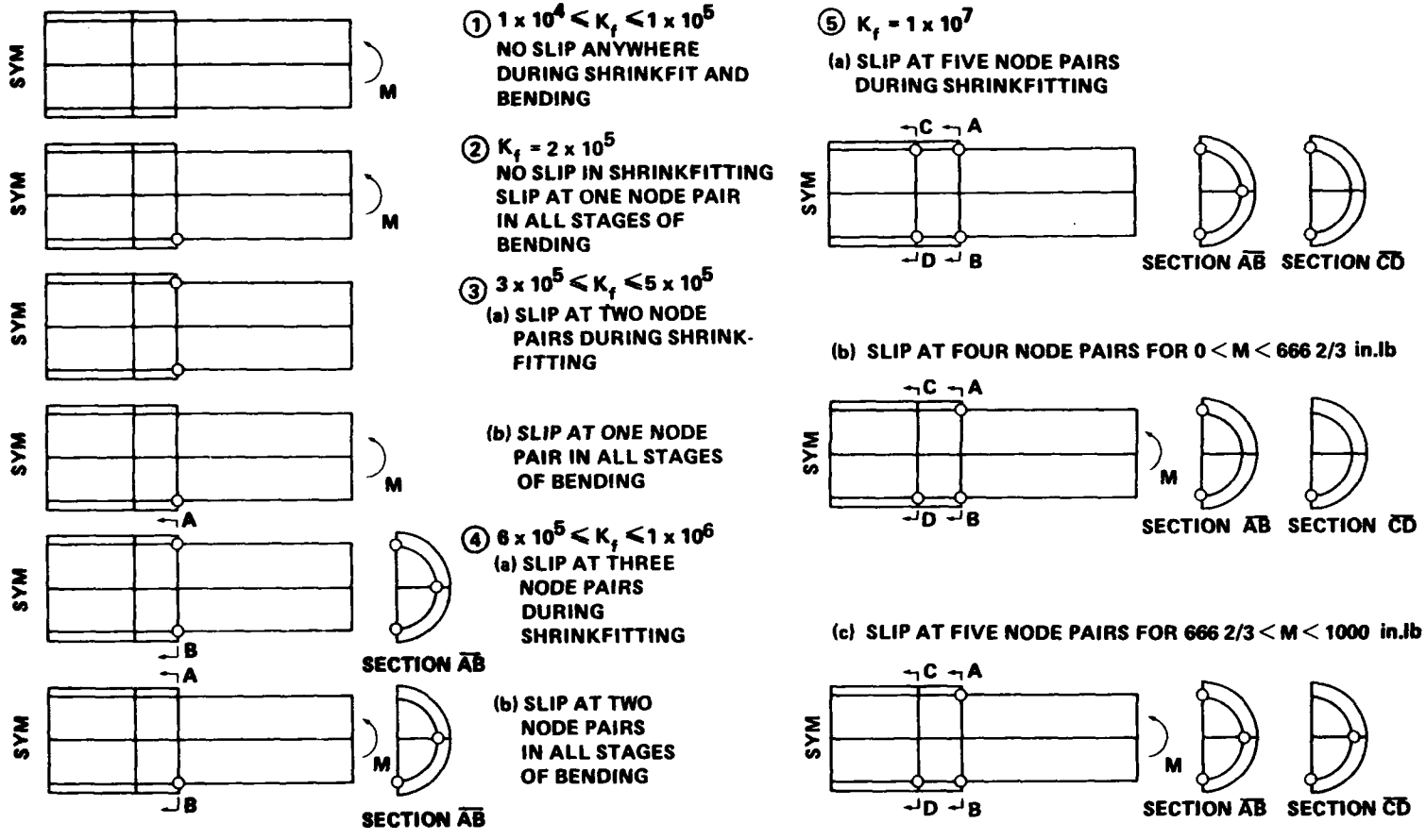

Figure 45 - Coarsely Discretized 3-D Shaft/Sleeve Shrinkfit with Bending and Friction, ABAQUS Frictional Slip Predictions for Various Frictional Stiffnesses

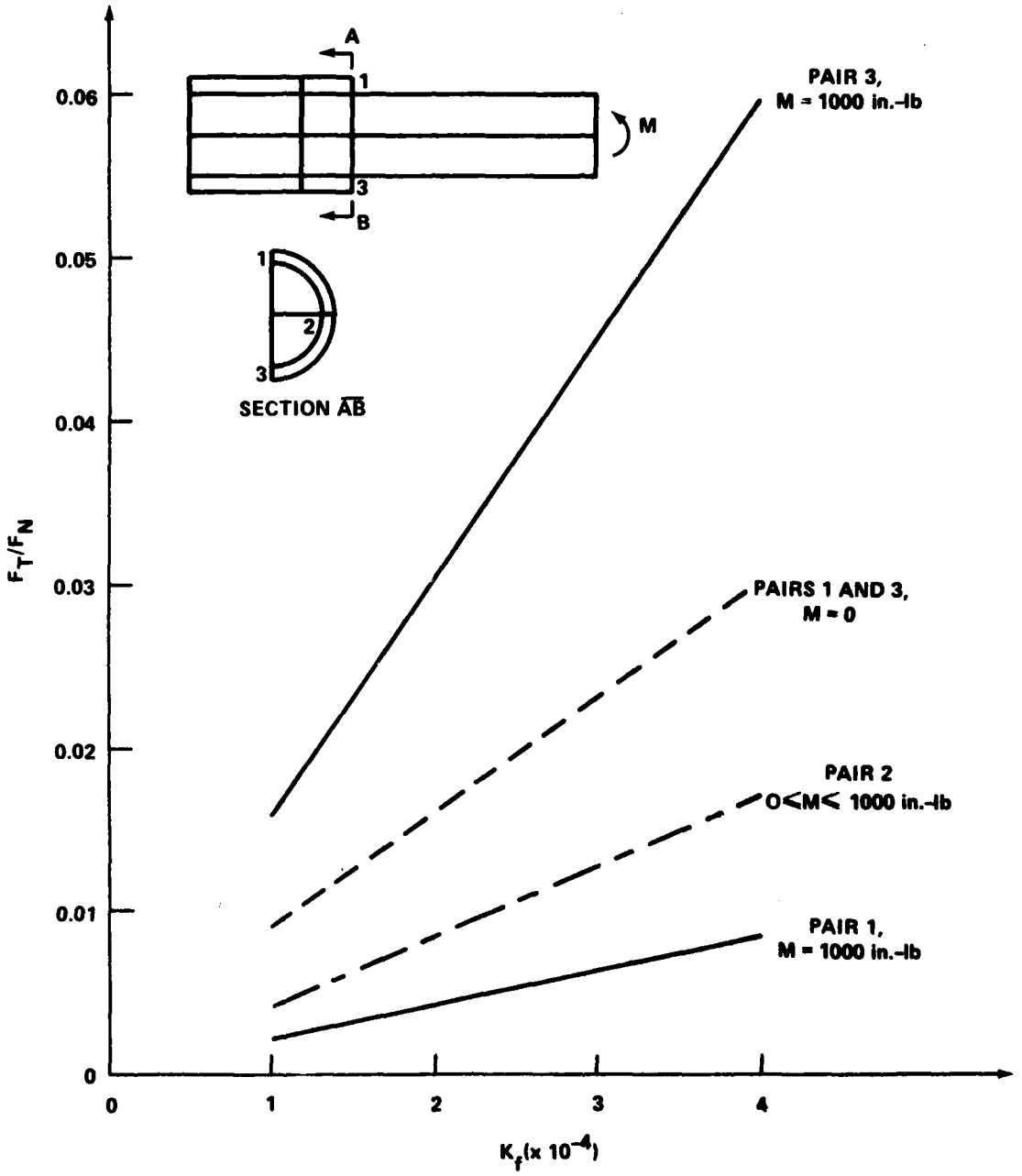

Figure 46 - Coarse 3-D Shrinkfit with Friction and Bending, ABAQUS Contact Force Ratio Predictions in Adherence Regime for Various Frictional Stiffnesses

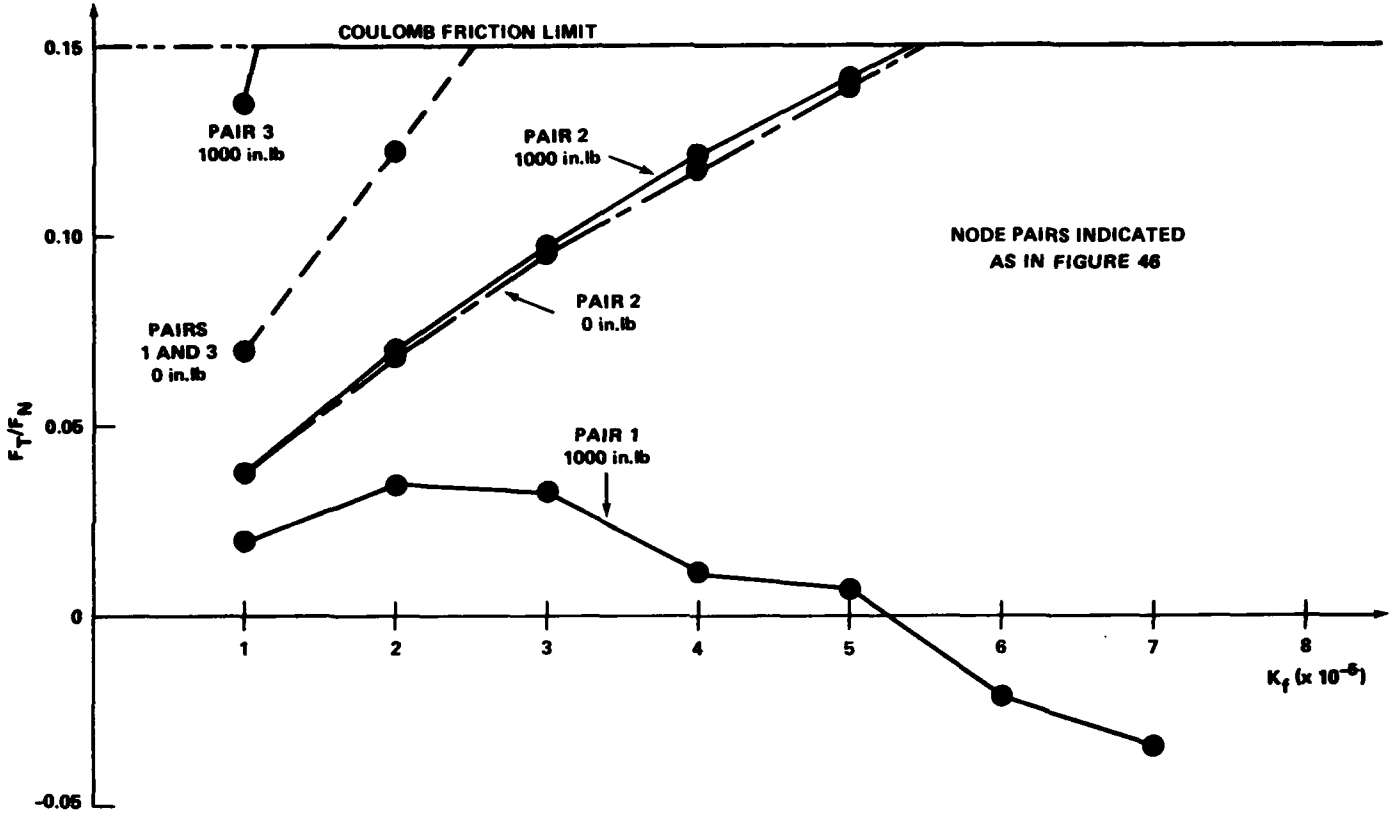

Figure 47 - Coarse 3-D Shrinkfit with Friction and Bending, ABAQUS Contact Force Ratio Predictions in Mixed Slip/Adherence Regime for Various Frictional Stiffnesses

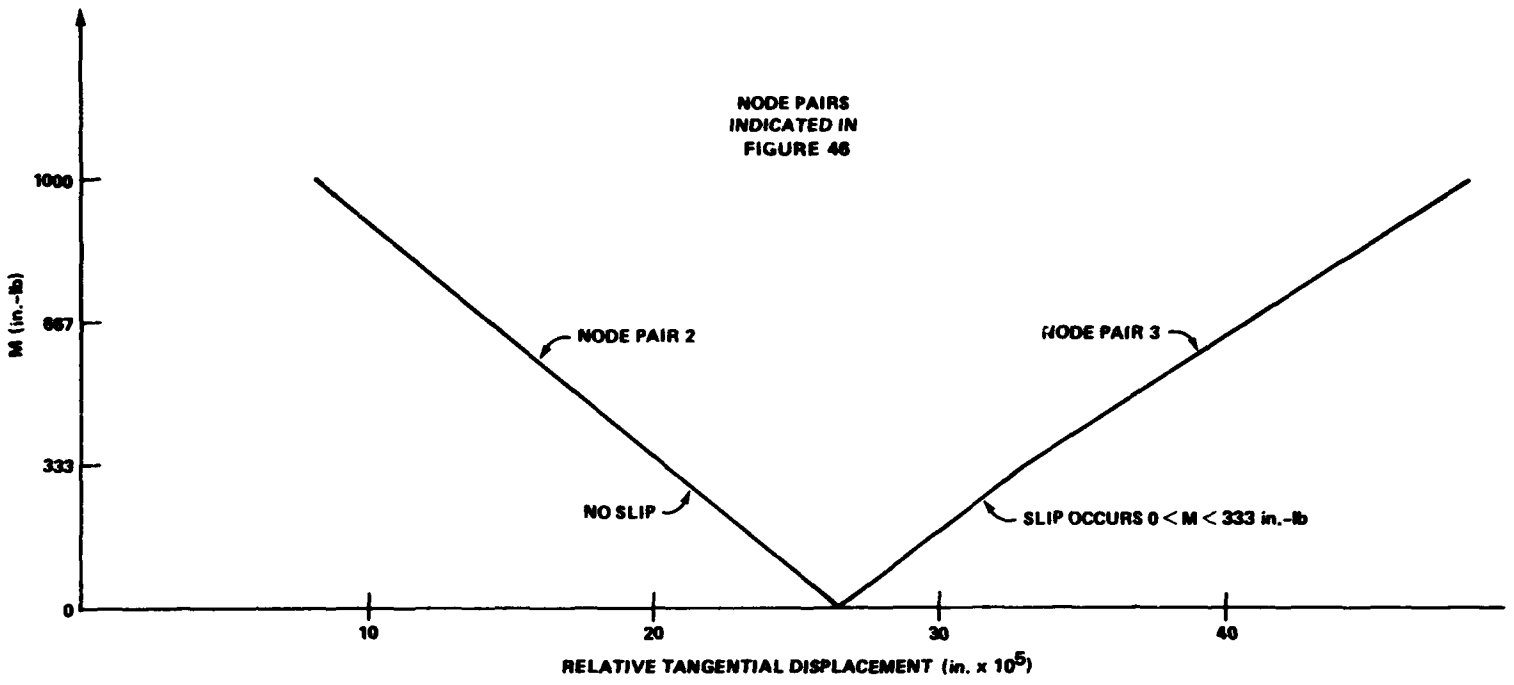

Figure 48 - Coarse 3-D Shrinkfit with Friction and Bending, ABAQUS Relative Tangential Contact Surface Displacement Predictions Versus Bending Load

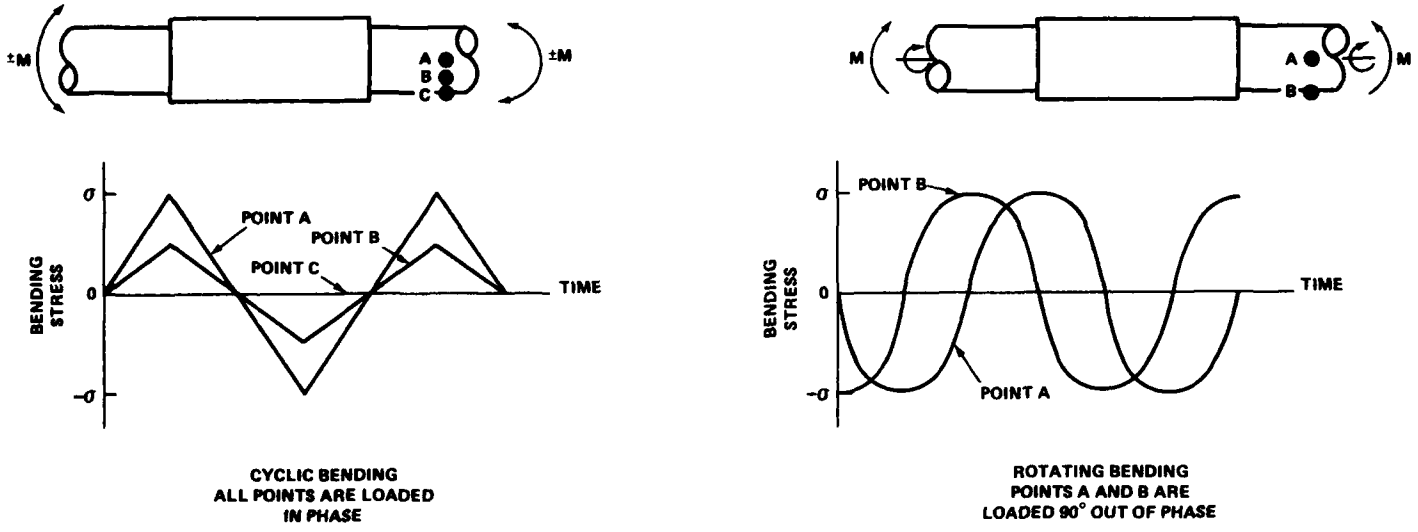

Figure 49 - Illustration of Differences Between Cyclic Bending and Rotating Bending

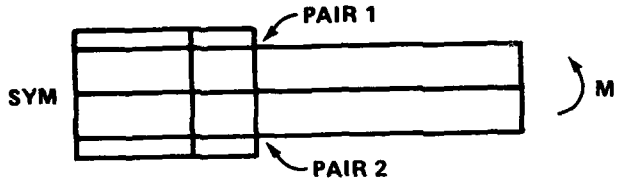

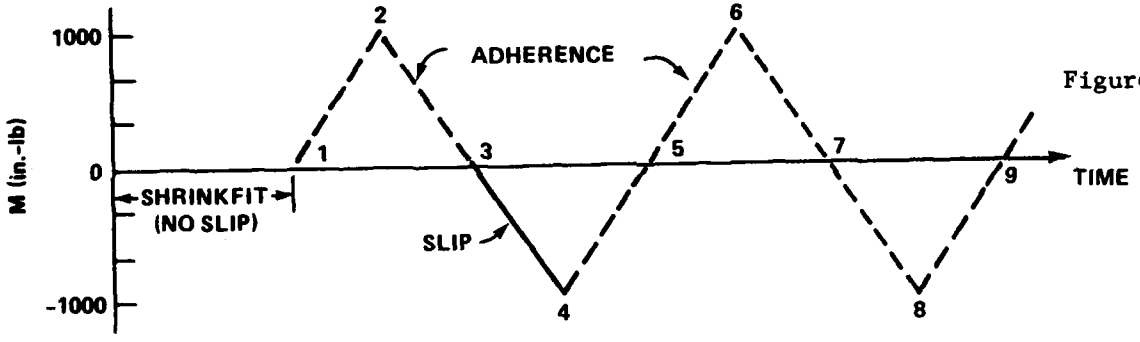

Figure 50a - Slip History at Node Pair 1

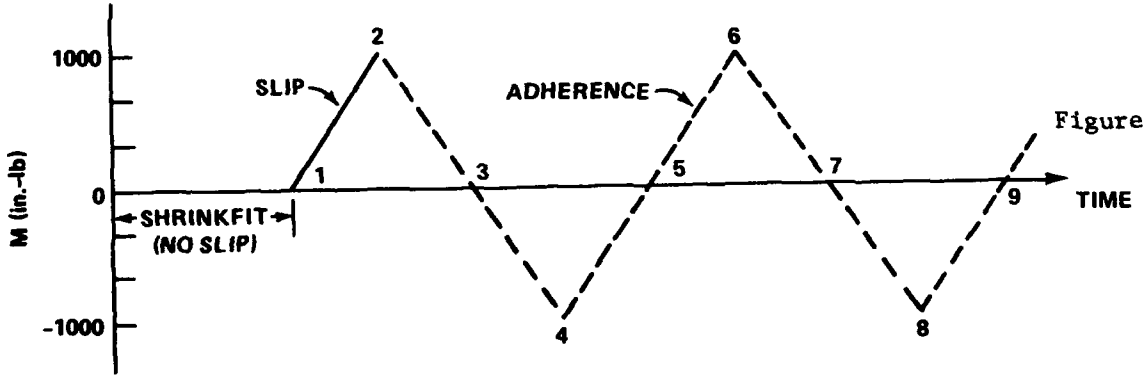

Figure 50b - Slip History at Node Pair 2

Figure 50 - Coarse 3-D Shrinkfit with Friction and Bending, Cyclic Slip Events at Crucial Locations for $K_f = 2 \times 10^5$

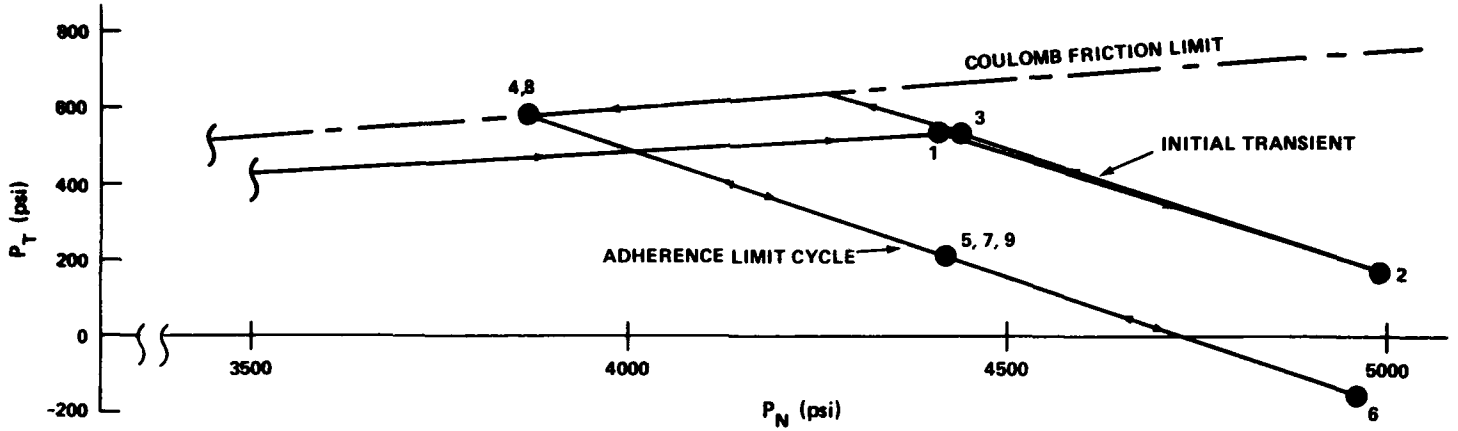

Figure 51a - Response of Node Pair 1 (Fig. 50)

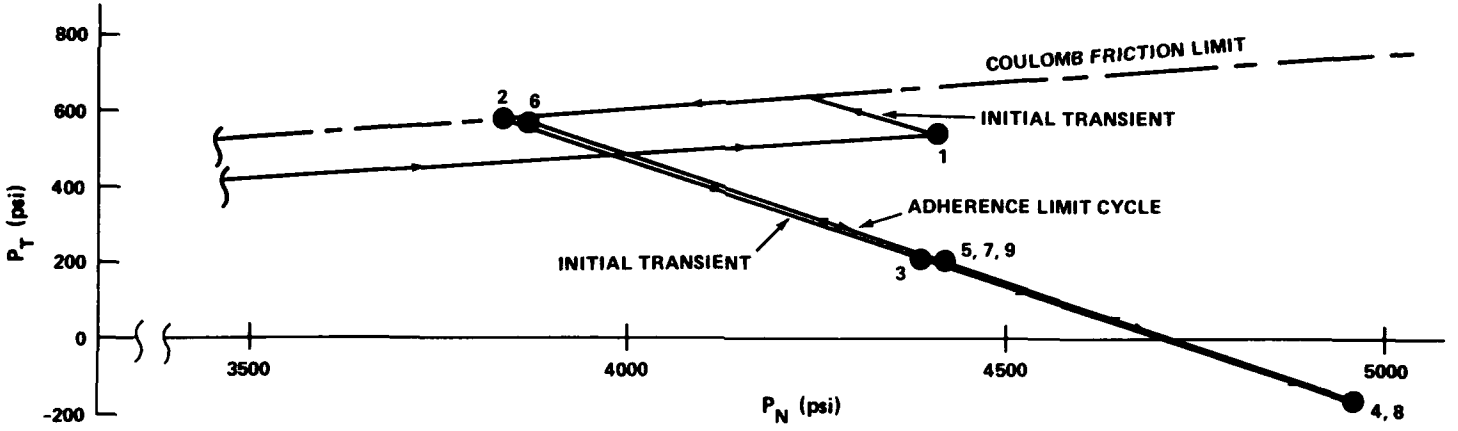

Figure 51b - Response of Node Pair 2 (Fig. 50)

Figure 51 - Coarse 3-D Shrinkfit with Friction and Bending, Cyclic Shear Versus Normal Stress at Crucial Locations for $K_f = 2 \times 10^5$

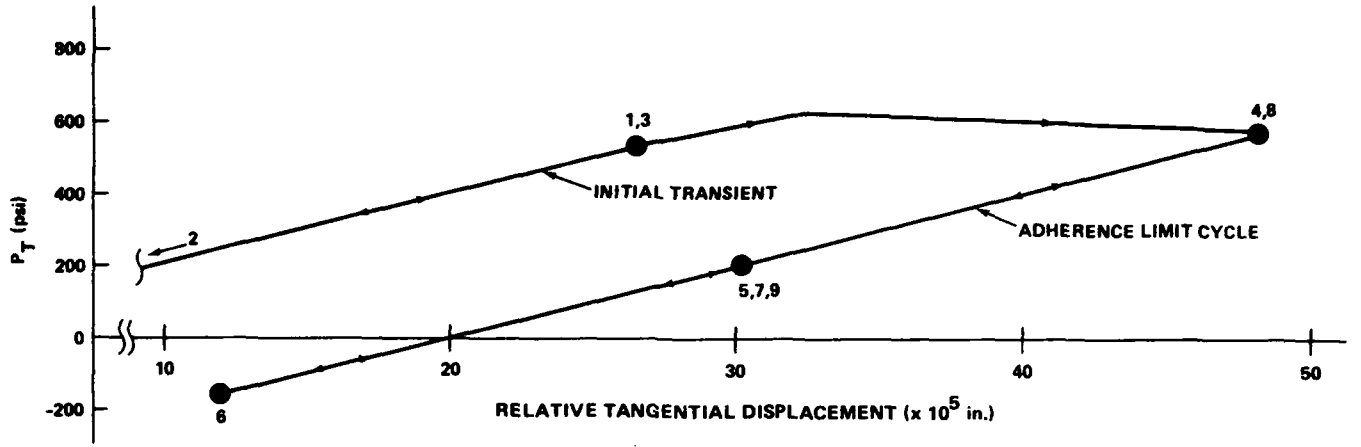

Figure 52a - Response of Node Pair 1 (Fig. 50)

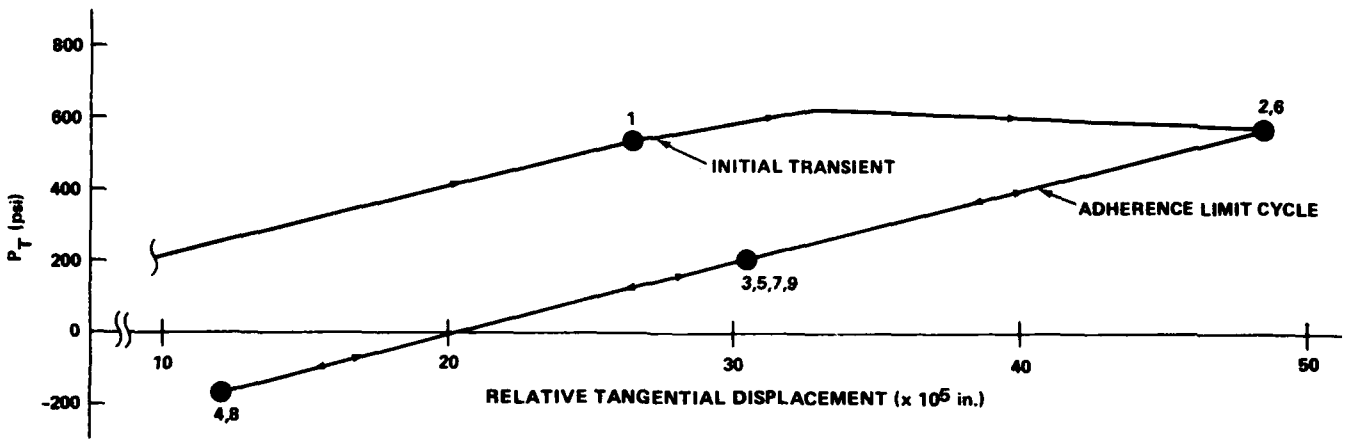

Figure 52b - Response of Node Pair 2 (Fig. 50)

Figure 52 - Coarse 3-D Shrinkfit with Friction and Bending, Cyclic Frictional Shear versus Relative Tangential Displacement at Crucial Locations for K_f = 2×10^5

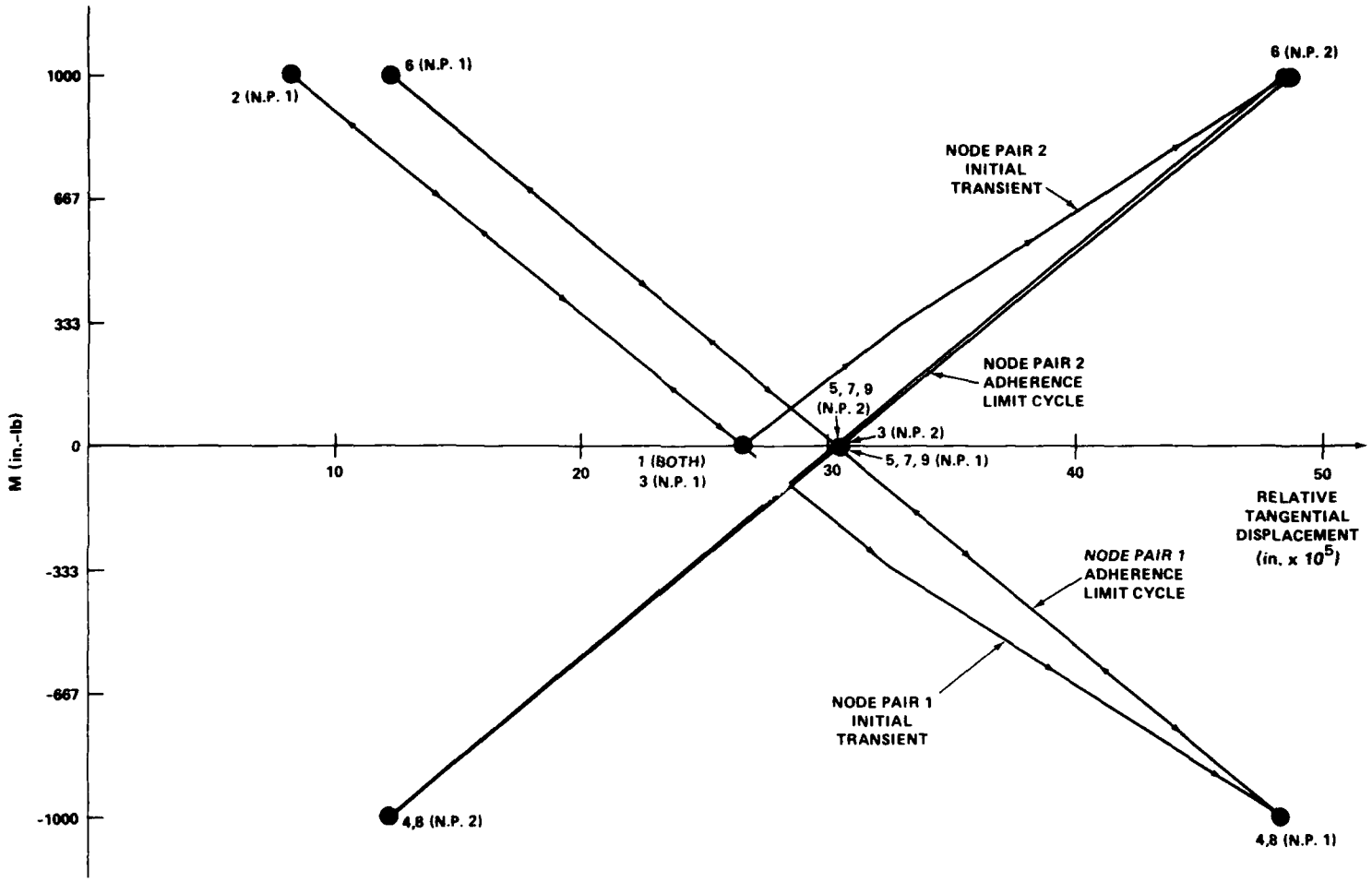

Figure 53 - Coarse 3-D Shrinkfit with Friction Bending, Cyclic Relative Tangential Displacements Versus Bending Load at Crucial Locations for $K_f = 2 \times 10^5$

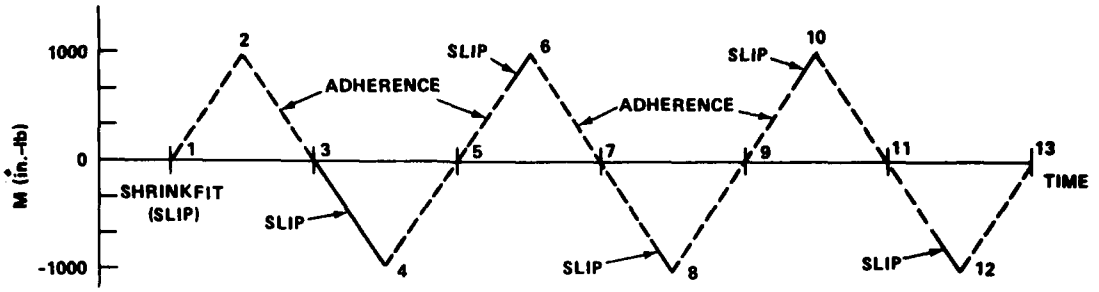

Figure 54a - Slip History at Node Pair 1

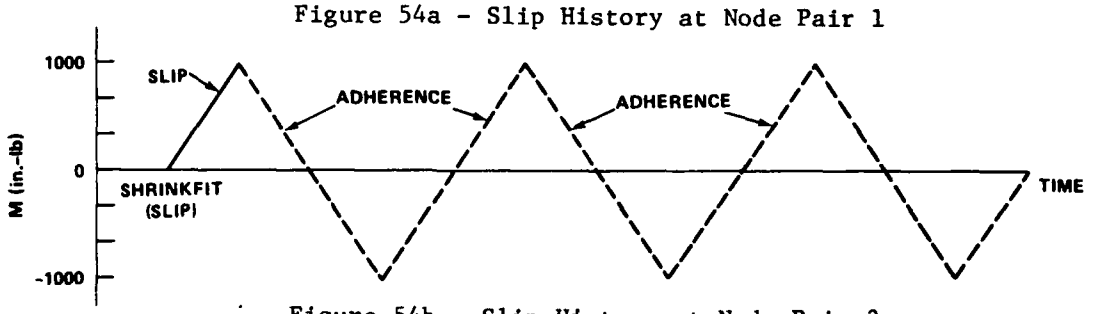

Figure 54b - Slip History at Node Pair 3

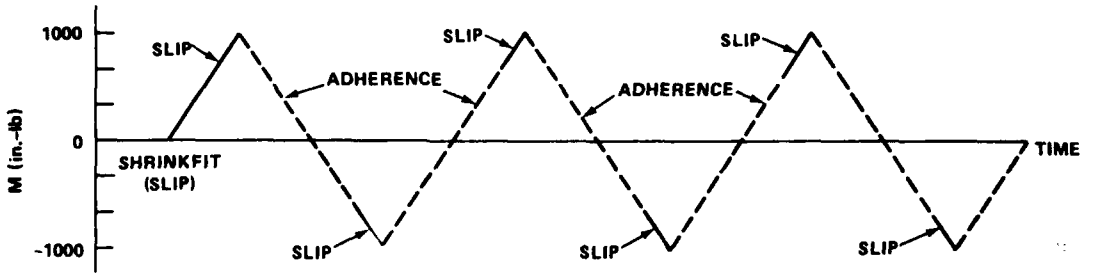

Figure 54c - Slip History at Node Pair 2

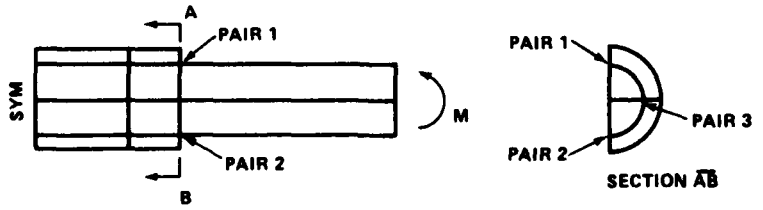

Figure 54 - Coarse 3-D Shrinkfit with Friction and Bending, Cyclic Slip Events at Crucial Locations for $K_f = 6 \times 10^5$

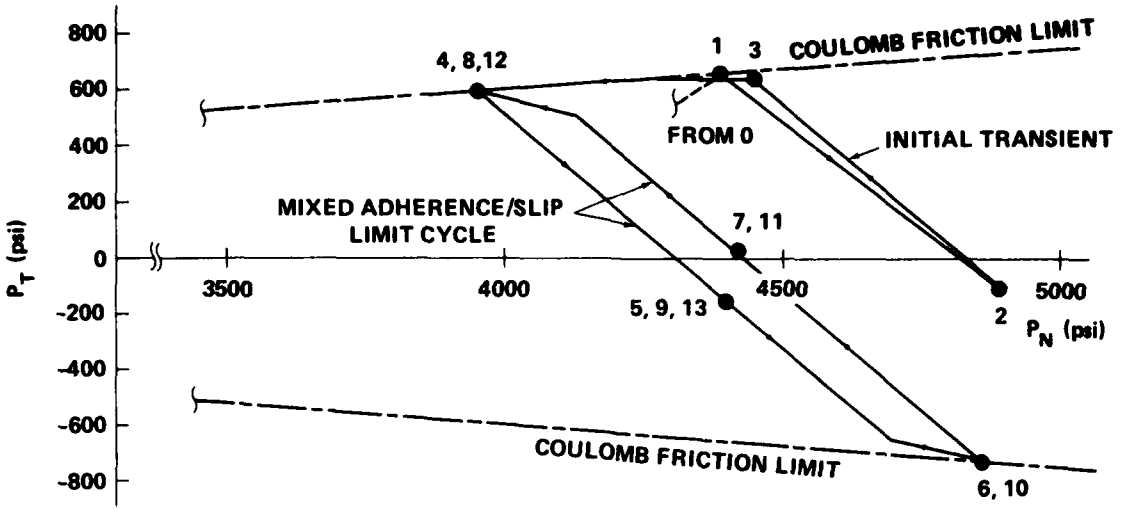

Figure 55a - Response of Node Pair 1 (Fig. 50)

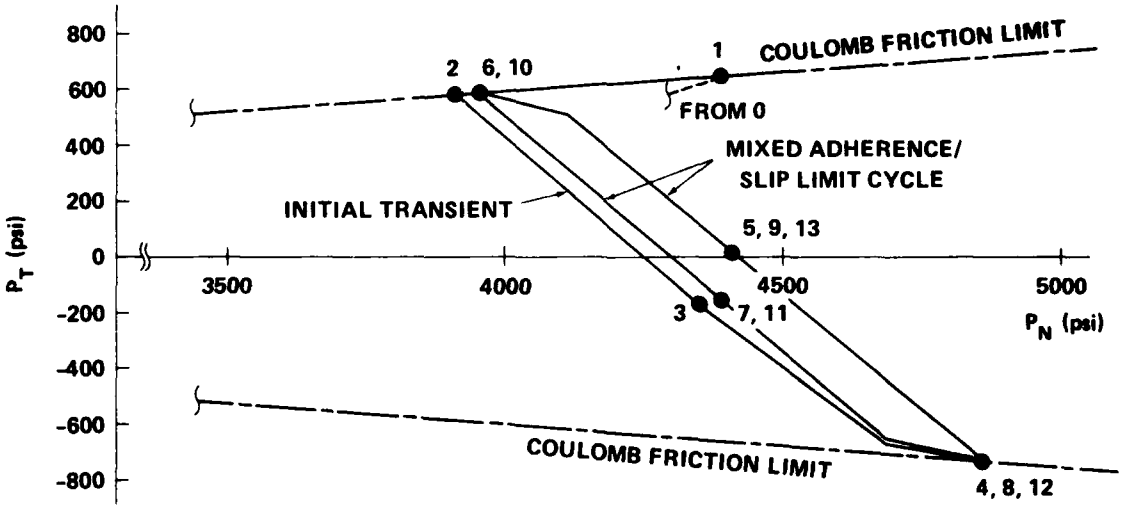

Figure 55b - Response of Node Pair 2 (Fig. 50)

Figure 55 - Coarse 3-D Shrinkfit with Friction and Bending, Cyclic Shear Versus Normal Stress at Crucial Locations for $K_f = 6 \times 10^5$

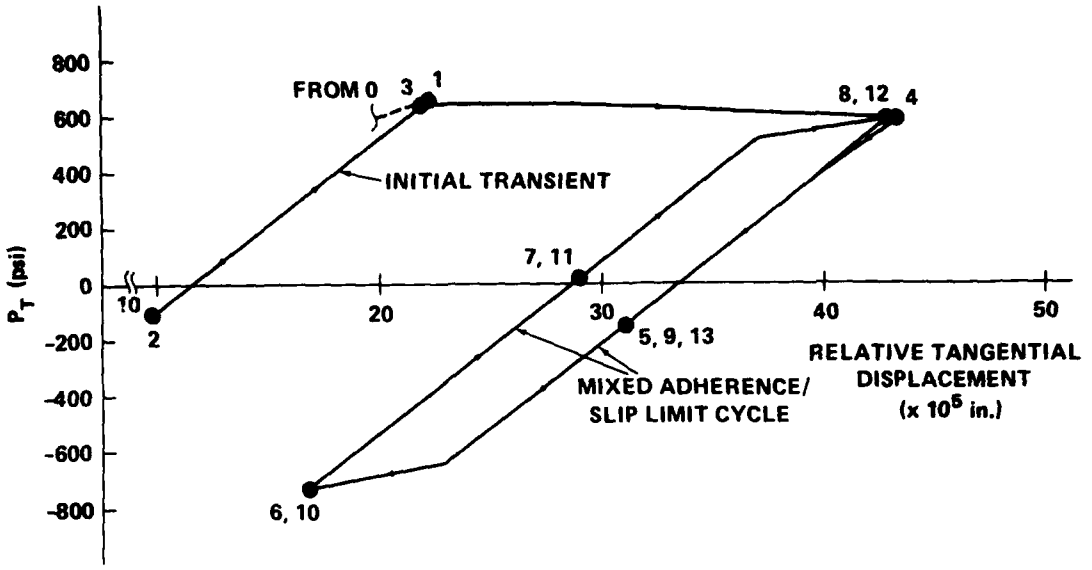

Figure 56a - Response of Node Pair 1 (Fig. 50)

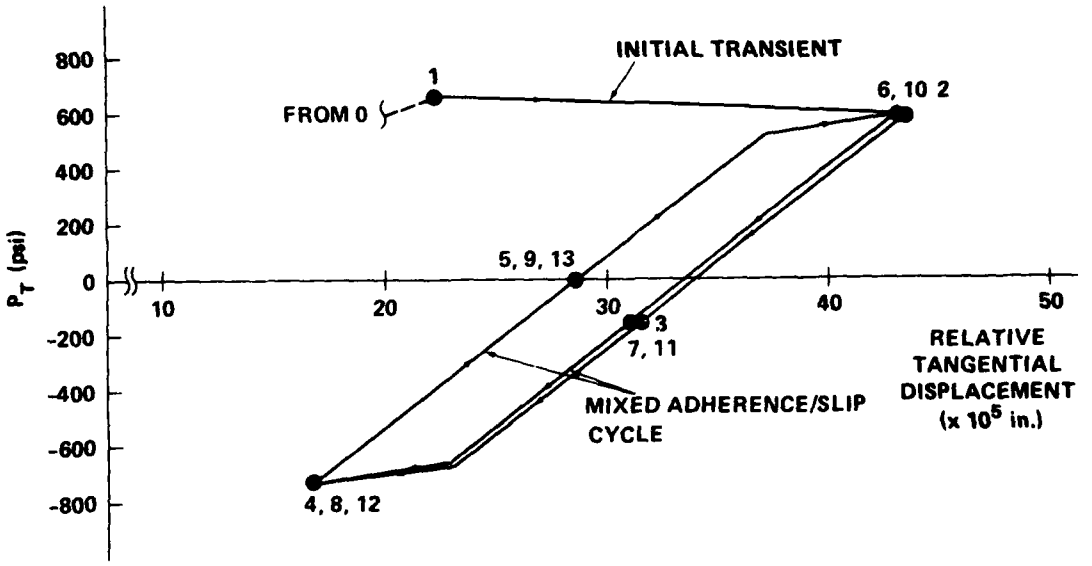

Figure 56b - Response of Node Pair 2 (Fig. 50)

Figure 56 - Coarse 3-D Shrinkfit with Friction and Bending Cyclic Frictional Shear Versus Relative Tangential Displacements at Crucial Locations for $K_f = 6 \times 10^5$

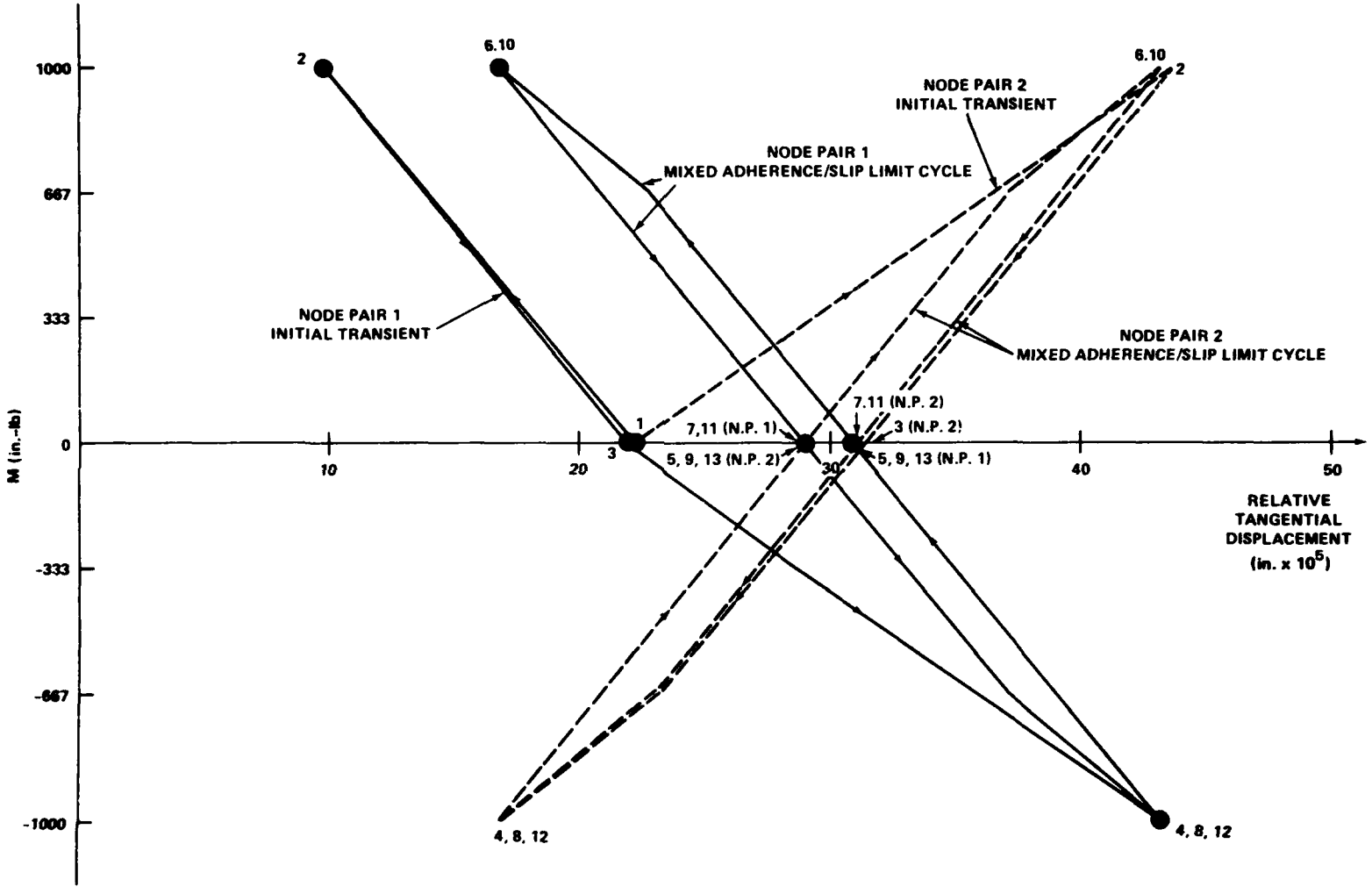

Figure 57 - Coarse 3-D Shrinkfit with Friction and Bending, Cyclic Relative Tangential Displacements Versus Bending Load at Crucial Locations for $K_f = 6 \times 10^5$

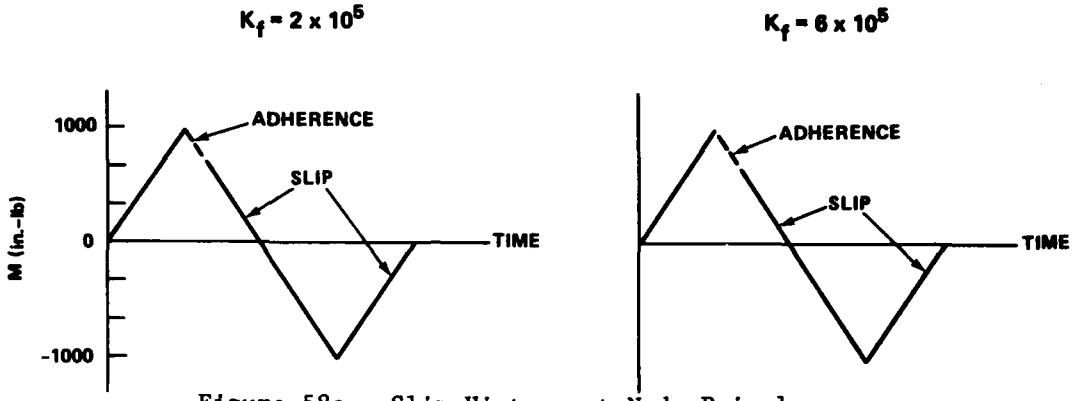

Figure 58a - Slip History at Node Pair 1

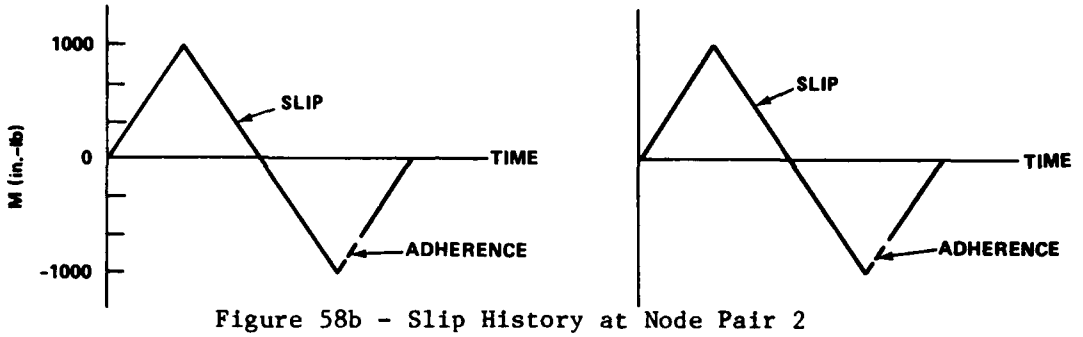

Figure 58b - Slip History at Node Pair 2

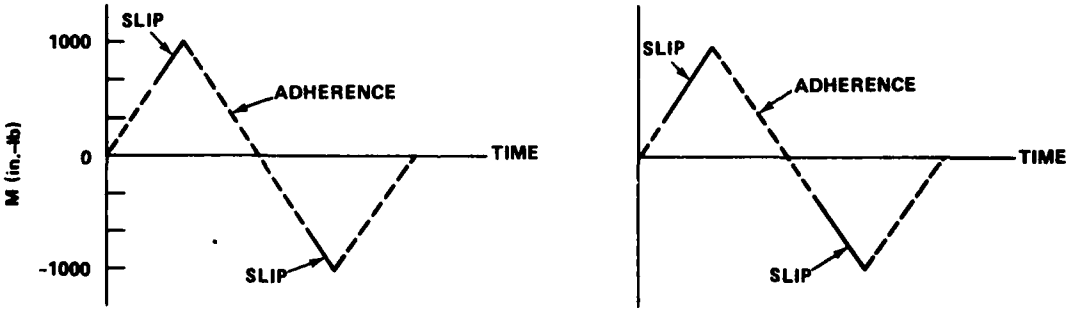

Figure 58c - Slip History at Node Pair 3

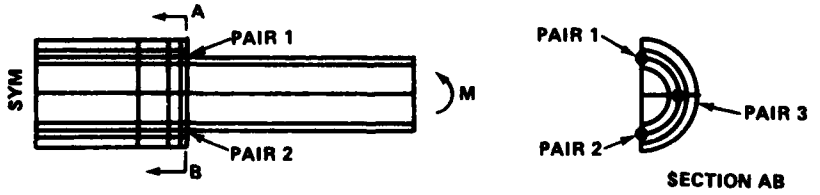

Figure 58 - Finely Discretized 3-D Shrinkfit with Friction and Bending, Comparison of Steady-State Slip Responses for $K_f = 2 \times 10^5$ and 6×10^5 at 1000 Inch-Pound Maximum Bending Load

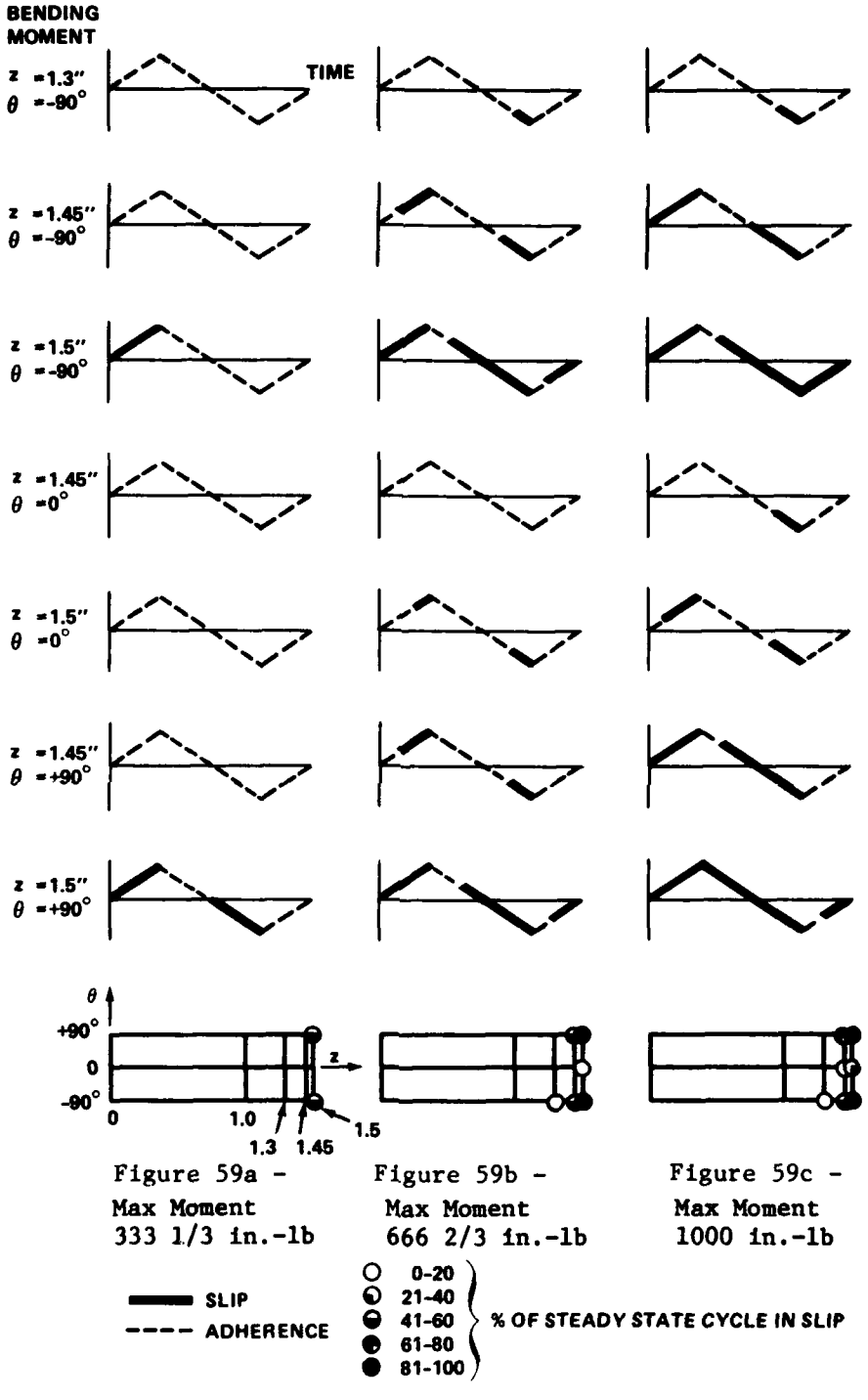

Figure 59a - Max Moment 333 1/3 in.-lb

Figure 59b - Max Moment 666 2/3 in.-lb

Figure 59c - Max Moment 1000 in.-lb

Figure 59 - Fine 3-D Shrinkfit with Friction and Bending, Comparison of Slip Predictions for Three Levels of Maximum Bending Moment for $K_f = 6 \times 10^5$

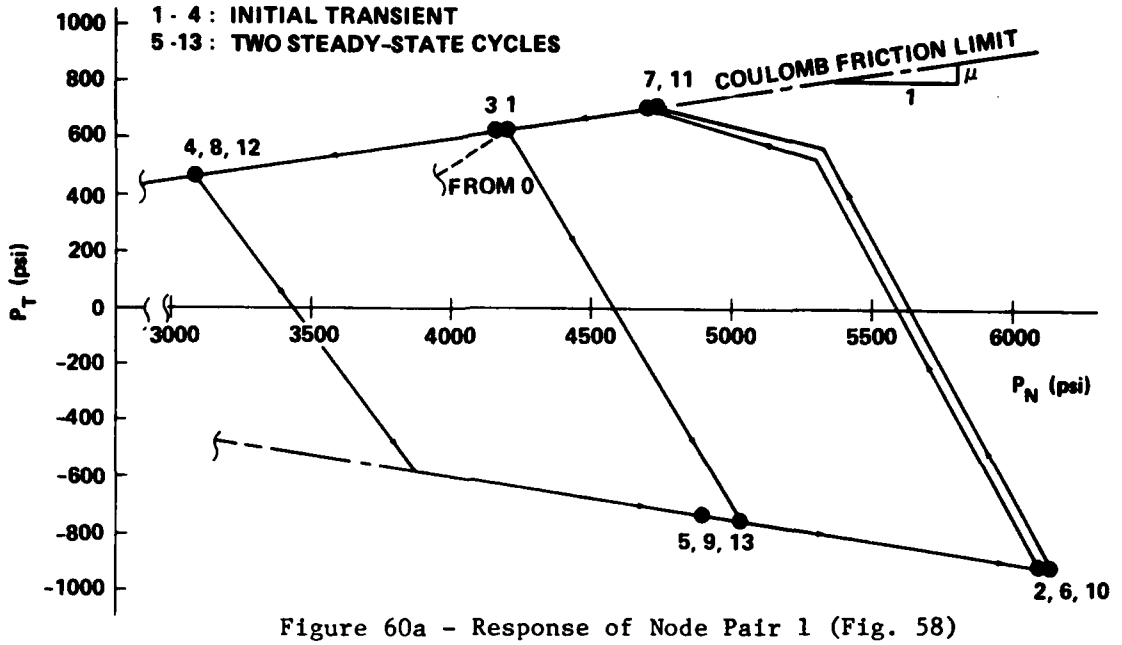

Figure 60a - Response of Node Pair 1 (Fig. 58)

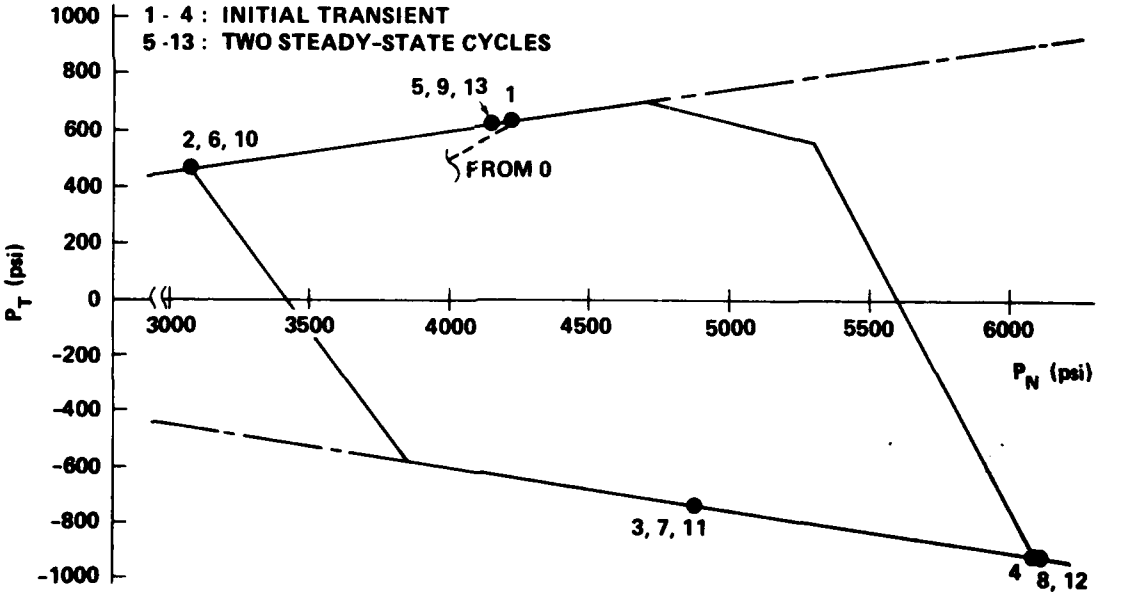

Figure 60b - Response of Node Pair 2 (Fig. 58)

Figure 60 - Fine 3-D Shrinkfit with Friction and Bending, Cyclic Shear Versus Normal Stress at Crucial Locations, $K_f = 6 \times 10^5$, Maximum Bending Load = 1000 Inch-Pounds

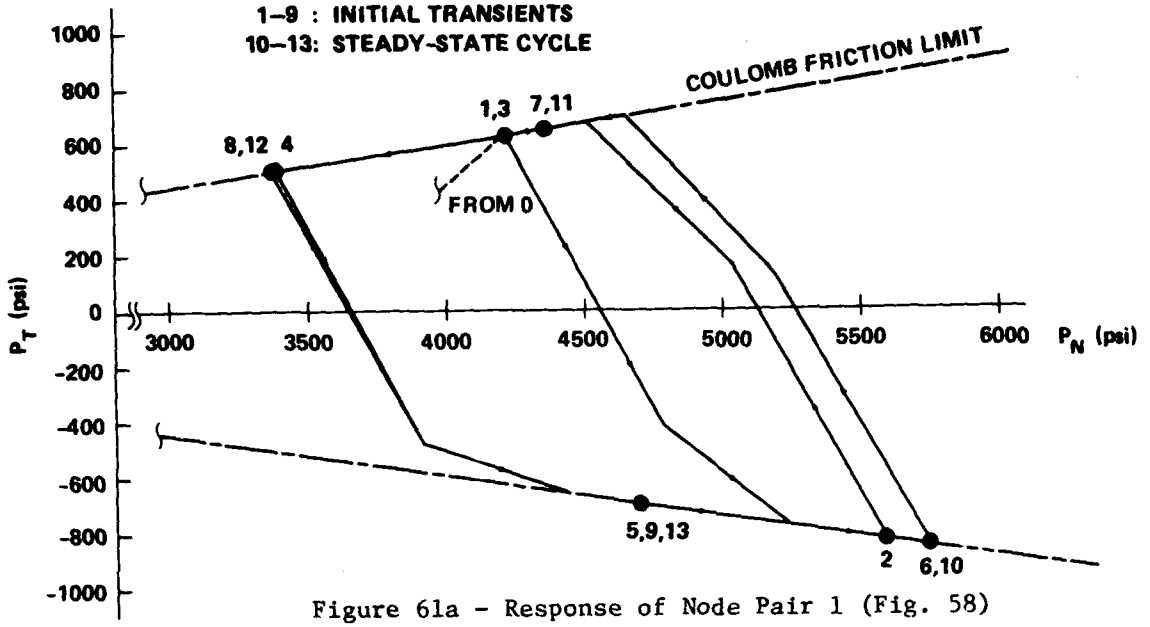

Figure 61a - Response of Node Pair 1 (Fig. 58)

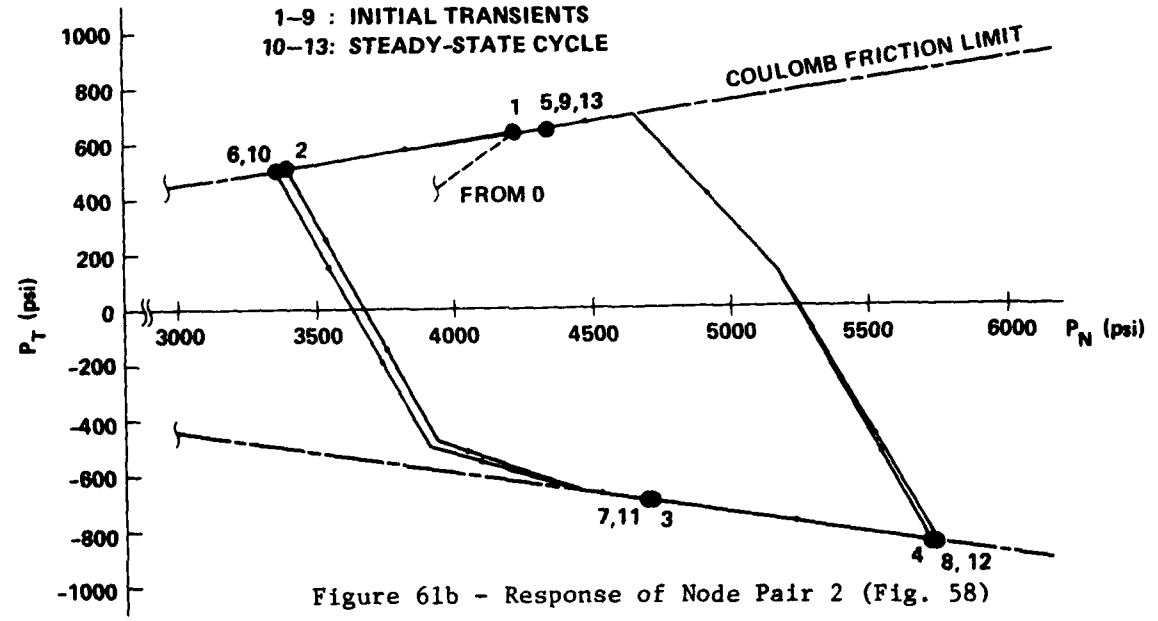

Figure 61b - Response of Node Pair 2 (Fig. 58)

Figure 61 - Fine 3-D Shrinkfit with Friction and Bending, Cyclic Shear versus Normal Stress at Crucial Locations, $K_f = 6 \times 10^5$, Maximum Bending Load = 666 2/3 Inch-Pounds

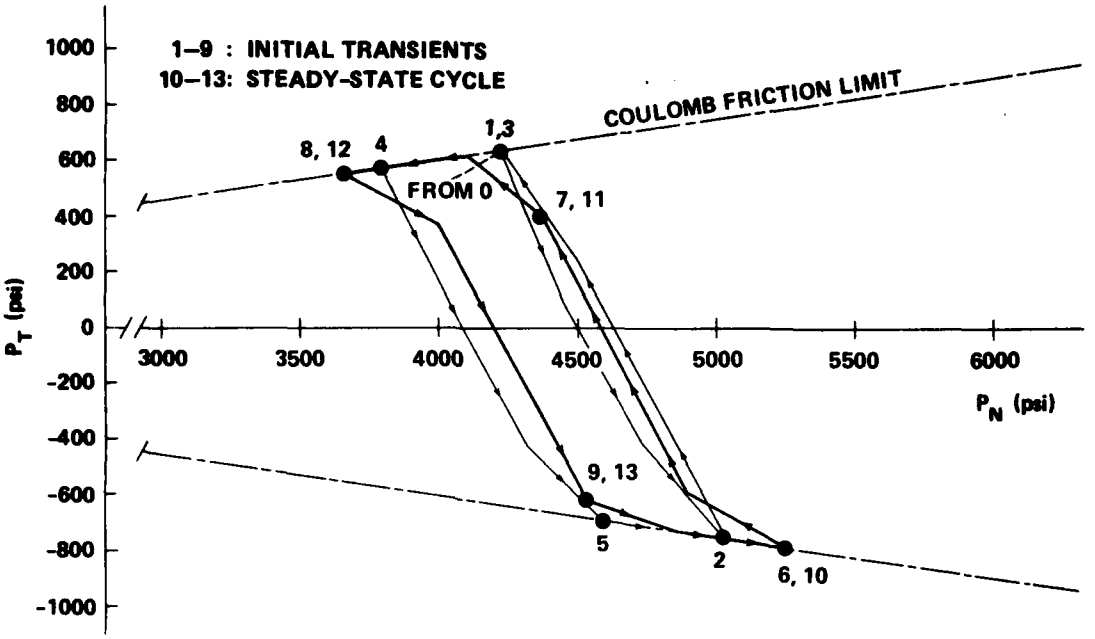

Figure 62a - Response of Node Pair 1 (Fig. 58)

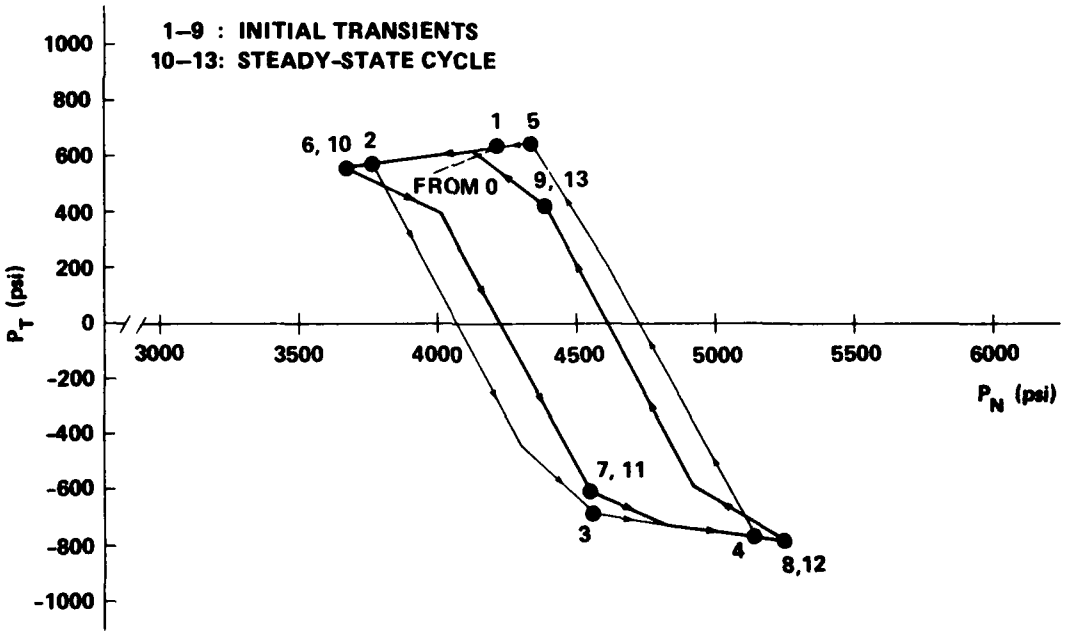

Figure 62b - Response of Node Pair 2 (Fig. 58)

Figure 62 - Fine 3-D Shrinkfit with Friction and Bending, Cyclic Shear Versus Normal Stress at Crucial Locations, $K_f = 6 \times 10^5$, Maximum Bending Load = 333 1/3 Inch-Pounds

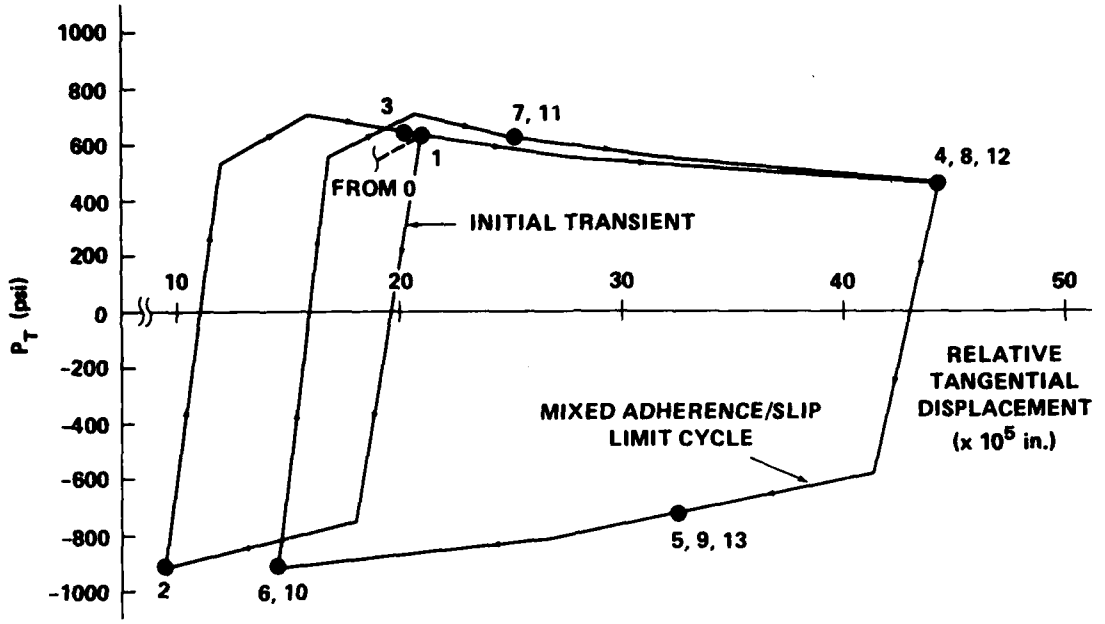

Figure 63a - Response of Node Pair 1 (Fig. 58)

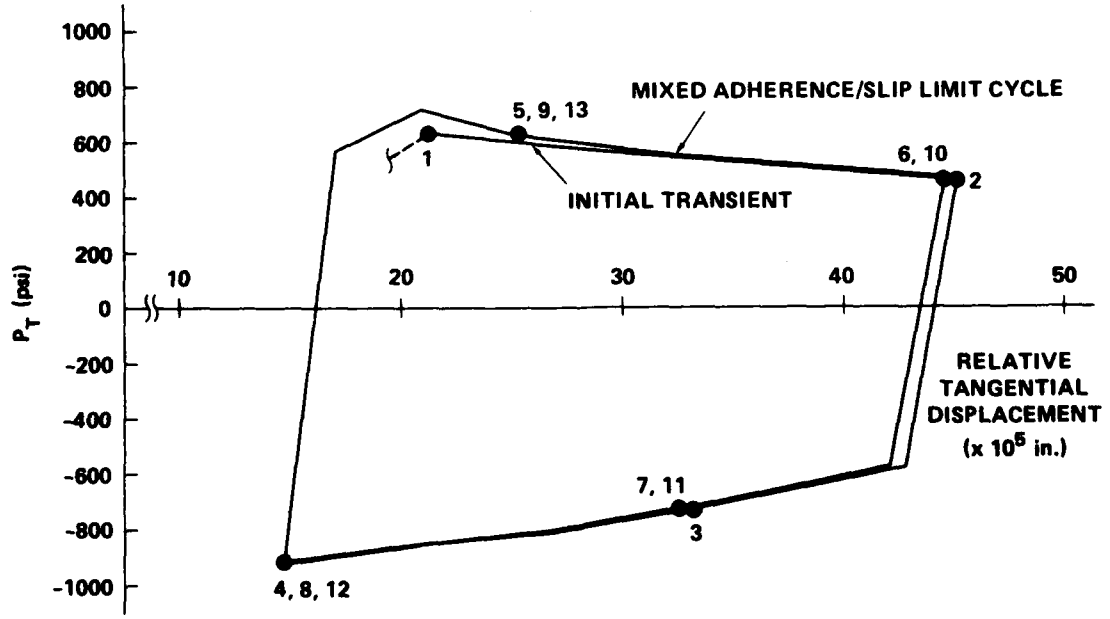

Figure 63b - Response of Node Pair 2 (Fig. 58)

Figure 63 - Fine 3-D Shrinkfit with Friction and Bending, Cyclic Frictional Shear versus Relative Tangential Displacements at Crucial Locations, K_f = 6 x 10^5, Maximum Bending Load = 1000 Inch-Pounds

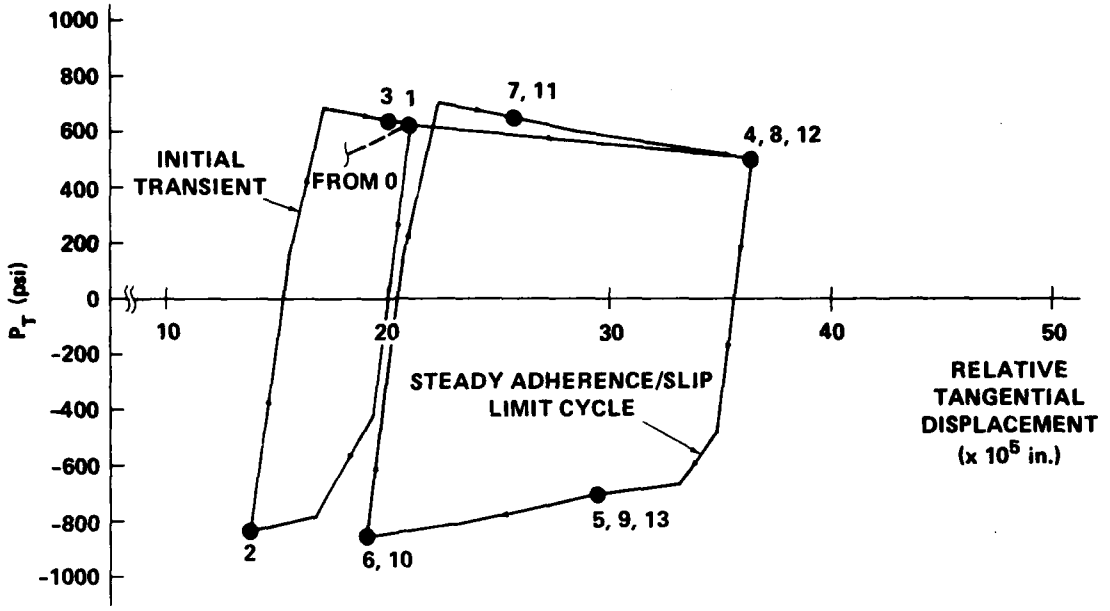

Figure 64a - Response of Node Pair 1 (Fig. 58)

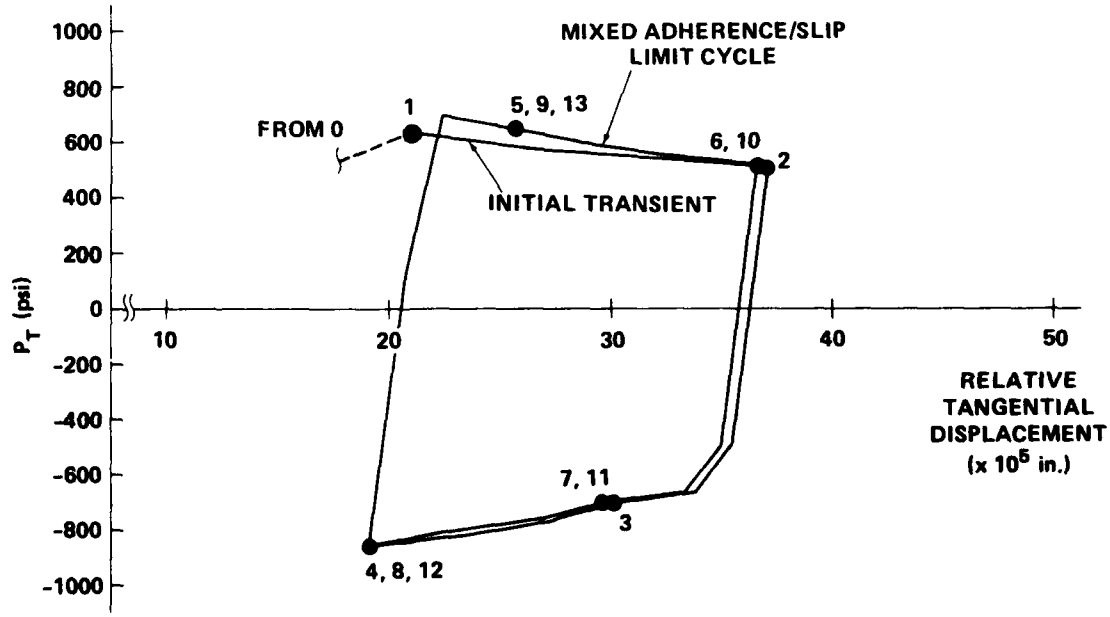

Figure 64b - Response of Node Pair 2 (Fig. 58)

Figure 64 - Fine 3-D Shrinkfit with Friction and Bending, Cyclic Frictional Shear versus Relative Tangential Displacements at Crucial Locations, K_f = 6 x 10^5, Maximum Bending Load = 666 2/3 Inch-Pounds

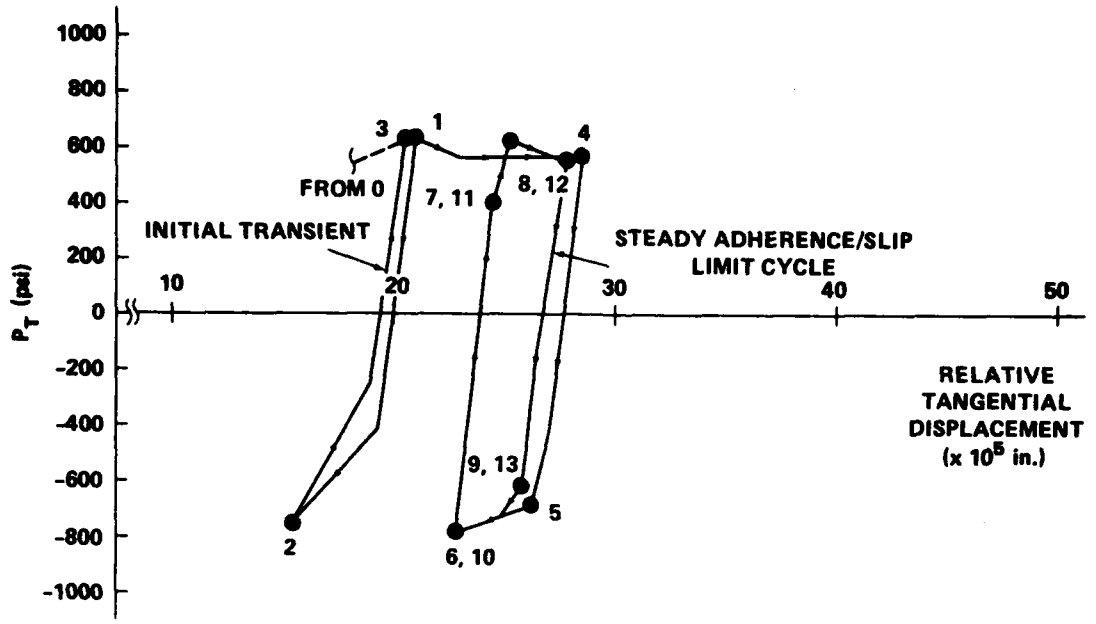

Figure 65a - Response of Node Pair 1 (Fig. 58)

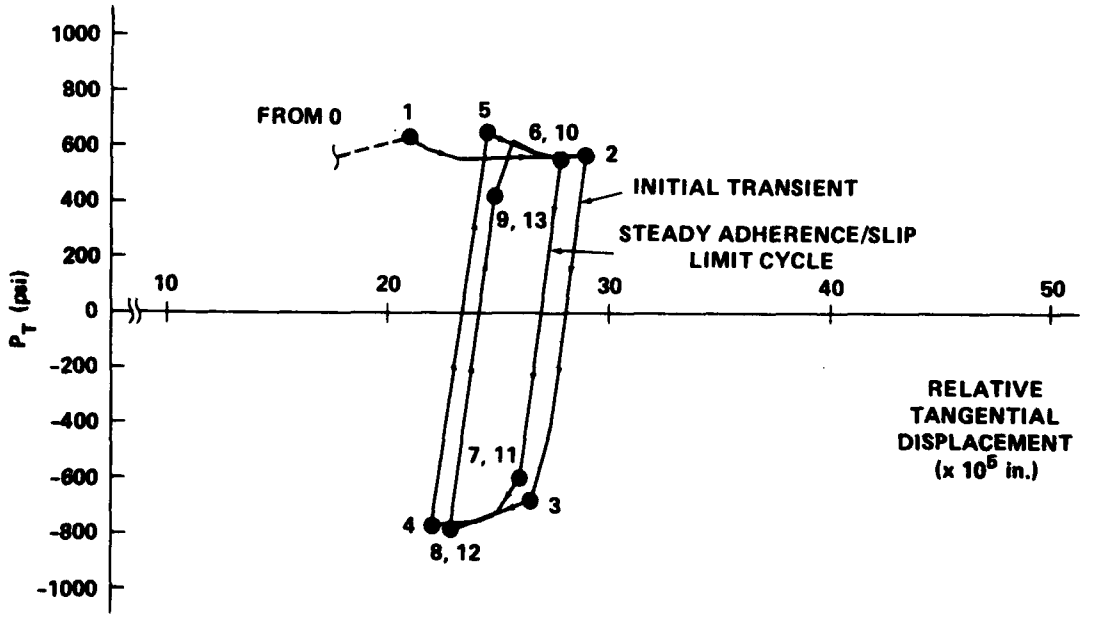

Figure 65b - Response of Node Pair 2 (Fig. 58)

Figure 65 - Fine 3-D Shrinkfit with Friction and Bending, Cyclic Frictional Shear Versus Relative Tangential Displacements at Crucial Locations, K_f = 6 x 10^5, Maximum Bending Load = 333 1/3 Inch-Pounds

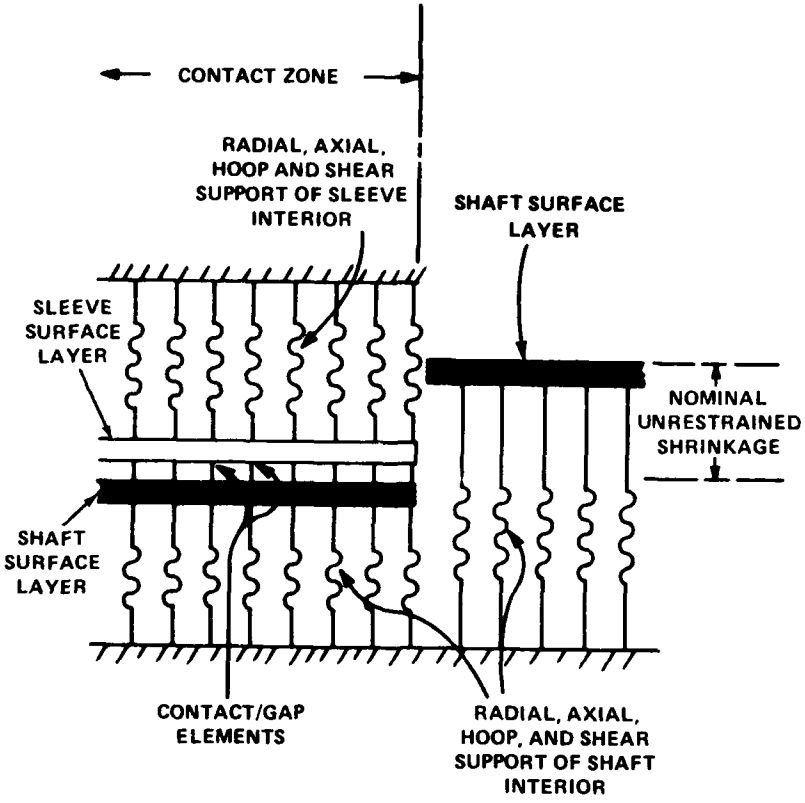

Figure 66a - Shaft/Sleeve System with Discontinuous Shaft Deformation

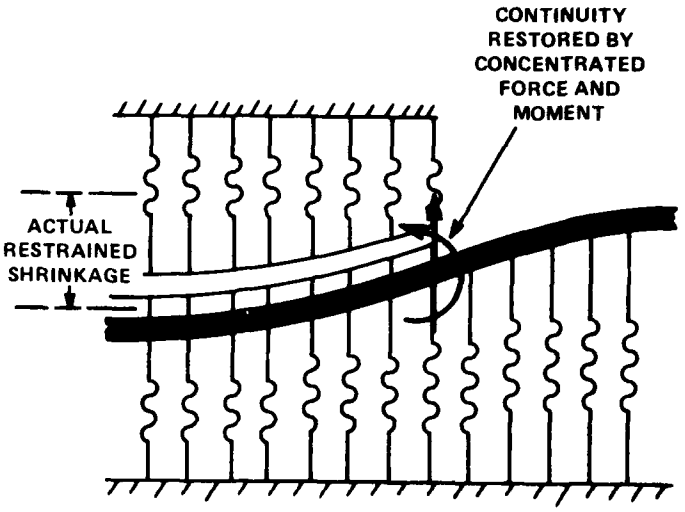

Figure 66b - Shaft/Sleeve System with Displacement Continuity Restored

Figure 66 - Shell on Elastic Foundation Model of Shaft/Sleeve Contact Problem

TABLE 1 - RESULTS OF MARC CALCULATIONS; ATTEMPTS TO SIMULATE CONWAY'S RIGID PUNCH/ELASTIC SLAB FRICTIONAL CONTACT PROBLEM

Friction Coefficient	Approximate % of Adherence (from Ref. 49, see Figure 38)	MARC Result	Validity of MARC Solution
Punch Half Width: Slab Depth = 1:4			
0.60	99	Full Adherence - Converged	Valid
0.50	97	Full Adherence - Slow Convergence	NV*
0.40	90	Full Slip - Slow Convergence	NV
0.30	78	Full Slip - No Convergence	NV
0.20	55	Partial Slip - No Convergence	NV
0.10	14	Full Adherence - Slow Convergence	NV
Punch Half Width: Slab Depth = 1:2			
0.60	99	Full Adherence - Converged	Valid
0.55	98	Full Adherence - Converged	Valid
0.50	97	Full Adherence - Slow Convergence	NV
0.45	94	Full Adherence - Slow Convergence	NV
0.40	90	Full Slip - Slow Convergence	NV
0.35	85	Full Slip - Slow Convergence	NV
0.30	78	Full Slip - No Convergence	NV
0.25	68	Full Slip - No Convergence	NV
0.20	55	Partial Slip - No Convergence	NV
0.15	33	Partial Slip - No Convergence	NV
0.10	14	Full Adherence - Slow Convergence	NV
0.05	4	Full Adherence - Slow Convergence	NV

*NV = Not Valid

TABLE 2 - RESULTS OF MARC CALCULATIONS; CONTACT SURFACE BEHAVIOR OF 3-D ELASTIC SHAFT/ELASTIC SLEEVE SHRINKFIT WITH BENDING AND FRICTION

Ratio F_T/F_N (Tangential Contact Force/Normal Contact Force) Brackets Indicate Slipping Condition				
Node Pair Number*	Shrinkfit and Bending	Shrinkfit and 333 1/3 in-lb	Shrinkfit and 666 2/3 in-lb	Shrinkfit and 1000 in-lb
1	0	0	0	0
2	0.0023	0.0059	0.0879	0.1275
3	0.0184	0.1188	[0.1491]	[0.1501]
4	0	0	0	0
5	0.0017	0.0403	0.0455	0.0523
6	0.0174	0.0549	0.0972	0.1433
7	0	0	0	0
8	0.0023	0.0392	0.1192	[0.1517]
9	0.0184	[0.1645]	[0.1480]	[0.1500]
% Shrinkfit Restraint (Percentage of Prescribed Shrinkfit Restrained by Shaft)				
1	86	85	85	84
2	85	89	94	98
3	87	99	112	125
4	86	86	86	86
5	85	85	85	85
6	87	87	87	87
7	86	65	65	64
8	85	60	55	49
9	87	54	40	25
*Location of Node Pairs.				

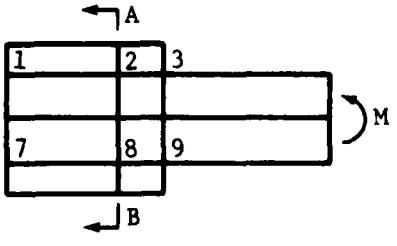

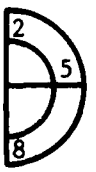

Section AB

TABLE 3 - ABAQUS ANALYSES OF RIGID PUNCH/ELASTIC SLAB CONTACT WITH FRICTION, μ = 0.35

Ratio F_T/F_N (Tangential Contact Force/Normal Contact Force) Brackets Indicate Slipping Condition						
Distance from Center Plane of Symmetry (in.)	Frictional Stiffness (K_f)					
	$3x10^6$	$1x10^7$	$1.1x10^7$	$1.36x10^7$	$1.37x10^7$	$5x10^7$
0.0	0	0	0	0		
0.250	0.017	0.019	0.019	0.019		
0.375	0.040	0.044	0.044	0.045		
0.500	0.054	0.063	0.064	0.065	Noncon-	Noncon-
0.625	0.070	0.087	0.088	0.092	vergent	vergent
0.750	0.114	0.142	0.144	0.150	Solution	Solution
0.8125	0.179	0.226	0.231	0.242		
0.875	0.197	0.276	0.285	0.311		
0.9375	0.212	0.341	[0.350]	[0.350]		
1.0	0.196	[0.350]	[0.350]	[0.350]		

TABLE 4 - ABAQUS ANALYSES OF RIGID PUNCH/ELASTIC SLAB CONTACT WITH FRICTION, $\mu = 0.80$

Ratio F_T/F_N (Tangential Contact Force/Normal Contact Force) Brackets Indicate Slipping Condition				
Distance From Centerplane of Symmetry (in.)	Frictional Stiffness (K_f)			
	1.1×10^7	1.14×10^7	1.15×10^7	1.36×10^7
0.0	0	0		
0.250	0.018	0.018		
0.375	0.041	0.041		
0.500	0.060	0.059	Noncon-	Noncon-
0.625	0.083	0.083	vergent	vergent
0.750	0.135	0.134	Solution	Solution
0.8125	0.214	0.214		
0.875	0.262	0.263		
0.9375	0.319	0.320		
1.0	0.424	0.431		

TABLE 5 - ABAQUS ANALYSES OF RIGID PUNCH/ELASTIC SLAB CONTACT WITH FRICTION, FRICTIONAL STIFFNESS = 1.1×10^7

Ratio F_T/F_N (Tangential Contact Force/Normal Contact Force) Brackets Indicate Slipping Condition						
Distance From Center Plane of Symmetry (in.)	Friction Coefficient (μ)					
	0.10	0.15	0.20	0.35	0.50	0.80
0.0	0	0	0	0	0	0
0.250	0.053	0.036	0.029	0.019	0.018	0.018
0.375	[0.100]	0.132	0.067	0.044	0.041	0.041
0.500	[0.100]	0.128	0.099	0.064	0.060	0.060
0.625	[0.100]	[0.150]	0.143	0.088	0.083	0.083
0.750	[0.100]	[0.150]	[0.200]	0.144	0.135	0.135
0.8125	[0.100]	[0.150]	[0.200]	0.231	0.214	0.214
0.875	[0.100]	[0.150]	[0.200]	0.285	0.262	0.262
0.9375	[0.100]	[0.150]	[0.200]	[0.350]	0.319	0.319
1.0	[0.100]	[0.150]	[0.200]	[0.350]	0.424	0.424

TABLE 6 - COMPARISON OF ABAQUS AND MARC ANALYSES OF COARSELY DISCRETIZED 3-D SHAFT/SLEEVE SHRINKFIT WITH BENDING AND FRICTION

Ratio F_T/F_N (Tangential Contact Force/Normal Contact Force) Axisymmetric Shrinkfit Only						
Node Pair Number*	MARC	ABAQUS Frictional Stiffness (K_f)				
		$1x10^4$	$2x10^4$	$3x10^4$	$4x10^4$	$5x10^4$
1	0	0	0	0	0	0
2	0.0023	0.0019	0.0038	0.0054	0.0071	0.0087
3	0.0184	0.0081	0.0161	0.0230	0.0303	0.0372
4	0	0	0	0	0	0
5	0.0017	0.0009	0.0019	0.0027	0.0036	0.0044
6	0.0174	0.0040	0.0081	0.0177	0.0156	0.0192
7	0	0	0	0	0	0
8	0.0023	0.0019	0.0038	0.0054	0.0071	0.0078
9	0.0184	0.0081	0.0161	0.0230	0.0303	0.0372
Ratio F_T/F_N, Maximum Bending Load 1000 in-lb Brackets Indicate Slipping Condition						
1	0	0	0	0	0	0
2	0.1275	0.0010	0.0021	0.0031	0.0041	0.0051
3	[0.1500]	0.0022	0.0043	0.0063	0.0083	0.0103
4	0	0	0	0	0	0
5	0.0523	0.0009	0.0019	0.0028	0.0036	0.0045
6	0.1433	0.0041	0.0082	0.0121	0.0160	0.0198
7	0	0	0	0	0	0
8	[0.1517]	0.0026	0.0052	0.0076	0.0100	0.0122
9	[0.1500]	0.0157	0.0310	0.0456	0.0597	0.0732

*Location of Node Pairs as Shown in Table 2.

TABLE 7 - FINE 3-D SHRINKFIT WITH FRICTION AND BENDING, COMPARISON OF EXPERIMENTAL FRETTING DAMAGE EXTENT WITH CALCULATED SLIP ZONE EXTENT

Maximum Bending Moment (in./lb)	Extent of Damage Observed in DTNSRDC Rotating Bending Experiment		Extend of Significant Slip Calculated in ABAQUS Cyclic Bending Analysis (in.)
	Average (in.)	Maximum (in.)	
333 1/3	None	None	At Edge Only
666 2/3	0.007	0.010	0.05
1000	0.009-0.011	0.018	0.05

APPENDIX
EDGE EFFECTS IN CONTACT PROBLEMS

An edge effect, in the form of a wiggly radial stress distribution, appears in the extrapolated MARC stress predictions for the elastic shaft/elastic sleeve shrinkfit problem. This same phenomenon was observed in a corresponding elasticity solution.[42] The edge effect was found to be more pronounced as the sleeve thickness become thinner in relation to shaft radius. The thin sleeve is modelled as a thin shell in Hill's work, and the influence of hoop restraint allows the use of a mathematical analogy to a beam on an elastic foundation (reference 73, pp. 30-33). This analogy gives rise to the edge effect.

This edge effect can be explained even for cases where the sleeve is not thin. If the shaft and sleeve surfaces are imagined as two thin shells, then the radial, axial and shear stiffnesses of the components' interiors may be imagined as arrays of attached discrete springs. The hoop restraint of both thick shells can, according to the analogy, be represented by a continuous elastic foundation. Both shaft and sleeve are now beams on elastic foundations, and the total effects of all spring and foundation restraint can be schematically pictured as two arrays of springs (Figure 70a).

This conceptual assembly of beams on foundations is now subject to the displacement condition that corresponds to the specified shrinkfit interference (the distance the sleeve would radially contract if unconstrained). This results in a physically impossible deformation as shown in Figure 66a. Displacement continuity can be restored by a concentrated force and moment at the sleeve edge, shown in Figure 66b. The shear force and bending moment patterns in beam/foundation assemblies take on the character of damped waves when acted upon by concentrated forces and moments (reference 73, Page 14). These disturbances gradually die out away from the loaded point. This fact explains, in part, why the stress distributions in the 3-D shaft/sleeve assembly are wiggly near the contact zone edge. It is a natural consequence of the localized forces needed to maintain displacement continuity at this edge.

The finite element procedure automatically accounts for such forces so that both continuity and equilibrium are maintained. The predicted displacements reflect some actual restrained shrinkage compatible with both the local and overall stiffnesses of both shaft and sleeve. Interior radial support of shaft and sleeve

augments the hoop restraint in the fictitious foundation quite directly, but the effects of axial and shear restraint on the beam-on-foundation wiggles are difficult to assess. The beam-on-foundation analogy is not perfect, but it at least provides a sensible explanation for the predicted wiggly stress distributions.

REFERENCES

1. Timoshenko, S. P. and J. N. Goodier, "Theory of Elasticity," 3rd Edition, McGraw-Hill Book Co. Inc., New York (1970).

2. "Handbook of Engineering Mechanics," Edited by W. Flugge, McGraw-Hill Book Co. Inc., New York (1962), "Contact Problems," (J. L. Lubkin), Chapter 42.

3. Love, A. E. H., "A Treatise on the Mathematical Theory of Elasticity," 4th Edition, Dover Publications Inc., New York (1944).

4. Shtaerman, I. Ya., "The Contact Problem of Elasticity Theory" (in Russian), Moscow-Leningrad (1949).

5. Galin, L. A. "Contact Problems in the Theory of Elasticity," Translated by H. Moss, Edited by I. N. Sneddon, Department of Mathematical Engineering Research, North Carolina State College, Raleigh (1961).

6. Lurye, A. I., "Three Dimensional Problems of Elasticity Theory," (in Russian), Moscow-Leningrad (1955).

7. Conway, H. D. and K. A. Farnham, "The Relationship Between Load and Penetration for a Rigid, Flat-Ended Punch of Arbitrary Cross Section," International Journal of Engineering Science, Vol. 6, No. 9, pp. 489-496, (Sep 1968).

8. Updike, D. P. and A. Kalnins, "Contact Pressure Between an Elastic Spherical Shell and Rigid Plate," Journal of Applied Mechanics, Vol. 39, No. 4, pp. 1110-1114 (Dec 1972).

9. Keer, L. M. et al., "Problems Involving a Receding Contact Between a Layer and a Half Space," Journal of Applied Mechanics, Vol. 39, No. 4, pp. 1115-1120 (1972).

10. Gladwell, G. M. L., "On Some Unbonded Contact Problems in Plane Elasticity Theory," Journal of Applied Mechanics, Vol 2, No. 43, pp. 263-267, (Jun 1976).

11. Steven, G. P., "A Non-Axisymmetric Cylindrical Contact Problem," International Journal of Engineering Science, Vol. 15, No. 2, pp. 99-103, (Feb 1977).

12. Gecit, M. R. and F. Erdogan, "Frictionless Contact Problem for an Elastic Layer under Axisymmetric Loading," International Journal of Solids and Structures, Vol. 14, No. 9, pp. 771-785 (Sep 1978).

13. Hardy, C. et al., "The Elasto-Plastic Indentation of a Half-Space by a Rigid Sphere," International Journal for Numerical Methods in Engineering, Vol. 3, No. 4, pp. 451-462, (Oct-Dec 1971).

14. Francavilla A. and O. C. Zienkiewicz, "A Note on Numerical Computation of Elastic Contact Problems," International Journal for Numerical Methods in Engineering, Vol. 9, No. 4, pp. 913-924, (Oct-Dec 1975).

15. Parsons, B. and E. A. Wilson, "A Method for Determining the Surface Contact Stresses Resulting from Interference Fits," Journal of Engineering for Industry, Vol. 92, No. 1, pp. 208-218 (Feb 1970).

16. Wilson, E. A. and B. Parsons, "Finite Element Analysis of Elastic Contact Problems Using Differential Displacements," International Journal for Numerical Methods in Engineering, Vol. 2, No. 3, pp. 387-395, (Jul-Sep 1970).

17. Gangal, M. K., "Direct Finite Element Analysis of Elastic Contact Problems," International Journal of Numerical Methods in Engineering, Vol. 5, No. 1, pp. 145-147, (Sep-Oct 1972).

18. Chan, S. K. and I. S. Tuba, "A Finite Element Method for Contact Problems of Solid Bodies - Part I. Theory and Validation and Part II. Application of Turbine Blade Fastenings," International Journal of Mechanical Sciences, Vol. 13, No. 7, pp. 615-639 (Jun 1971).

19. Ohte, S. "Finite Element Analysis of Elastic Contact Problems," Bulletin of the Japan Society of Mechanical Engineers, Vol 16, No. 95, pp. 797-804, (May 1973).

20. Gaertner, R., "Investigation of Plane Elastic Contact Allowing for Friction," Computers and Structures, Vol. 7, No. 1, pp. 59-63, (Feb 1977).

21. Okamoto, N. and M. Nakazawa, "Finite Element Incremental Contact Analysis with Various Frictional Conditions," International Journal for Numerical Methods in Engineering, Vol. 14, No. 3, pp. 337-357, (Mar 1979).

22. Hibbitt, H. D. and D. M. Rubin, "New Gap and Friction Element," Report to DTNSRDC by MARC Analysis Research Corporation, Palo Alto, Cal., Report No. 77-52, (June 1977).

23. Stadter, J. T. and R. O. Weiss, "Analysis of Contact Through Finite Element Gaps," Computers and Structures, Vol. 10, No. 6, pp. 867-873, (Dec. 1979).

24. Heermann, L. R., "Finite Element Analysis of Contact Problems," Journal of Engineering Mechanics Division, ASCE, Vol. 104, No. EM5, pp. 1043-1056, (Oct 1978).

25. Buragohain, D. and V. L. Shah, "Curved Isoparametric Interface Surface Element," Journal of Structural Division, ASCE, Vol. 104, No. ST1, pp. 205-209, (Jan 1978).

26. Hsu, T. R. and A. W. M. Bertels, "Application of Elastoplastic Finite Element Analysis to the Contact Problems of Solids," AIAA Journal, Vol. 14, No. 1, pp. 121-122, (Jan 1976).

27. ANSYS User Information Manual for Revision 3, (1979) Swanson Analysis Systems Inc., Houston, Pennsylvania, 15342.

28. Benda, B. J. and R. C. Greenlaw, "Application of ADINA to Nonlinear Contact Problems," Proceedings of the ADINA Conference, Massachusetts Institute of Technology, Cambridge (4-5 Aug 1977).

29. Schafer, H. "A Contribution to the Solution of Contact Problems with the Aid of Bond Elements," Computer Methods in Applied Mechanics and Engineering, Vol. 6, No. 3, pp. 335-354, (Nov 1975).

30. Fredriksson, B., "Finite Element Solution of Surface Nonlinearities in Structural Mechanics with Special Emphasis to Contact and Fracture Mechanics Problems," Computers and Structures, Vol. 6, No. 4/5, pp. 281-290, (Aug-Oct 1976).

31. Fredriksson, B., "Elastic Contact Problems in Fracture Mechanics," Fracture 1977, Vol. 3, ICR4, Waterloo, Canada (19-24 Jun 1977).

32. Hughes, T. J. R. et al., "A Finite Element Method for a Class of Contact-Impact Problems," Computer Methods in Applied Mechanics and Engineering, Vol. 8, No. 3, pp. 249-276 (Jul-Aug 1976).

33. Taylor, R. L. and J. L. Sackman, "Contact-Impact Problems - Volume 1; Engineering Report and User's Manual," U.S. Department of Transportation Report DOT HS-805629 (Aug 1980).

34. MARC-CDC General Purpose Finite Element Analysis Program, Volume 1, User Information Manual for Revision J, (1977), MARC Analysis Research Corp., Palo Alto, Cal., 94306.

35. Hibbitt, H. D. Private Communication (June 1981).

36. MARC-CDC General Purpose Finite Element Analysis Program, Volume 1, User Information Manual for Revision H (1976), MARC Analysis Research Corp., Palo Alto, Cal., 94306.

37. ABAQUS Users Manual (Version 3, June 1979 (Revised Sep 1980)), Hibbitt and Karlsson Inc., Providence, R.I., 02903.

38. Sorensen, E. P. and H. D. Hibbitt, "Contact/Friction Interaction and the Analysis of Shaft-Sleeve Interference," Report to DTNSRDC by Hibbitt, Karlsson and Sorensen, Inc., Providence, R.I., 02906 (Apr 1982).

39. Zienkiewicz, O. C., "The Finite Element Method," 3rd Edition, McGraw-Hill Book Company (UK) Ltd., Maidenhead, England, U.K. (1977).

40. ABAQUS Users Manual (Version 4, May 1982), Hibbitt, Karlsson and Sorensen, Inc., Providence R.I., 02906.

41. Poritsky, H. "Stresses and Deflections of Cylindrical Bodies in Contact with Application to Contact of Gears and Locomotive Wheels," Journal of Applied Mechanics, Vol. 72, pp. 191-201 (Jun 1950).

42. Hill, L. R. et al., "Shrink Fit of a Thick-Walled Cylinder with Contact Shear," Journal of Applied Mechanics, Vol. 90, pp. 729-736, (Dec 1968).

43. Conway, H. D. and K. A. Farnham, "The Shrink Fit of a Flexible Sleeve on a Shaft," International Journal of Mechanical Sciences, Vol. 10, No. 10, pp. 757-764 (Oct 1968).

44. Shibahara, M. and J. Oda, "Problems on the Finite Hollow Cylinders under the Axially Symmetrical Deformations," Bulletin of the Japan Society of Mechanical Engineers, Vol. 11, No. 48, pp. 1000-1014, (Dec 1968).

45. Loubignac, G. et al., "Continuous Stress Fields in Finite Element Analysis," AIAA Journal, Vol. 15, No. 11, pp. 1645-1647 (Nov 1977).

46. Hinton, E. and J. S. Campbell, "Local and Global Smoothing of Discontinuous Finite Element Functions Using a Least Squares Method," International Journal for Numerical Methods in Engineering, Vol. 8, No. 3, pp. 461-480, (1974).

47. Hinton, E. et al., "Local Least Squares Stress Smoothing for Parabolic Isoparametric Elements," International Journal for Numerical Methods in Engineering, Vol. 9, No. 1, pp. 235-238 (1975).

48. Juvinall, R. C., "Engineering Considerations of Stress, Strain, and Strength," McGraw-Hill Book Co. Inc., New York (1967) pp. 128-130.

49. Conway, H. D. and K. A. Farnham, "The Contact Stress Problem for Indented Strips under Conditions of Partial Slipping," International Journal of Engineering Science, Vol. 5, No. 2, pp. 145-154, (Feb 1967).

50. Roark, R. J. and W. C. Young, "Formulas for Stress and Strain," 4th Edition, Mc Graw-Hill Book Co. Inc., New York (1965), p. 158, Example 1.

51. Hibbitt, H. D., Private Communication, (Jun 1981).

52. White, G. N., Jr., "Application of the Theory of Perfectly Plastic Solids to Stress Analysis of Strain Hardening Solids," Technical Report No. 51, Graduate Division of Applied Mathematics, Brown University (Aug 1950).

53. Besseling, J. F., "A Theory of Elastic, Plastic, and Creep Deformation of an Initially Isotropic Material Showing Strain Hardening, Creep Recovery and Secondary Creep," Journal of Applied Mechanics, Vol. 25, No. 4., pp. 529-536 (Dec 1958).

54. Burdekin, M. et al., "Experimental Study of Normal and Shear Characteristics of Machined Surfaces in Contact," Journal of Mechanical Engineering Science, Vol. 20, No. 3, pp. 129-132, (Jun 1978).

55. Burdekin, M. et al., "An Elastic Mechanism for the Microsliding Characteristics Between Contacting Machined Surfaces," Journal of Mechanical Engineering Science, Vol. 20, No. 3, pp. 121-127, (Jun 1978).

56. Duquette, D. J., "The Role of Cyclic Wear (Fretting) in Fatigue Crack Nucleation in Steels," Strength of Metals and Alloys, Vol 1, Fifth International Conference, Aachen, W. Germany, pp. 213-218, (27-31 Aug 1979).

57. Nishioka, K. et al., "Fundamental Investigations of Fretting Fatigue, (Part I, on the Relative Slip Amplitude of Press-Fitted Axle Assemblies)," Bulletin of the Japan Society of Mechanical Engineers, Vol. 11 No. 45, pp. 437-445, (Jun 1968).

58. Smith, E. "The Application of Fracture Mechanics Principles to Stress Corrosion Fractures Arising from Contact Stresses," Proc. Conf. Fracture Mechanics in Engineering Practice, Sheffield, England, U.K., pp. 257-270 (1976).

59. Rooke, D. P. and D. A. Jones, "Stress Intensity Factors in Fretting Fatigue," Journal of Strain Analysis, Vol 14, No. 1, pp. 1-6, (Jan 1979).

60. Tong, P. and T. H. H. Pian, "On the Convergence of the Finite Element Method for Problems with Singularity," International Journal of Solids and Structures, Vol. 9, No. 3, pp. 313-321, (Mar 1973).

61. Tseng, J. and M. D. Olson, "The Mixed Finite Element Method Applied to Two-Dimensional Elastic Contact Problems," International Journal for Numerical Methods in Engineering, Vol 17, No. 7, pp. 991-1014, (1981).

62. Seguchi, Y. et al., "Sliding Rule of Friction in Plastic Forming of Metal," Computational Methods in Nonlinear Mechanics, Proceedings of the International Conference on Computational Methods in Nonlinear Mechanics, University of Texas, pp. 683-692, (Sep 1974).

63. Kennedy, F. E. and F. F. Ling, "A Thermal, Thermo-elastic and Wear Simulation of a High-Energy Sliding Contact Problem," Journal of Lubrication Technology, Vol. 96, No. 3, pp. 497-507, (Jul 1974).

64. Reddi, M. M., "Finite Element Solution of the Incompressible Lubrication Problem," Journal of Lubrication Technology, Vol. 91, No. 3, pp. 524-533, (Jul 1969).

65. Reddi, M. M., and T. Y. Chu, "Finite Element Solution of the Steady-State Compressible Lubrication Problem," Journal of Lubrication Technology, Vol. 92, No. 3, pp. 495-503 (Jul 1970).

66. Wada, S. et al., "Application of Finite Element Method to Hydrodynamic Lubrication Problems, (Part I, Infinite-Width Bearings)," Bulletin of the Japan Society of Mechanical Engineers, Vol. 14, No. 77, pp. 1222-1233, (Nov. 1971).

67. Wada, S. and H. Hayashi, "Application of Finite Element Method to Hydrodynamic Lubrication Problems, (Part 2, Finite Width Bearings)," Bulletin of the Japan Society of Mechanical Engineers, Vol. 14, No. 77, pp. 1234-1244, (Nov 1971).

68. Booker, J. F. and K. H. Huebner, "Application of Finite Element Methods to Lubrication: An Engineering Approach," Journal of Lubrication Technology, Vol. 94, No. 4, pp. 313-323, (Oct 1972).

69. Taylor, C. and J. F. O'Callaghan, "A Numerical Solution of the Elastohydrodynamic Lubrication Problem Using Finite Elements," Journal of Mechanical Engineering Science, Vol. 14, No. 4 pp. 229-237 (Aug 1972).

70. Rohde, S. M. and K. P. Oh, "A Unified Treatment of Thick and Thin Film Elastohydrodynamic Problems by Using Higher Order Element Methods," Proc. Royal Society of London, Series A, Vol. 343, No. 1634, pp. 315-331, (13 May 1975).

71. Oh, K. P. and S. M. Rohde, "Numerical Solution of the Point Contact Problem Using the Finite Element Method," International Journal for Numerical Methods in Engineering, Vol 11, No. 10 pp. 1507-1518, (1977)

72. Huebner, K. H., "Application of Finite Element Methods to Thermohydrodynamic Lubrication," International Journal for Numerical Methods in Engineering, Vol. 8, No. 1, pp. 139-165, (1974).

73. Hetenyi, M., "Beams on Elastic Foundation," University of Michigan Press, Ann Arbor (1946).

INITIAL DISTRIBUTION

Copies	
1	CNO, Code 987
1	CHONR, Code 431 (M. K. Ellingsworth)
1	ONR BOSTON
1	ONR CHICAGO
1	ONR LONDON, ENGLAND
1	ONR PASADENA
3	NRL 1 2627 1 5800 1 6300
1	USNA
1	NAVPGSCOL LIB
1	NROTC & NAVADMINU, MIT
1	NSWC WHITE OAK
1	NOSC
1	NCEL
11	NAVSEA 1 03R 1 03R24 (J. Gagorik) 1 323 1 3232 (R. Provencer) 1 32321 (R. Keltie) 1 32322 (D. Nichols) 1 32323 (R. McCarthy) 1 05H 1 05R22 (H.D. Marron) 1 052 (R.J. Cauley) 1 524 (R.M. Petros)
1	USDRE/TWP/SA (Dr. P. Genalis)

Copies	
5	DTIC
1	NSF ENGR DIV LIB
1	DOT LIB
1	Dr. T. Dow North Carolina State University
1	Prof. E. Rabinowicz MIT
1	Dr. H. D. Hibbitt Hibbit, Karlsson and Sorensen, Inc. Providence, R.I.
1	Dr. S. Chander Control Data Corp. Rockville, MD
1	Prof. D. Duquette Rensselaer Polytechnic Institute
1	Dr. P. Marcal MARC Analysis Research Corp. Palo Alto, CA
1	Prof. Francis Kennedy Dartmouth University
1	Prof. Frederick Ju University of New Mexico

CENTER DISTRIBUTION

Copies	Code	Name
1	012.3	D. Jewell
1	11	W. M. Ellsworth
1	17	W. W. Murray
1	1702	

Copies	Code	Name
1	1706s	C. Eynon (m)
1	172	M.A. Krenzke
1	1720.1	T.J. Kiernan
1	1720.1	G.L. Becker
1	1720.1	D. Lesar
1	1720.2	K. Hom
1	1720.3	R.F. Jones Jr.
1	1720.4	A.J. Wiggs
1	1720.5	D.T. McDevitt
1	1720.6	R.D. Rockwell
1	173	
1	174	
1	175	
1	177	
1	177.4	M. Wright (m)
1	18	G.H. Gleissner
1	1844	S. Dhir
1	27	
1	2723	A. Harbage
1	28	
1	2814	J. Gudas
1	2832	J. Dray
5	5211.1	Reports Distribution
1	522.1	Unclass Lib (C)
1	522.2	Unclass Lib (A)

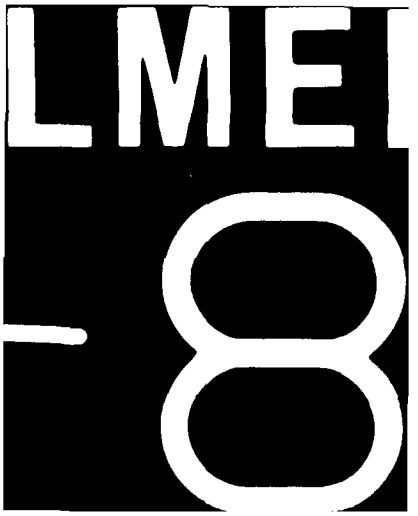
LME
8